THESIS
2
(1994)

MICHIGAN STATE LIBRARIES
3 1293 01801 7404

LIBRARY
Michigan State
University

This is to certify that the

dissertation entitled

31P-NMR SPECTROSCOPY OF PHOSPHOCREATINE
RECOVERY TRANSIENTS IN RAT SKELETAL MUSCLE

presented by

Anthony Toby Paganini

has been accepted towards fulfillment
of the requirements for

Ph.D. degree in Physiology

Major professor

Date 12/10/98

MSU is an Affirmative Action/Equal Opportunity Institution

O-12771

PLACE IN RETURN BOX to remove this checkout from your record.
TO AVOID FINES return on or before date due.
MAY BE RECALLED with earlier due date if requested.

DATE DUE	DATE DUE	DATE DUE
JAN 2 0 8 2007		

1/98 c/CIRC/DateDue.p65-p.14

^{31}P-NMR SPECTROSCOPY OF PHOSPHOCREATINE RECOVERY TRANSIENTS IN RAT SKELETAL MUSCLE

By

Anthony Toby Paganini

A DISSERTATION

Submitted to
Michigan State University
in partial fulfillment of the requirements
for the degree of

DOCTOR OF PHILOSOPHY

Department of Physiology

1998

^{31}P-NMR S
RECOVERY

The first part o
the oxidative
mammal work
influence of in
phosphorous n
study the temp
superficial gastroc
endothelial con
splenectomy (10
caused by progr
normal regimen
Chinese treatm
the superficial g
corresponding con
(P<0.01 be
relation and a
two groups, th

ABSTRACT

^{31}P–NMR SPECTROSCOPY OF PHOSPHOCREATINE RECOVERY TRANSIENTS IN RAT SKELETAL MUSCLE

By

Anthony Toby Paganini

The first part of this dissertation examines the effect of perturbations in skeletal muscle oxidative capacity on phosphocreatine (PCr) recovery kinetics after submaximal workloads (8 minutes of isometric twitch stimulation) in addition to the influence of intracellular acidosis on the PCr recovery rate constant. In vivo 31–phosphorous nuclear magnetic resonance spectroscopy (^{31}P–NMRS) is used to quantify the temporal changes of phosphagens and intracellular pH in the rat superficial gastrocnemius (approximately 85% fast–twitch–glycolytic fibers) after mitochondrial content is either decreased by chronic hypothyroidism via chemical thyroidectomy [10–weeks of 0.025% w/v methimazole (MMI) in drinking water] or increased by progressive, interval, aerobic training [10–weeks on a running wheel to a final regimen of 37m/minute, 60 minutes/day, five days/week ($\approx$ 85% $VO2_{max}$)]. After these treatments, citrate synthase activity (an index of mitochondrial content) of the superficial gastrocnemius was 29% and 179%, respectively, of that in the corresponding control groups. The results indicate a significant linear correlation ($r = 0.84$, $P<0.01$) between the PCr recovery rate constant after submaximal stimulation and a 6–fold range of citrate synthase activity. Additionally, within the control groups, there was a significant correlation ($r=0.73$, $P<0.01$) between the

recovery rate

ages miracl

very rate con

the second ;

mapping distr

mative oxida

ments. High

ized by summ

ial Principal C

ssion to Fou

ement instab

xponential

ssed Nor

ple, discret

ssate applyi

eak bimodal

ification of

ted by non-ir

ecidedly, thes

e first thr

may confoun

ocean metabo

'run-up' perio

PCr recovery rate constant and the intracellular pH at the end of stimulation. This suggests intracellular acidification complicates the correlation between PCr recovery rate constants and muscle oxidative capacity.

In the second part of this dissertation, an attempt was made to identify the underlying distribution of distinct muscle fiber type populations as differentiated by relative oxidative capacity from decomposition of global PCr recovery transients. High signal–to–noise ^{31}P–NMRS data from the posterior rat leg were obtained by summing across eight contiguous, stimulation–recovery cycles. The novel Principal Component Analysis (PCA) method for spectral processing was used prior to Fourier transformation to correct for frequency drifting and other equipment instabilities. Experimental results indicates the apparent monoexponential PCr recovery can be resolved into multiple components using the unbiased Non–negative Least Squares (NNLS) analysis method. This suggests multiple, discrete, fiber type populations may exist. Modelling studies, however, illustrate applying the NNLS method to two disparate fiber type distributions (discrete bimodal versus Gaussian) gives similar results. Therefore unambiguous identification of the distribution of fiber type populations in mammalian mixed muscle by non–invasive, high–resolution, NMR spectroscopy remains elusive. Secondarily, these results document significant differences in end–stimulation pH over the first three cycles of an intermittent, constant, supramaximal workload. This may confound the interpretation of gated–NMR experiments which assume invariant metabolic responses from cycle to cycle and point to the importance of a "warm–up" period prior to engaging in short bursts of high–intensity workloads.

first and fore
intellectual g
shape rather
ship about mat
reading scie
merely leads b
their senior lab
their profession
data protocols
will have been
write assays, sp
ships. Many th
ears I have spen
ks and the fir
ends Tom, yo
Brent and Jim
dissertation.
Dan and espe
8 years. Jack,
much time as
dressing help
lyze my data
am extreme
Brooks at Mich
Sisters, Bob W

ACKNOWLEDGMENTS

First and foremost, I genuinely thank my research mentor, Dr. Ron Meyer, for his intellectual guidance, impeccable scientific integrity, and treating me like a colleague rather than just another minion. You have shown me how to think deeply about nature, balance skepticism with open–mindedness, wear many hats while "doing science", and have fun doing it all. You are one of the very few people who truly leads by example rather than decree. I am also deeply indebted to my former senior lab colleague, Dr. Jeanne Foley. I've always been able to count on you for professional guidance, lively scientific discourse, friendship, and help with the lab protocols when I was wet behind the auricles. I loathe to think where I would have been without your detailed lab notes and patience showing me how to run the assays, spin the dials on the Bruker spectrometer, and perform the rat surgery. Many thanks go to my teaching mentor, Dr. Tom Adams, for the countless hours I have spent in his office discussing physiology pedagogy, class management skills, and the finer points of heat transfer in Australian Brush Turkey nest mounds. Tom, you are a genuine Renaissance man. Thanks also go to Drs. Rudy Bernard and Jim Pivarnik for their valuable perspectives and thorough review of my dissertation. I also want to thank Drs. Dick Heisey, Burnell Selleck, Bob Pitman and especially the late Jack Krier for their tutelage and sage advice over the years. Jack, I'll never forget your passion for research and willingness to spend as much time as I needed discussing neurophysiology. Without the spectral processing help of Dr. Truman Brown and Radka Stoyanova at Fox Chase Cancer Center my data would seem much less interesting.

I am extremely grateful to my friends and current and former colleagues while I've been at Michigan State (Marya Liimatta, Roop Jayaraman, Barry Prior, Marco Cabrera, Bob Wiseman, Rick Kustasz) and Ohio State (Ken–"Kenny H"–Helal,

[illegible] R[illegible]

[illegible] or [illegible]

[illegible] but cert[illegible]

[illegible] Marilyn[illegible]

[illegible] Jo[illegible]

[illegible] Plant, [illegible]

[illegible] Tom[illegible]

[illegible] much [illegible]

[illegible]

[illegible] Dissertat[illegible]

[illegible]skeletal [illegible]

[illegible] was fina[illegible]

[illegible] at Mich[illegible]

Jim–"Jimmy R"–Raeburn) for the many thought provoking discussions, help with homework or lab techniques, and general inspiration.

Last, but certainly not least I'd like to thank the Physiology (Amylou, Jan, Barb, Nancy, Marilyn, Sharon, Shirley, Bobby, Greg, Vance), Anatomy (Judy, Jill), and Kinesiology (Jo Ann, Jan, Verna, Darcie) department support staff; Dan from Physical Plant, Jim from the Physics machine shop, and Ron's former lab technicians (Tom, Mary, Rob). All of you have kept the gears well greased and made life much easier for me over the years. To all who have help me, thanks a googolplex!

This dissertation was supported by National Institute of Arthritis and Musculoskeletal and Skin Diseases Grant AR–38972. A portion of my graduate program was financed by a Recruiting Fellowship from the College of Human Medicine at Michigan State University.

ST OF TABLES

ST OF FIGURES

hapter 1 INTR
ENERAL ORIE
ACKGROUND
SCOPE OF THE
ORGANIZATIONS

HAPTER 2 LITE
keletal mus
ERGY CONVER
nergy for mu
nergy for mu
nergy for mu
E RADLE REVI
ATP energies a
Myothermal te
Phosphorylati
CONTEMPORARY
The connection
PCr and the che
Oxidative capa
Respiratory NM
Transient and

HAPTER 3 Line
muscle oxida
TRODUCTION
THODS
Animal care an
Treatment grou
Muscle surgical
Spectral acquis
Spectral analy
Statistical ana
SULTS
Treatment effe
Effect of subma
Effect of 2 CHz
SCUSSION

TABLE OF CONTENTS

LIST OF TABLES ix

LIST OF FIGURES x

Chapter 1 INTRODUCTION 1
GENERAL ORIENTATION 1
BACKGROUND OF THE PROBLEM AND SPECIFIC AIMS 2
SCOPE OF THE DISSERTATION 4
LIMITATIONS OF THE DISSERTATION 4

CHAPTER 2 LITERATURE REVIEW The role and utility of phosphocreatine in skeletal muscle energy metabolism 5
EARLY CONCEPTS (1880S–1940S) 5
Energy for muscle contraction was viewed as a heat transfer phenomenon 5
Energy for muscle contraction was related to biochemical phenomena 6
Energy for muscle contraction was explained by PCr hydrolysis 9
THE ROLE REVERSAL (1940S–EARLY1970S) 12
ATP emerges as the primary energetic determinant of contraction 12
Myothermal techniques refine the bioenergetic role and experimental utility of PCr 14
PCr hydrolysis helps estimate muscle efficiency 20
CONTEMPORARY VIEWS (EARLY1970S–PRESENT) 23
The connection between PCr kinetics and oxidative capacity and its implications 23
PCr and the chemical energy balance method 29
Oxidative capacity exhibits plasticity in skeletal muscle fibers 31
Phosphorus NMR spectroscopy becomes an important tool in bioenergetics 32
Transient and steady–state analysis of PCr kinetics 38

CHAPTER 3 Linear dependence of phosphocreatine kinetics on skeletal muscle oxidative capacity 46
INTRODUCTION 46
METHODS 46
Animal care and feeding 46
Treatment groups 47
Muscle surgical protocol 48
Spectral acquisition parameters and muscle stimulation protocol 50
Spectral analysis 50
Statistical analysis 51
RESULTS 51
Treatment effects 51
Effect of submaximal stimulation 55
Effect of 2.0Hz Stimulation 61
DISCUSSION 64

CHAPTER 4 Est
phosphocre
INTRODUCTION
METHODS
Animal care a
Muscle surgi
Stimulation-h
Spectra acqu
Spectra pro
Spectra anal
Statistical an
RESULTS
Spike changes
Theory of Pmi
Decomposition
Modeling of Pi
DISCUSSION
Decomposition
Temporal meta
Validity of in v
CHAPTER 5 SUM
SUMMARY
RECOMMENDATI
APPENDICES
LIST OF REFERE
INDEX

CHAPTER 4 Estimation of skeletal muscle fiber distributions by phosphocreatine transient analysis **69**
INTRODUCTION 69
METHODS 71
Animal care and feeding 71
Muscle surgical protocol 71
Stimulation–Recovery protocol 72
Spectral acquisition parameters 73
Spectral processing 74
Spectral analysis 76
Statistical analysis 77
RESULTS 77
Cyclic changes in metabolites and force 77
Utility of Principal Component Analysis 110
Decomposition of global PCr time constants 112
Modelling of fiber type distributions 116
DISCUSSION 120
Decomposition of PCr recovery transients 120
Temporal metabolite patterns during prolonged intermittent exercise 124
Viability of in vivo fiber typing by ^{31}P–NMRS 126

CHAPTER 5 SUMMARY AND RECOMMENDATIONS **130**
SUMMARY 130
RECOMMENDATIONS FOR FUTURE STUDIES 131

APPENDICES **134**

LIST OF REFERENCES **143**

INDEX **170**

Table 1: Biochem
Table 2: Treatm
Table 3: Mother
Table 4: Metabo
Table 5: PCr kine
Table 6: Treatm
Table 7: NMRS A
Table 8: Time co
Appendix B Figu

LIST OF TABLES

Table 1: *Evolution of fiber type classification schemes* 28

Table 2: *Treatment groups and effects* 52

Table 3: *Mechanical characteristics–Bench experiment* 54

Table 4: *Metabolites in resting superficial gastrocnemius* 55

Table 5: *PCr kinetics and pH during submax. stimulation* 58

Table 6: *Treatment groups* 73

Table 7: *NMRS Acquisition parameters* 74

Table 8: *Time constants from NNLS output* 116

Appendix B Figure 28 & Table 9: *Leg cross–section* 136

Figure 1: Sampl
Figure 2: Time
Figure 3: PCr re
Figure 4: 2.5Hz
Figure 5: 2.5Hz
Figure 6: Rate co
Figure 7: Sampl
Figure 8: Time co
Figure 9: Time co
Figure 10: Time
Figure 11: Steady
Figure 12: Time
Figure 13: Time
Figure 14: Time
Figure 15: End-s
Figure 16: Time
Figure 17: Time
Figure 18: Time
Figure 19: Initia
Figure 20 Force
Figure 21: Spect
Figure 22: Samp
Figure 23: NNLS
Figure 24: Hypo
Figure 25: Synch
Figure 26: NNLS

LIST OF FIGURES

Figure 1: Sample ^{31}P–NMR spectra stackplots 56

Figure 2: Time course of PCr changes (submaximal stim.) 57

Figure 3: PCr recovery rate constant v. oxidative capacity 60

Figure 4: 2.0Hz Stimulation time courses 62

Figure 5: 2.0Hz Recovery time courses 63

Figure 6: Rate constant v. pH (supramaximal stim.) 64

Figure 7: Sample ^{31}P–NMR spectra stackplots 79

Figure 8: Time course of PCr changes (0.75Hz) 80

Figure 9: Time course of PCr changes (2.0Hz) 82

Figure 10: Time course of PCr changes (5.0Hz) 84

Figure 11: Steady–state PCr characteristics vrs. cycle # 87

Figure 12: Time course of ICF pH changes (0.75Hz) 89

Figure 13: Time course of ICF pH changes (2.0Hz) 91

Figure 14: Time course of ICF pH changes (5.0Hz) 93

Figure 15: End–stimulation ICF pH vrs. cycle # 95

Figure 16: Time course of isometric twitch force (0.75Hz) 97

Figure 17: Time course of isometric twitch force (2.0Hz) 100

Figure 18: Time course of isometric twitch force (5.0Hz) 103

Figure 19: Initial and end–stimulation peak twitch force 108

Figure 20 Force kinetics of single twitches vrs. cycle # 109

Figure 21: Spectral correction by PCA 111

Figure 22: Sample high signal–to–noise ^{31}P–NMR spectra 113

Figure 23: NNLS applied to a PCr recovery transient 114

Figure 24: Hypothetical fiber type distributions 117

Figure 25: Synthesized global PCr recovery time–courses 118

Figure 26: NNLS output of hypothetical distributions 119

Appendix A Figure 27: ^{31}P–NMR Probe Photographs 135

Appendix B Figure 28 & Table 9: *Leg cross–section* 136

Appendix C Figure 29: Temperature Homeostasis 137

Appendix D Figure 30: N versus Cycle Number 138

Appendix E Figure 31: Methimazole Inhibition 139

Appendix F Figure 32: Intensity–Duration Protocol 140

Appendix G Figure 33: Training Compliance 141

Appendix H Figure 34: Methimazole Effects 142

General Or

major thre

ing in mamm

uscle spect

humans in t

biochemical ch

and degener

ease over whe

maximal w

$\dot{V}O_{2max}$ is

$\dot{V}O_{2max}$ is

ities Support

servations tha

mption QC

al 39. This p

dependent on

Maximal AT

Maine enzyme

ggests that t

$\dot{V}O_2$ compon

ained from obs

ults and grea

Speed to Typ

Chapter 1
INTRODUCTION

General Orientation

A major thrust of this dissertation explores the viability of non–invasive fiber typing in mammalian skeletal muscle using 31–phosphorus nuclear magnetic resonance spectroscopy (^{31}P–NMRS). Fiber typing has been of perennial interest to clinicians in the rehabilitative medicine fields who wish to catalog the histochemical changes from muscle tissue biopsies as a result of acute trauma or chronic degenerative processes. More recently, in the applied exercise sciences, the debate over whether central cardiovascular factors or peripheral muscle factors limit maximal whole–body oxygen consumption (VO_{2max}) has been re–ignited. Since VO_{2max} is synonymous with a person's aerobic capacity, determining what limits VO_{2max} is of profound interest to cardiologists, exercise scientists, and coaches. Support for limitation by peripheral muscle factors comes from observations that over 80% of the slow VO_2 component reflects the oxygen consumption (QO_2) kinetics of the exercising muscle mass (for reviews see Refs. 246, 309). This phenomenon necessarily reflects muscle fiber QO_2 kinetics which are dependent on the communication between cytosolic ATP demand and mitochondrial ATP supply. Invasive fiber typing protocols based upon staining for oxidative enzyme contents and isoenzymes of myosin ATPase have led to the conjecture that the fast VO_2 component is due to Type I fiber recruitment and the slow VO_2 component is due to Type II fiber recruitment (18). This explanation is derived from observations that Type I fibers generally have higher mitochondrial contents and greater capillary densities resulting in greater oxidative capacities compared to Type II fibers (261). The greater the oxidative capacity, the greater the

ract to which

ated by the

Backgroun

Consequently

ercising skel

The Tradit

echemical st

ep numerous

rmed a corr

d and they t

mate FG v

Unfortunately

ized muscle

aphic locati

reamore, m

ater discomfor

because of the

already beer

ber type distrib

especially imp

ed muscle. No

mical power

ional limitati

Consequently,

ated paramete

ious theoreti

extent to which fibers rely on oxygen consumption to meet the instantaneous ATP demand by the contractile apparatus.

Background of the Problem and Specific Aims

Consequently, it is incumbent to systematically classify fiber type distributions in working skeletal muscle to provide a basis for mechanistic interpretations of VO_{2max}. Traditional fiber typing methods over the past 40 years have employed histochemical stains, immunocytochemical markers, and/or gel electrophoresis to assay numerous enzyme activities and protein constituents. These methods have provided a cornucopia of information unattainable through other techniques (261, 242), and they have led to the commonly reported bipartite (Type I v. Type II) or tripartite (FG v. FOG v. SO) fiber type taxonomy.

Unfortunately, these traditional methods require *in vitro* assays of freeze–clamped muscle biopsies, and several biopsies are usually needed with respect to geographic location within the muscle and/or time during the experiment. Furthermore, multiple biopsies necessitate halting the experiment and may cause patient discomfort once the local anesthetic has worn off.

Because of these limitations, measuring oxidative capacity via *in vivo* ^{31}P–NMRS has recently been proposed as a non–invasive alternative for estimating muscle fiber type distributions. The promise of ^{31}P–NMRS is it offers real–time tracking of energetically important intracellular metabolites (PCr, ATP, Pi, pH) within the same muscle. Not only does this greatly increase time resolution, it also increases statistical power over the one–muscle–one–time–point (and/or one–geographic–location) limitation of the muscle biopsy method.

Consequently, a necessary prerequisite would be to correlate a ^{31}P–NMRS derived parameter to an energy supply or energy demand fiber type parameter. Previous theoretical and empirical studies have shown that the steady–state PCr

during stim

recovery aft

ome content

leads to the

Specif

relative

^{31}P-NM

constant

ffirmative.

Specif

distribut

oxidativ

answering

ased over a

ty and the t

and superfic

ed on previou

osely propor

max 203).

Specific Aim

^{31}P-NMR spectr

ues with phas

Dependent Ana

ulate a de

ulate a hetero

for the global

ing the unbia

level during stimulation scales with oxygen consumption, and the time constant of PCr recovery after submaximal stimulation should be directly proportional to total creatine content and inversely proportional to oxidative capacity (192, 203, 208). This leads to the first specific aim of this dissertation:

> **Specific Aim #1**: Does skeletal muscle oxidative capacity in a relatively homogeneous fiber population scale with an *in vivo* ^{31}P–NMRS derived parameter such as the PCr recovery time constant?

If affirmative, this leads to the second specific aim of this dissertation.

> **Specific Aim #2:** Can ^{31}P–NMRS be used to elucidate the distribution of discrete fiber type populations based upon relative oxidative capacity in a known heterogenous fiber population?

In answering Specific Aim #1, skeletal muscle mitochondrial content will be perturbed over a six–fold range, a range significantly larger than in any human study, and the time constant of PCr recovery will be measured with ^{31}P–NMRS in the rat superficial white gastrocnemius (mostly fast–glycolytic fibers, (8). This is based on previous studies which suggest the time constant of PCr recovery is inversely proportional to oxidative capacity when normalized to total creatine content (203).

Specific Aim #2 will be addressed by first constructing a high signal–to–noise ^{31}P–NMR spectral time course from repeated, contiguous, stimulation–recovery cycles with phase and frequency correction performed by the novel Principal Component Analysis (PCA) method. An intentional effort will be made to interrogate a deeper volume of muscle in the rat hindlimb which is known to contain a heterogenous population of fibers with respect to oxidative capacity (8). Next, the global, NMR–derived, PCr recovery time course will be decomposed using the unbiased Non–Negative Least Squares (NNLS) algorithm. This is done to

extract time–constant amplitudes and durations in an effort to elucidate the distribution of discrete fiber type populations within heterogeneous mammalian skeletal muscle.

Scope of the Dissertation

The primary focus of this study is to clarify the potential utility of ^{31}P–NMRS to discern discrete fiber type populations in mixed mammalian muscle. No attempt will be made to directly contribute to the ongoing, high–profile debates of muscle fatigue or metabolic control theory.

Limitations of the Dissertation

1) This is an *in vivo* study using genotypically and phenotypically similar rodents. These rodents spend nearly all of their time within the confines of a small cage, are under general anesthetic during the experiment, and undergo supramaximal sciatic nerve stimulation simultaneously activating all motor units. The results of this study, therefore, may not be directly applicable to human muscle biology and routine locomotion patterns.

2) The *in vitro* enzymatic assay used to assess mitochondrial content may not be representative of *in vivo* cellular activities.

3) Oxidative capacity in the working skeletal muscle is dependent not only on mitochondrial content but also on capillary density. Capillary density was not measured.

The following Literature Review places the investigation of phosphocreatine and its kinetics in energy metabolism in a historical context as a preface for the Specific Aims mentioned above.

Th
ir

arly Conc

ergy for mu
nomenon

Since the la
ntinuum meta
e, a para
ption to ta
um-mechan
1930s 225
ure like a he
ntinuum mecha
ssor to a lo
based on
ounding the
ciple in phy
ederation o
Copenhagen, Da
proximately d
ending the law
No surprising
ciples such a
Bohr, Engel
ermodynamics
temperature

CHAPTER 2
LITERATURE REVIEW
The role and utility of phosphocreatine in skeletal muscle energy metabolism

Early Concepts (1880s–1940s)

Energy for muscle contraction was viewed as a heat transfer phenomenon

Since the late 1920s phosphocreatine (PCr) has been recognized as an important metabolite in mammalian skeletal muscle energy metabolism. Prior to this time, a paradigm shift occurred in muscle bioenergetics that allowed this recognition to take place. The contemporary archetype of muscle as a biological chemo–mechanical energy transducer was not the prevailing theory during most of the 1800s (225). During that century, muscle energy conversion was believed to behave like a heat engine. A heat engine is a device, such as a steam engine, performs mechanical work when heat is transferred from a high temperature reservoir to a low temperature reservoir. The explanation of a muscle's mechanical output based on heat engine principles was undoubtedly linked to the excitement surrounding the birth of classical (a.k.a. macroscopic) thermodynamics as a new discipline in physics during the nineteenth century (88). This was accomplished by a confederation of physicists, chemists, and engineers such as Carnot, Clausius, Clayeperon, Dalton, Gibbs, Helmholtz, Joule, Kelvin, and Mayer who all lived approximately during the same time and were all instrumental in formalizing and extending the laws of classical thermodynamics (196).

Not surprisingly this excitement in physics over thermodynamics infected other disciplines such as physiology. As an illustration of the muscle–heat engine paradigm, Engelmann in 1895 (88) attempted to apply the second law of thermodynamics to muscle by postulating the existence of numerous intracellular high temperature foci. These foci were to provide the muscle with the necessary

cellular te

chemical wor

energize the

cleaves intra

cycles norm

reaction occu

cosphere. If

ring contract

ngle paradigm

ng favor at t

Energy for mu

Muscle physi

biochemical mec

ng 1930s PCr

muscle force

ical role in th

was well kn

s that the tem

Setine, Cr, and

traction. Uyer

keletal muscle

ching season t

ntractions of ca

data 297 and

humans after e

ctor to the la

ther catabolic

intracellular temperature gradients for sufficient heat transfer in order to perform mechanical work in a thermodynamically reversible fashion. Unfortunately, the heat engine theory was seriously flawed on two accounts. First, it required numerous intracellular high temperature foci be maintained at more than three to ten times normal physiological temperatures (314). Second, Hill (130) showed heat production occurs during the recovery period from contraction in an oxygen atmosphere. If muscle were a heat engine, then heat should be produced only during contraction and not during recovery as Hill showed. Consequently, the heat engine paradigm as an explanation for the energy of muscular contraction was losing favor at the beginning of this century.

Energy for muscle contraction was related to biochemical phenomena

Muscle physiologists sought to explain muscle contraction based upon biochemical mechanisms as a way to supplant the heat engine paradigm. By the early 1930s PCr hydrolysis emerged as the leading process most closely associated with muscle force development; however, as discussed next, PCr arrived at this central role in the early history of muscle biochemistry through a circuitous route.

It was well known before the discovery of PCr in 1927 by Fiske and Subbarow (94) that the temporal change in the concentrations of PCr hydrolysis products (creatine, Cr, and inorganic phosphate, Pi) was strongly correlated with muscle contraction. Uyeno noticed a greater creatine content in tonically contracting pectoralis muscles of mating male frogs engaged in clasping females during the breeding season than non–mating male frogs (301). Thompson showed ischemic contractions of cat hindlimb increased the creatine released by the muscle into the plasma (297) and Embden was able to show increased urine inorganic phosphate in humans after exhaustive exercise (86).

Prior to the late 1920s creatine was considered a waste product of generalized protein catabolic processes occurring during muscle contraction (238). Moreover,

during this time frame, most muscle biochemists investigating creatine did so for the purpose of understanding the factors that caused increased creatinuria under pathological conditions such as myasthenia gravis, kidney disease, starvation, or diabetes mellitus (20, 147, 202, 237). Interestingly, it was recognized early on, creatine had its greatest concentration in tissues with capacity for large *changes* in metabolic demand (e.g. skeletal muscle, brain, heart), but not necessarily in tissues with large *constant* metabolic demand, per se, such as kidney or liver (20, 147). Furthermore, as early as 1911, Thunberg showed adding creatine to muscle extracts proportionally increased O_2 consumption and CO_2 production (298). Unfortunately, these observations did not resonate in the muscle bioenergetic community prior to the 1930s since increased creatine during contraction was not viewed as being directly tied to the energy supply of the contractile apparatus but rather the result of muscle protein catabolism.

During the same time frame the emerging role of inorganic phosphate in muscle bioenergetics was far more captivating to bioenergeticists than the putative waste by–product role of creatine. The metabolic significance of inorganic phosphate evolved from being considered as an obscure anion known to promote plant and yeast growth (117) into an essential ionic species covalently bonded to key glycolytic intermediates involved with lactic acid formation. Much of the motivation behind Embden's ground breaking work on the glycolytic pathway during the 1920s was the result of tenacious attempts to isolate a carbohydrate–based intermediate that liberated phosphate during muscle contraction, resulting in the observed increased urine phosphate and increased intramuscular lactic acid. Of course, it was later determined the phosphorylated C_3 and C_6 intermediates Embden isolated were directly or indirectly involved in substrate level phosphorylation of adenosine diphosphate (ADP) and were not intimately linked to providing the immediate energy for the contractile machinery.

Throughout

ion add form

ion acid? It h

on animals k

ile while res

hemins ident

on The early

ship motivat

ressing Buch

operations 3

element sugar

ylated hexo

ys directly co

monophosphates

ugest the proc

ursor in skel

ulate hypothes

onstituted fro

n unknown pre

lation during

ons of Embde

ulated the gl

ose monophos

ursor' 162, 2

As the glycoge

ose necessary

ction: I. wh

Throughout most of the first three decades of the 20th century the process of lactic acid formation was seen as *the* energy source for muscular contraction. Why lactic acid? It has been well appreciated by hunters since the beginning of time that animals killed after a pursuit will have more sour tasting flesh than animals killed while resting. According to Needham (225) in the middle of the 19th century Berzelius identified the ultimate source of this sourness in hunted stags as lactic acid. The early interest in the biochemical process of lactic acid formation was largely motivated by developments in the alcoholic fermentation process by yeast. Extending Buchner's earlier work for the German beer industry on intact yeast preparations (34), Harden and Young where able to show yeast–juice was also able to ferment sugars, thereby producing ethanol and CO_2 (105, 117). They later postulated hexoses (of unknown structure at the time) plus inorganic phosphates were directly converted in a single reaction step into CO_2, ethanol, and hexose monophosphates. These insights encouraged Fletcher and Hopkins (99, 100) to suggest the process by which lactic acid is anaerobically formed from an unknown precursor in skeletal muscle could provide the energy for contraction–the so called 'lactate hypothesis'. During recovery, this unknown precursor would be reconstituted from intramuscular lactic acid. This instigated an intensive search for the 'unknown precursor' and the catabolic pathway that resulted in lactic acid formation during muscle contraction. Toward this end, the collective seminal efforts of Embden, Meyerhof, Parnas, and the Cori husband and wife team elucidated the glycogenolytic/glycolytic pathways and identified glycogen and hexose monophosphates as putative candidates for the role of the 'unknown precursor' (162, 215).

As the glycogenolytic/glycolytic metabolic pathway began to materialize it became necessary to explain two experimental observations during muscle contraction: 1) why does muscle Pi increase above resting levels 2) how does

...ctic buffer ...

...the 1920s F...

...in the increa...

...ns although ...

...ressive lactic

...knew were

...pothesis' doc...

...ential factor

...significance

...ght closer t...

...ning to tur...

...timate hyp...

...ergy for mu...

...the start o...

...ect energy so...

...T. Lundsgaar...

...still occur ...

...ptic flux sh...

...Furthermore, he

...tly proportio...

...ues together th...

...gy is supplie...

...By the mid 19...

...nosis, creati...

...ified as a 'py...

...ctosine trip...

...reakdown was e...

muscle buffer the lactic acidosis that occurs under anaerobic conditions. At the end of the 1920s Fisk and Subbarow (95, 96) proposed PCr hydrolysis would explain both the increased Pi during contraction and the buffering of lactic acid. At the time, although lactate formation was seen as necessary for muscle contraction, excessive lactic acidosis was thought to be the cause of muscle fatigue. Fisk and Subbarow were able to dovetail their findings into the prevailing 'lactate hypothesis' doctrine by suggesting the buffering action of PCr hydrolysis was the essential factor allowing the muscle to contract without fatigue. Retrospectively, the significance of their studies was that PCr, Pi, and Cr were simultaneously brought closer to the energetic determinants of muscle contraction thereby beginning to turn attention away from carbohydrate catabolism as articulated by the lactate hypothesis.

Energy for muscle contraction was explained by PCr hydrolysis

At the start of the 1930s, the sovereignty of carbohydrate catabolism as the direct energy source in muscle contraction was being seriously called into question (131). Lundsgaard used iodoacetate to block glycolysis and showed contractions could still occur (190). If the lactate hypothesis were operative, then blocking glycolytic flux should have resulted in no contractile response upon stimulation. Furthermore, he also showed PCr breakdown, assessed by increasing Pi, was directly proportional to the external work (force x distance) done by the muscle. Taken together these observations suggested to Lundsgaard that the "contraction energy is supplied directly and exclusively by phosphagen breakdown" (190).

By the mid 1930s, Lohmann had discovered the enzyme responsible for PCr hydrolysis, creatine kinase, and the existence of an indispensable coenzyme he identified as a 'pyrophosphate of adenylic acid' (AMP–PPi) more commonly known as adenosine triphosphate (ATP) (189). More importantly, he suggested PCr breakdown was energetically coupled to the immediate resynthesis of ATP via the

ing react..

#1

#2

Net react..

ser observat..

modynamic

ergetically

ion could e

anced 22

mediary m

ions to less

more specifi

first hydroly

kdown. From

ration and t

ganic phosph

cetic acid 189

abolite respo

During the beg

ck of cellular b

mediary me

ater potentia

ber of carbo

eased via oxi

ber of phosph

e phosphate–g

ential phosph

following reaction catalyzed by creatine kinase:

#1	ATP		——>	AMP +	2Pi
#2	AMP +	2PCr	<——>	ATP +	2Cr
Net reaction:		2PCr	——>	2Pi +	2Cr

These observations broke new ground on two different fronts. First, from a general thermodynamic perspective, Lohmann provided the first experimental evidence of an energetically coupled chemical process. Prior to this time the idea one chemical reaction could energetically drive another chemical reaction was only theoretically entertained (225). Since then it has been repeatedly shown that most of intermediary metabolism occurs due to energetic coupling of highly exergonic reactions to less exergonic reactions or to endergonic reactions (14, 105). Second, and more specific to muscle bioenergetics, Lohmann suggested muscle contraction will first hydrolyze ATP which is then quickly resynthesized at the expense of PCr breakdown. From Lohmann's perspective, PCr was the direct energy source for contraction and the near constant level of the ATP provided the necessary inorganic phosphate donor pool to sustain glycogenolytic/glycolytic flux resulting in lactic acid (189). He viewed ATP as only a "coenzyme" and not the central metabolite responsible for muscle contraction.

During the beginning of the 1940s Lipmann published a seminal paper in the field of cellular bioenergetics in which he suggested the central purpose of intermediary metabolism was to generate compounds of high phosphate–group transfer potential (188). In other words, the chemical potential energy of a large number of carbohydrate intermediates (lipids were acknowledged later) is harnessed via oxidation–reduction reactions and stored in a relatively small number of phosphate based molecules. The major mammalian molecules with high phosphate–group transfer potential are (in order of decreasing transfer potential): phosphoenolpyruvate (PEP) > 1,3–bisphosphoglycerate > PCr > ATP.

The simpl
acetoxyl ma
ed as glucos
ng phosphate
ecules havin
enzymatic re
s. There wer
for the phosp
ewer higher
mental groups
ATP as the s
ercles are ul
ved PCr as a
explain. This
enzymic "curre
ew of the role o
ceptually simi
ellector storing
ckeept phosph
redox reactio
ells were. Li
stream whereb
xidation and
from the lacta
ility of PCr h

These compounds would transfer their phosphate group (technically, the phosphoryl moiety, (91)) to molecules of lower phosphate group transfer potential such as glucose–6–phosphate (G6P) > glycerol–3–phosphate. In most cases the high phosphate–group transfer potential of a molecule arises from its hydrolysis products having greater resonance stabilization plus lower intramolecular electrostatic repulsions plus a greater ability to be solvated in the aqueous cytosol (14). There were two important insights Lipmann provided in this paper (188). First, the phosphate–group transfer potential of ATP was viewed as intermediate between higher transfer potential groups such as PEP and PCr and lower transfer potential groups such as G6P. This realization is tantamount to the characterization of ATP as the single universal energy "currency" of the cell whereby all metabolic networks are ultimately linked to the production and utilization of ATP. Second, he viewed PCr as a metabolic "capacitor" that could store "charge" in the form of phosphate. This phosphate charge would flow through the cell forming a metabolic "current" that is utilized to do work. It is worthwhile to note Lipmann's view of the role of PCr as metabolic capacitor storing phosphate charge was conceptually similar to the view that A.V. Hill held in 1913 of lactate as a metabolic capacitor storing redox charge (128). Lipmann also suggested the role of ATP was to accept phosphates as a mechanism that prevents phosphates from clogging up the redox reactions of the triose phase of glycolysis. As significant as the above insights were, Lipmann did not waver from the view held by Lundsgaard and Lohmann whereby PCr hydrolysis was the direct energetic determinant of muscle contraction and ATP was simply a coenzyme. But compared to nearly two decades wherein the lactate hypothesis was the solitary working theory, the unrivaled primacy of PCr hydrolysis as the direct energy supply was relatively shorted lived.

The Role P

ATP emerges

As mention
sphate d
wer, this
ughout th
med at
sphanhydr
cle contract
ein of muscl
osin was n
ase activity
ving the ques
major intrace
lyze ATP m
the mid 1940s
mentous acti
entration, a
ted for diss
ments by sh
sphate suc
lecule myosi
ers were well
imately lin
molecule tha
ost collective
ense from th

The Role Reversal (1940s–early 1970s)

ATP emerges as the primary energetic determinant of contraction

As mentioned above, the initial function assigned to ATP was a coenzyme role as a phosphate donor to the glycolytic/glycogenolytic cascade and to creatine; however, this subordinate role was slowly phased out by the early 1960s. Throughout the 1940s there was mounting, persuasive, circumstantial evidence that turned attention away from the phosphoguanidine bonds of PCr toward the phosphoanhydride bonds of ATP as *the* source of chemical potential energy for muscle contraction. Although myosin had been considered the major structural protein of muscle since the middle of the 1800s (225), the ATPase enzymatic activity of myosin was not firmly established until 1939 (87). This discovery of myosin's ATPase activity had a profound effect on the muscle bioenergetic community. Forcing the question: is the functional connection between the role of myosin as the major intracellular structural protein of muscle and myosin's ability to hydrolyze ATP more than just coincidence? To make matters even more intriguing, by the mid 1940s, Szent–Gyorgyi and his Hungarian colleagues had discovered filamentous actin, another intracellular muscle protein found in high concentration, and showed under optimal Mg^{2+} and K^{+} concentrations, ATP was required for dissociation of myosin from actin (286). Dainty et al. (64) honed these key results by showing only *adenosine* triphosphate–not simply any generic triphosphate such as various purines, pyrimidines, or inorganic triphosphates–will dissociate myosin from actin. Consequently, by the end of the 1940s two general tenets were well appreciated: **(#1)** based upon Lipmann, all metabolic networks are ultimately linked to the production and utilization of ATP; and **(#2)** ATP is the only molecule that dissociates the two structural proteins coincidentally having the highest collective concentration of any chemical species in skeletal muscle. The inference from these tenets was inescapable to the muscle physiology community–

ff's the dir

Thermate

rmet exper

ent necessar

n approache

nake contrac

ements" I

nake prepar

ppen that mo

ntilateral co

mperature to

n down the re

ineration co

nations of the

challenge W

ermated mu

rkets and

nake compare

n consistent

Neither resu

hydrolysis a

ver the nex

anged from o

the investiga

Nitrides, Cha

ions in the

Decomplation

ATP is the direct source of energy in muscle contraction.

Unfortunately, as seductive as the above hypothesis was at the time, there was no direct experimental evidence ATP actually broke down during contraction to the extent necessary to drive the contractile apparatus. Sensing a need for infusion of new approaches to directly determine if ATP was significantly hydrolyzed during muscle contraction, the esteemed Nobel laureate A.V. Hill issued a "Challenge to Biochemists" (134). He made several suggestions in his challenge: use *in vivo* muscle preparations rather than *in vitro* muscle extracts, use muscles from species that move slower (i.e. tortoise rather than a frog), use limb muscles so a contralateral control muscle can easily be obtained, and decrease the operating temperature to slow the reactions. The overall objective of this challenge was to slow down the reaction velocity such that statistically significant changes in ATP concentration could be observed during contraction within the frequency response limitations of the instrumentation available at the time. A year later in response to this challenge Weber and Weber showed the tension developed by single glycerinated muscle fibers depends on the ATP concentration (310), and Mommarets and Rupp showed ATP is broken down during contraction in frog limb muscle compared to contralateral resting controls (220). Both of these experiments were consistent with the view that ATP serves as the direct energetic determinant, but neither result could also exclude the chemical potential energy provided by PCr hydrolysis as a direct energetic determinant of muscle contraction.

Over the next ten years additional incidental evidence of the central role of ATP emerged from other domains of muscle physiology and bioenergetics. Based on earlier investigators' work with cytochromes, flavoproteins, and pyridine nucleotides, Chance and Williams elucidated the precise sequence of redox reactions in the mitochondrial respiratory chain responsible for oxidative phosphorylation (52). They also suggested mitochondrial oxygen consumption

ing switch
cipitate acc
ipated the
ements t
mplification
m the "slide
Huxley pos
amiotonin
ATP, a hydr
ments, to in
ntanization
1950s. H. E.
anism expla
raction of ra
sicles in th
ing contracti
finally, in 19
ction of the
ched the cre
ctus abdo
ferent ten-f
aining no ch
ctively ans
like contracti

during twitch contractions of frog sartorius muscle is limited by the amount of phosphate acceptor (i.e. ADP) within the matrix (53). Taken together their results supported the idea of oxidative phosphorylation as a third ATP supply system that complements the other two ATP supply systems based upon substrate level phosphorylations, i.e. the creatine kinase reaction and glycolysis. This is consistent with the "linked hydraulic reservoir model" of interdependent ATP supply systems Lundsgaard postulated in 1932 (190)–well before the tricarboxylic acid cycle and the mitochondrial respiratory chain were discovered! Chance's results also neatly tied ADP, a hydrolysis product of increased ATP demanded by the contractile apparatus, to increased ATP supply, thereby supporting Lipmann's characterization of ATP as the cell's energy currency. At the same time during the mid 1950s, H. E. Huxley and Hanson articulated the Sliding Filament Theory as a mechanism explaining the changes in the cross–striation patterns occurring during contraction of rabbit psoas myofibrils (148). Although they entertained other possibilities in their paper, they strongly felt the interdigitation of actin and myosin during contraction was driven by the enzymatic splitting of ATP.

Finally, in 1962, direct experimental evidence ATP actually broke down during activation of the cross–bridge machinery was obtained when Cain and Davies inhibited the creatine kinase reaction with fluorodinitrobenzene (FDNB) in isolated frog rectus abdominus (40). The results were unequivocal: FDNB treated muscle underwent ten–fold fewer contractions and consumed significantly more ATP while sustaining no change in PCr as compared to controls. A.V Hill's challenge had been conclusively answered–ATP was the indisputable primary energetic determinant of muscle contraction.

Myothermal techniques refine the bioenergetic role and experimental utility of PCr

With the basic bioenergetic interrelationship between ATP as the primary energy metabolite and PCr as its phosphagen capacitor now clearly delineated, several camps within the muscle energy metabolism community turned their attention toward more precise characterization of the thermochemistry and the time dependent behavior of PCr changes during and after stimulation. In general, the thermochemical lines of investigation stemmed from motivation to quantify changes in enthalpy, free energy, and work as a way to assess the thermodynamic efficiency of muscle as a chemomechanical energy transducer (219, 314, 316). Interest in the time–dependent behavior of PCr was based upon exploring the ramifications of a corollary to Cain and Davie's unequivocal answer to A.V. Hill's challenge. That is, since ATP is temporally buffered by PCr during contraction (40, 45) and PCr donates its phosphoryl group to ATP through a single, biomolecular, equilibrium, phosphoryl–transfer reaction catalyzed by creatine kinase (91, 137, 171, 230), then it is reasonable to infer measuring PCr changes during and after contraction will provide a direct measure of the energy cost of the underlying metabolic processes. As will be discussed later, tracking phosphocreatine's behavior became, and remains today, an important experimental technique to discern the fundamental bioenergetic properties of muscle efficiency, metabolic energy costs, and oxidative metabolism. What follows next is a brief survey of pragmatic reasons as well as methodological and technological advancements that facilitated understanding of the thermochemistry and kinetic behavior of PCr.

The pragmatic reason was simply experimental convenience–that is, the "when Nature hands you lemons you make lemonade" maxim. Unlike all of the other important energy metabolites (AMP, ADP, ATP, NAD, FAD) in skeletal muscle, phosphocreatine is found at much higher concentrations (53, 91, 146, 230) *and* undergoes readily detectable changes even during mild stimulations. Without

FDNB, the creatine kinase inhibitor, only the most severe stimulation protocols, which may require blocking blood flow, will significantly change the [ATP]. Consequently, PCr was a prime candidate for investigation since it was the most experimentally accessible energy metabolite and was intimately linked to buffering ATP, the primary energy molecule.

Methodological and technological advancements between the 1940–1970s also greatly facilitated the growing interest in PCr kinetics that continues to this day. Two examples relevant to myothermal techniques include: **1)** The development of more thorough rapid–freezing procedures for excised muscle tissue, which greatly reduced artifactual hydrolysis of labile phosphate groups prior to extraction and chemical assay (170), resulted in more accurate determination of [PCr] with less variability. **2)** Measurement of muscle heat production was substantially improved compared to the pre–W.W.II era due to construction of thermopiles from individual thermocouples which greatly improved temperature sensor gain (135). Moreover, the temperature sensor's response time was significantly reduced to ≈ 10msec by the newly available commercialized engineered plastics (e.g. Teflon) and epoxy resins which abated nuisance heat capacity (101, 321).

Given PCr's experimental accessibility, its role as ATP's phosphagen capacitor, and the improvements in temperature measurements previously noted, bioenergeticists in the 1960s exploited the behavior of PCr during and after stimulation as a way to understand the efficiency and energy costs involved with muscle contraction and relaxation. Selected highlights are discussed below, for comprehensive reviews see (63, 219, 320). In an effort to simplify the metabolic systems under study, all of the myothermic experiments mentioned below used isolated frog muscle at 0°C with glycolysis blocked by iodoacetate and oxidative phosphorylation inhibited by a 100% nitrogen atmosphere.

Carlson showed there was a linear relationship between the extent of PCr

ction and

smic switch-

emical pe

ress of the

mented buff

ew that mu

n in the en

mible by

phosphor

ing reactio

metric

was based

ction in is

ply produc

A few years la

nergeticist

hydrolysis.

ion during i

mption ha

netic tensio

mum aroun

ed at $L_o \approx 2$

o. When t

o-minimi

ssible they

ical ATP co

on. Sandbe

utilization and the number of isometric twitches (45) or external work done during isotonic twitches (44). Coincidentally, he also confirmed the Fenn Effect (93) from a biochemical perspective by showing the extra energy liberated during shortening in excess of the isometric condition can be accounted for by PCr hydrolysis and associated buffer reactions. In Fenn's particular frog muscle preparation it was shown that muscles undergoing isotonic contractions, thereby performing external work on the environment, liberate an extra amount of heat beyond that accountable by the work performed. Carlson also argued in his two papers that PCr dephosphorylation and its associated buffer reactions are the major net energy yielding reactions taking place during a complete contraction and recovery cycle in either isometric, lightly–loaded isotonic, or heavily–loaded isotonic contractions. This was based upon the observation that thermopile–measured global enthalpy production in isolated frog muscle was not significantly different than the predicted enthalpy production of PCr hydrolysis from thermochemical tables.

A few years later in 1966, Sandberg analyzed the Sliding Filament Theory from a bioenergeticist's perspective (264). He found ATP consumption, as estimated by PCr hydrolysis, had both a length–dependent fraction and a length–independent fraction during isometric contractions. The length–dependent fraction of ATP consumption had the same qualitative dependence upon sarcomere length as isometric tension. That is, both ATP consumption and isometric tension reached a maximum around the optimal length, L_o, (0.26μmole ATP per gram muscle per second at $L_o \approx 2.25\mu m$) and both dropped off precipitously below 70%L_o or above 140%L_o. When they stretched the sarcomeres to various fixed lengths greater than 140%L_o–minimizing myosin's ability to form crossbridges with actin–and stimulated the muscle they found ATP consumption was approximately 25–50% of the maximal ATP consumption at L_o. They termed this the length–independent fraction. Sandberg astutely suggested this length–independent ATP consumption

probably
ATP use
ked with
ysis and
ming proc
ming cal
m handl
decade ear
ction bas
his Ca
nnected
sed in resp
r system.
plasmic ret
sed the C
brane netw
ew muscle t
ultramicro
sses in the
scopy to un
ences other
Calcium
scle micros
phragm musc
s of radiola
ergeticists
total ATP c

was probably due to calcium pumping and represented a significant fraction of the total ATP use during a complete stimulation and recovery cycle. This result conflicted with Carlson's two papers a few year's earlier which suggested net PCr hydrolysis and its associated buffer reactions are the only significant ATP consuming process. Furthermore, this indirect energetic evidence of an ATP consuming calcium pump nicely complemented the 1960s surge of interest in calcium handling by muscle cells as summarized in the next paragraph.

A decade earlier Sandow (265) formulated the "Calcium Theory" of muscle contraction based upon electrophysiological measurements and light microscopy studies. His Calcium Theory proposed that calcium is stored in an intricate interconnected network of internal membranes (the sarcoplasmic reticulum), is released in response to sarcolemmal depolarization that requires a transverse–tubular system, binds to the contractile apparatus and is taken back up into the sarcoplasmic reticulum. Unfortunately, most muscle physiologists in the 1950s dismissed the Calcium Theory largely on the grounds that they saw the internal membrane network as simply an optical artifact from the fixation process required to view muscle tissue slices under a light microscope. It required the development of the ultramicrotome, freeze–fracture techniques, and heavy–metal shadowing processes in the 1950s (275) that allowed thin–slice transmission electron microscopy to unveil the structural detail required to pique the curiosity of audiences other than histologists and cell biologists. Persuasive functional evidence for the Calcium Theory came after Ebashi discovered calcium uptake required ATP in muscle microsomes (79), Padykula localized an ATPase in the SR of rat diaphragm muscle (233), and Winegrad (317) elucidated transient intracellular fluxes of radiolabeled calcium during and after tetanic contractions. To bioenergeticists these studies suggested muscle cells must budget at least some of their total ATP currency toward handling calcium during and after contractions. As

ained ab

muscle es

ming at L

the latter

ermal e

ed a vital

ments re

ermodynam

metric, c

ndings. T

hemically e

lysis, lacta

metric o

py ΔH p

ets of reacti

ed muscle

erations i

limb mu

ction is m

ctions onl

suring force

ermal ene

account fo

ured exter

hermoche

ect the ob

py prod

mentioned above, Sanberg's discovery of length–independent ATP consumption in frog muscle estimated this allocation at 25–50% of the maximal ATP consumption occurring at L_o.

In the latter half of the 1960s a fresh experimental paradigm, called the "myothermal energy balance method", emerged in which measuring PCr changes played a vital role. The basic premise behind all myothermal energy balance experiments rested upon a conspicuous application of the First Law of Thermodynamics and assumed isolated skeletal muscle behaves as an isothermal, isovolumetric, closed system–able to exchange heat but not matter with its surroundings. The principle is that one should be able to correlate all of the "biochemically explained" enthalpy production of known reactions (e.g. PCr hydrolysis, lactate production) to the observed enthalpy production during, and after isometric or isotonic contractions (63, 141, 219). The biochemically explained enthalpy (ΔH) production requires knowing *in vitro* ΔH values plus measuring the extents of reactions via direct chemical assay of metabolites extracted from freeze–clamped muscles. The extent of reaction is evaluated by comparing metabolite concentrations in the stimulated limb muscle versus its unstimulated contralateral control limb muscle. The contribution of heat to the total observed enthalpy production is measured by thermopiles; the contribution of external work (isotonic contractions only) to the total observed enthalpy production is determined by measuring force acting through a distance. So, within experimental error, the myothermal energy balance method dictates it should be possible to quantitatively fully account for the observed enthalpy production by comparing it to the measured extent of the biochemical reactions multiplied by *in vitro* ΔH values from thermochemical tables. If there was a statistically significant difference between the observed enthalpy production and the biochemically explained enthalpy production then it would be concluded some unknown reaction(s) was or

were taking place. The enthalpy of the unknown reaction(s) would comprise the total "unexplained enthalpy".

Applying the myothermal energy balance principle, Woledge (320) using frog sartorius and Gower using rat soleus (111) found the enthalpy (heat + work) produced during contraction and relaxation is *greater* than can be accounted for by the biochemically explained enthalpy of PCr hydrolysis and lactic acid formation as measured calorimetrically. But over an entire contraction–relaxation–oxidative recovery cycle the total energy measured as heat plus work was not significantly different than the enthalpy produced by the known metabolic reactions occurring. After numerous investigations (cf. (63, 141, 321)) the major observations were that the unexplained enthalpy is dependent upon the stimulus duration, exhibits a Q_{10} effect, is greater if a muscle rapidly shortens than if it isometrically contracts, and is quantitatively and qualitatively different than the isometric maintenance heat. (The Q_{10} effect is a generic term describing the increase in reaction rate seen when temperature increases by 10°C.) It is believed the unexplained enthalpy is primarily due to the heats of binding, ionization, and solvation associated with calcium movements during contraction and relaxation. This includes release from the terminal cisternae of the sarcoplasmic reticulum (SR), binding to troponin, binding to parvalbumin (in fast twitch fibers only) binding to the longitudinal segments of the SR and binding to calsequestrin within the SR.

PCr hydrolysis helps estimate muscle efficiency

In addition to quantifying the energetic costs of contraction and calcium movements, the simultaneous measurement of enthalpy production and PCr breakdown provided necessary data to attempt to estimate skeletal muscle efficiency during shortening. Without requiring a derivation from first principles, an intuitive notion of machine efficiency became obvious when the first steam engine, a heat engine, was developed by James Watt in 1769 (196). Simply put, a

heat engine's efficiency is the ratio of its work output to heat input. Unfortunately for bioenergeticists, this straightforward interpretation of efficiency is not applicable since muscles are isothermal energy converters. Up until the 1960s, the efficiency definition most widely used by muscle physiologists was the one suggested by A.V. Hill. He defined the mechanical efficiency (e_{mech}) of a muscle as the ratio of total work done to enthalpy produced (129, 133), $e_{mech} = W/(W+\Delta H)$. Total work done includes both external work of the muscle exerting a force acting through a distance plus internal work against an ill–defined elastic component in series with the contractile component of muscle. Enthalpy is the sum of heat produced plus total work. Using this definition, Hill found mechanical efficiency during an isotonic contraction was dependent upon shortening velocity and had a maximum of almost 40% at 88% of the maximal velocity of shortening (132). In his 1960 paper (314), Wilkie suggested Hill's mechanical efficiency concept is imprecise because the thermopile–measured ΔH term is actually the sum of the free energy available to do work, ΔG, plus an entropy creation term, $T\Delta S$ (i.e. $\Delta H=\Delta G+T\Delta S$). He argued it is only the free energy term, exclusive of entropy creation, driving the cyclic changes in the myosin kinetic states during contraction. Wilkie suggested a thermodynamic efficiency, e_{therm}, be used in place of e_{mech}, where $e_{therm} = \Delta H_{ATP}/\Delta G_{ATP}(e_{mech})$. ΔH_{ATP} and ΔG_{ATP} were to be obtained from *in vivo* measurements of ATP hydrolysis. Toward this goal, Wilkie's laboratory measured phosphocreatine hydrolysis as a way to estimate the *in vivo* value of ΔH_{ATP} during isometric and isotonic contractions (43, 315). Using frog muscle at 0°C with glycolysis and oxidative phosphorylation inhibited they found that for either isometric twitch or tetanic contractions the *in vivo* ΔH_{PCr} was ≈10.6kcal/mol. By taking the ratio of heat produced before inhibiting creatine kinase to heat produced after inhibiting creatine kinase they estimated the *in vivo* ΔH_{ATP} value to be 11.0kcal/mole based on knowing ΔH_{PCr} (315) . ΔG_{ATP} was not directly measured in

paper and

$\Delta G^{\circ}_{\text{interm}}$

CNB poiso

and was a

$\Delta G^{\circ}_{\text{ATP}}$ =

Asmewhat

mpled the

ical model V

rmodynamic

mation is t

Energy defi

Park's strai

ass of work

Ebert const

estimated

n strength

n species of

ntrations

ability erg

asures the

Systems. In

Vol. 174,

Na+ ATPas

he experime

N-order pol

to the exter

proximately

their paper and so they did not calculate e_{therm}. Instead, they inferred the upper limit of e_{therm} would be approximately 80%. This was based upon previous studies in FDNB poisoned frog muscle that showed $\Delta G_{ATP} \approx$ mechanical work/mole of ATP split and was at least 5.5 kcal/mole (numerically: $e_{therm} = \Delta H_{ATP}/\Delta G_{ATP}(e_{mech}) = 11.0/5.5(40\%) = 80\%$).

A somewhat more direct approach toward estimating muscle efficiency was attempted the following year by Kushmerick and Davies (173) with the same animal model Wilkie's group used. Kushmerick and Davies suggested the thermodynamic efficiency of chemo–mechanical energy conversion during contraction is the ratio between work done and *in vivo* ΔG_{ATP}. (Note: their efficiency definition, $e_{therm} = W/\Delta G_{ATP}$, is intuitively appealing since it is analogous to Watt's straightforward definition of heat engine efficiency, $e = W/\Delta Q$.). Different values of work done were obtained by integrating the force versus time record for different constant distances shortened. *In vivo* ΔG_{ATP} at different values of work was estimated by a formula requiring educated assumptions about intracellular ionic strength based on Debye–Hückel theory and activities of all of the various ionic species of the adenine nucleotides based on chemically assayed concentrations. A unique aspect of their experimental design was the use of an isovelocity ergometer which, in contrast to an isotonic work measurement, measures the work done by the muscle exclusive of the passive series elastic components. In conjunction with results from their companion paper in the same journal (174), this permitted them to directly measure the work done by the myosin ATPase or the SR Ca^{2+} ATPase or both during shortening. The key result of their experiment was they found e_{therm} is not constant, but exhibited a complex high–order polynomial dependence on shortening velocity. More specifically, they found the e_{therm} of the myosin ATPase, per se, reached a maximum of 97% at approximately 30% of the maximum shortening velocity. The e_{therm} of the myosin

ATPase plus the SR Ca^{2+} ATPase reached a maximum of 66% at the same $\%V_{max}$. For comparison, the thermal efficiency of a typical four–stroke gasoline engine reaches a maximum of about 28% at approximately 50% of its maximum revolutions per minute (227) and the photosynthetic efficiency of C_3 plants in strong sunlight is around 30% (249). (C_3 plants are so-named since they initially fix CO_2 in the form of three–carbon acids.)

In summary, simultaneous measurement of the enthalpy and chemical extent of PCr hydrolysis before and after contraction provided bioenergeticists of the 1960s a "measuring stick" to routinely estimate energetic costs of isometric or isotonic contractions, estimate the energetic costs of the newly discovered calcium–ATPase required for muscle fiber relaxation, and quantify the thermodynamic efficiency of contraction.

Contemporary Views (early1970s–present)

The connection between PCr kinetics and oxidative capacity and its implications

By the mid to late 1970s most of interesting experimental permutations using the myothermal energy balance method had been done: "unexplained" enthalpy was explained, global thermodynamic efficiency of contraction was estimated, and more accurate assessments of the value and temporal distribution of activation heat, shortening heat, and maintenance heat evolved during contraction were obtained (172, 321). During this same time period, attention in the bioenergetic community began to be directed toward assessing the interrelationship between PCr kinetics and oxidative metabolism. The purpose was to gather a functional assessment of the extent and rate of ATP demand during a contraction–relaxation–recovery cycle and the capacity of the ATP supply systems to meet these demands. This rebirth of interest in this interrelationship was based upon three historical lines of inquiry that converged in the early 1970s.

One of these lines was the discovery of the temporal association between oxidative recovery and PCr resynthesis. Almost fifty years earlier, A.V. Hill documented that recovery heat is only produced in an oxygen, not pure nitrogen, atmosphere (130). This showed recovery processes, of unspecified mechanisms at the time, must consume oxygen. Building upon this, Margaria showed recovery oxygen consumption after an intense workload was composed of three exponential components (193): a fast component ($t_{1/2} \approx 30$ seconds) necessary for regenerating the ATP and PCr used during contraction which he coined the "alactacid oxygen debt", a slow component ($t_{1/2} \approx 15$ minutes) necessary for regenerating intramuscular glycogen from lactic acid–the "lactacid oxygen debt", and a very slow component ($t_{1/2} > 60$ minutes) due to a thermogenic effect raising the basal metabolic rate. In 1940, A.V. Hill's son, D.K. Hill, showed recovery oxygen consumption and recovery heat production followed qualitatively similar monoexponential time courses over a thirty minute period (136). He also showed it was possible to titrate the recovery rate of oxygen consumption with the degree of inhibition of cytochrome oxidase by sodium azide. This latter observation was the first study using whole skeletal muscle to show the rate of oxidative recovery is strongly dependent on the oxidative enzyme content. By 1970, Hultman and then Piiper showed the above correlations between PCr kinetics and oxidative metabolism were not limited to isolated *in vitro* amphibian muscles at low temperatures. Hultman was the first to illustrate using human subjects that PCr declines rapidly and reaches a steady–state that is a function of workload intensity (146). The higher the workload, the lower the steady–state value of [PCr] during exercise. Upon cessation of exercise, PCr immediately begins to exponentially return to resting levels. Using an *in situ* dog preparation, Piiper showed the exponential time course of recovery oxygen consumption after moderate workloads had two components mechanistically corresponding to the fast and very

slow components that Margaria elucidated (244, 245). Because of the moderate workload Piiper used, he was able to unambiguously correlate the fast component of oxygen recovery with the regeneration of PCr and ATP. Lastly, Sahlin and Harris showed neither PCr nor lactate returned to their resting levels after intense exercise in humans as long as blood flow was restricted with a pressure cuff during recovery (120, 258). Taken together these studies empirically linked ATP production by oxidative recovery processes to PCr resynthesis via the creatine kinase reaction and established the rate of oxidative recovery is dependent on mitochondrial content.

A second line of investigation coming to fruition by the early 1970s involved understanding the mechanistic link between oxygen consumption and the adenine nucleotides. In a brilliant piece of deductive reasoning based on mitochondrial inhibitors and uncouplers, Peter Mitchell concluded that the reduction of oxygen to water was directly coupled to the phosphorylation of ADP to ATP by a proton electrochemical potential difference across the inner mitochondrial membrane–the chemiosmotic hypothesis (216). Furthermore, it was recognized and verified that all adenine nucleotides (ATP, ADP, AMP), both pyridine nucleotides (NAD, NADP), PCr and Pi were interlinked by a network of near–equilibrium reactions even though oxidative metabolism is a non–equilibrium process *in toto* (42, 157, 158, 169, 306). The profound significance of these insights is that tracking the steady–state and transient behavior of oxygen consumption kinetics not only provides information about PCr kinetics (and vice versa), but it also indirectly allows one to monitor the kinetics of the major metabolic networks responsible for providing phosphorylation chemical potential and redox chemical potential in the muscle fiber. The phosphorylation chemical potential provides free energy to drive the myosin kinetic state changes during contraction, the SR calcium pump during contraction and relaxation, and the sarcolemmal Na^+/K^+ pump at all times. The

redox chemical potential provides free energy to drive the first reaction of the triose phase of glycolysis in the cytosol and several reactions of Krebs cycle and fatty acid β–oxidation in the mitochondrial matrix.

The third and final line of inquiry arose from recognition that muscle tissue was a heterogeneous population of cells with respect to the rate of ATP demand and the capacity of its ATP supply systems. As summarized in Table 1 below, it was first documented in the late 19th century that the commonly observed color differences of poultry, fish, and rabbit meat had physiological manifestations. Visibly red rabbit skeletal muscle tissue ("dark meat") generally developed tension more slowly–i.e. took longer to reach peak tension–than white muscle (251). Due to the time required for the discovery and cataloging of most of the key enzymes and intermediates found in skeletal muscle, a period of almost 90 years elapsed before muscle fiber classification was systematically revisited in the 1960s. Dubowitz extended Ranvier's basic result by correlating an ATP demand parameter with an ATP supply parameter. He suggested there were two fiber type populations arbitrarily designated as Type I, that had low ATPase activity and high oxidative enzyme content, and Type II fibers, which had the opposite profile (76). This classification was expanded by Brooke who exploited the differential pH sensitivity of the myosin ATPase staining process and suggested a total of four fiber type populations could be discerned: Type I plus three subtypes of Type II–IIA, IIB, IIC (32). Focusing on the ATP supply capacity, Stein characterized three fiber type populations as White–A, Red–B, or Red–C based upon the relative intensity of staining of succinate dehydrogenase (SDH) (280). Burke showed the muscle fibers making up a single motor unit are functionally identical with respect to rate of force development and fatigue characteristics (36, 38). He classified three motor unit populations as Fast Fatigable, Fast Fatigue Resistant, or Slow Fatigue Resistant. More comprehensive attempts relating several mechanical

characteristics to numerous metabolic capacity measurements were performed by Barnard (15) and then Peter (239), with the general consensus that three fiber type populations could be identified: Fast–Oxidative–Glycolytic, Fast–Glycolytic, or Slow–Oxidative. It is important to emphasize that the tripartite scheme discussed above is simply a less verbally cumbersome approximation of the *in vivo* reality. In his 1968 Ph.D. thesis at Michigan State University, V.R. Edgerton, who later worked with Barnard, Burke, and Peter, astutely pointed out that an individual muscle fiber's metabolic characteristics are more appropriately considered as part of a continuum (80). The point along the continuum an individual fiber occupies is a function of its developmental stage (81, 253), motorneuron innervation (35), the intensity and duration of chronic training (10, 11, 16, 17, 55, 77, 82) or chronic electrical stimulation (242), volumetric location within the muscle tissue (47, 70, 90) and thyroid hormone level (150, 181, 197). Furthermore, the metabolic capacity of a muscle's fiber population resembles a slightly skewed quasi–Gaussian distribution (242). The degree of skew and standard deviation depends upon the specific enzyme used to classify the fiber type (e.g. succinate dehydrogenase, phosphofructokinase, malate dehydrogenase, hexokinase) and species. In most cases the quasi–Gaussian distribution nature arises from fiber–specific genetic expression of varying amounts of enzyme content rather than expression of different isoforms with different kinetic properties (240). This is based upon a literature search turning up tissue specific differences but not skeletal muscle fiber specific differences in most key flux regulating enzymes. (The major exception was lactate dehydrogenase which showed isoform switching that promoted the conversion of lactate to pyruvate after aerobic training (156, 163)).

Table 1: E

Classifi Sche
Slow-Red
Fast-Wh
Type I-v
Type II-Fa
Fiber-A v
- Red-C
Fast Fati
Fast Fati
Resistant
Slow Fati
Resistant
Fast-Twi
Fast-Twi
- Slow-T
Intermedi
Type I v
- Type II
Type IIC
Fast-Oxi
Fast-Gly
Slow-Oxi

Table 1: ***Evolution of fiber type classification schemes***

Classification Scheme	Basis of Classification	Year, Author (Reference)
Slow–Red v. Fast–White	macroscopic inspection of muscle color and measurement of time to peak tension	**1873**–Ranvier (225)
Type I–v Type II–fast	enzymatic assay of ATPase activity correlated with NADHase activity	**1960**–Dubowitz (76)
White–A v. Red–B v. Red–C	histochemical metabolic profiling based upon differential SDH staining density	**1962**–Stein (280)
Fast Fatigable v. Fast Fatigue Resistant v. Slow Fatigue Resistant	time to fatigue of different motor units (that contain homogenous fiber types) under continuous electrical stimulation	**1967, 1971**–Burke, (36, 38)
Fast–Twitch–Red v. Fast–Twitch–White v. Slow–Twitch–Intermediate	histochemical metabolic profiling based upon differential NADHase staining density and enzymatic assay of myosin ATPase activities correlated with time to peak tension and half–relaxation time	**1971**–Barnard (15)
Type I v. Type IIA v. Type IIB v. Type IIC	improved on Dubowitz, '60, differential myosin ATPase stains with preincubation in additional pH mediums	**1970**–Brooke (32)
Fast–Oxidative–Glycolytic v. Fast Glycolytic v. Slow–Oxidative	extends Barnard, '71, adds assay for glycogen, myoglobin, and cytochrome contents and assaying for enzyme activities of LDH, GPDH, HK, SDH	**1972**–Peter (239)

The mecha

examine tis

for think a

army. The

army. To c

amphibres

mas heavy

spleen 1

mass 12

Toxicity, de

mechanism

structure o

mild rash.

Trauma

presented

fluoride po

burning s

Other mon

Are metab

Apple in A

Walking fib

Mild rate

Mild adec

Sleep fibe

Hand the

Splinting

Normally

The mechanical performance characteristics (e.g. time to peak tension, relaxation time) of a muscle's fiber population are functions of the binding kinetics of the thick and thin microfilaments as well as the SR's calcium release and uptake capacity. These characteristics have a slightly different distribution than metabolic capacity. To date, in adult mammalian skeletal muscle, various regimens of gel electrophoresis and immunocytochemistry have uncovered four isoenzymes of myosin heavy chain (268), three isoenzymes with fast and slow subtypes of myosin light chain (13, 285), fast and slow isoenzymes of each of the three troponin subunits (121) and fast and slow isoenzymes of the SR calcium ATPase (186, 322). Curiously, despite the theoretically large number of combinations of the above protein isoforms that could be assembled in a sarcomere, it appears the frequency distribution of a muscle's fibers' mechanical characteristics, per se, resembles a bimodal rather than Gaussian lineshape (81, 98, 110, 256).

To summarize, the three lines of investigation converging in the early 1970s documented that PCr kinetics, oxygen consumption kinetics, and the adenine nucleotide pool are interdependent. This interdependency suggested that monitoring the temporal changes in one of the three parameters may allow indirect monitoring of temporal changes in one or both of the others as the muscle fibers' metabolic networks relax to a new steady–state after perturbation by changes in ATP demand. Moreover, there was accumulating documentation regarding fiber type heterogeneity with respect to oxidative capacity and ATP demand rate. This suggested the transient and steady–state responses of PCr, O_2, and the adenine nucleotides to changes in ATP demand may be different for different fiber types.

PCr and the chemical energy balance method

Exploiting this convergence of ideas, Kushmerick's lab in the mid–1970s sought to functionally assess the extent and rate of ATP demand during a contraction–

relaxation–recovery cycle and relate this to the extent of recovery metabolism required to meet these demands (69, 177, 178). Previously, Carlson had shown a positive linear relationship between the extent of PCr hydrolysis and the isometric tension–time–integral, TTI (43). (TTI, when normalized on a per muscle mass basis and assuming a constant tissue density, is the time integral of the isometric force per unit cross–sectional area. Since the development and maintenance of force requires ATP, TTI is an indirect measure of energy cost of contraction that does not require a chemical assay as well as a direct measure of force per unit fiber area (159).) As mentioned above, D.K. Hill, Hultman, Margaria, and Piiper had independently shown a temporal correlation between PCr resynthesis and oxygen consumption in a variety of species. Completing the triad of interconnecting PCr kinetics, O_2 consumption, and force development, Stainsby showed oxygen consumption scales with isometric tension in the *in situ* dog gastrocnemius (278, 279). There were, however, no studies simultaneously measuring all three.

Addressing this need, Kushmerick and Paul (177, 178) used the experimental framework called the "chemical energy balance method" which seeks to equate the extent of high–energy phospate utilization during contraction to the extent of recovery oxygen consumption above basal levels (ΔQO_2) during recovery. Phosphate utilization is quantified by the extent of PCr breakdown, and recovery oxygen consumption is measured with an oxygen electrode. Their major findings using frog muscle include: **1)** both PCr breakdown and ΔQO_2 have independent positive linear regressions with TTI that coincidentally have essentially the same slope and y–intercept, i.e. ΔPCr/gram versus TTI and ΔQO_2/gram versus TTI are superimposable plots. **2)** both PCr breakdown and ΔQO_2 follow a time course best described by a monoexponential function **3)** ΔQO2 is proportional to the initial extent of PCr hydrolysis for tetanic durations between 5–20 seconds. In a later paper, Crow and Kushmerick (61) applied these results to mouse muscle and

found fast twitch muscle had a threefold greater cost of briefly maintaining the same isometric tension than slow twitch muscle (i.e. the fast muscle was less economical). Interestingly, during longer duration tetani. the fast twitch muscle reduced its energy usage (i.e. became more economical) to a level only 50% greater than the slow twitch muscle, which did not change its energy cost. This reduction in energy cost was explained by a reduction in the myosin ATPase rate.

Oxidative capacity exhibits plasticity in skeletal muscle fibers

During this same time frame of the 1970s there were numerous studies, largely extending the work of John Holloszy, showing increased oxidative enzyme activities in response to chronic endurance training. In retrospect, it could be argued Holloszy ascended to the patriarch of modern exercise biochemistry when he published his seminal findings that treadmill exercise will increase the concentration of flux–regulating enzymes in Krebs cycle and electron transport chain constituents (138). Prior to this paper it was widely believed the cardiovascular system was the exclusive limiting factor of endurance capacity (292). Holloszy's results revealed peripheral muscle adaptations must also be considered. He also showed both prolonged (120 minutes/day, 5 days/week for 12 weeks) *and* vigorous (>80% VO_{2max}–based upon treadmill speed of 31m/min for rats from Ref. (270)) exercise is required to garner impressive increases in oxidative capacity. This strenuous experimental protocol was used repeatedly in the 1970s to confirm the intuitive notions that chronic endurance training has the following consequences: increased pyruvate oxidation and alanine export for use in the alanine–glucose cycle (218), increased citrate synthase activity (97) and NADH–linked dehydrogenases' activity in the mitochondrial matrix (140), minimal effect on most glycolytic enzymes' activity (12), increased surface area and cytochrome C content of the inner mitochondrial membrane (97, 139), and prolonged time to exhaustion as well as sparing liver and muscle glycogen (97). Furthermore, it was shown,

although all fiber types can increase oxidative capacity in response to endurance training (10), the extent of the increase is fiber type specific, and for oxidative fibers improvement is generally proportional to the extent of chronic motor unit recruitment required during the training period (294). Terjung showed in rats who underwent only the most intense aerobic training did the Fast–Glycolytic (FG) fibers significantly increase (+60%) their oxidative capacity. On the other hand the Fast–Oxidative–Glycolytic (FOG) and Slow–Oxidative (SO) fibers increased oxidative capacity in all training regimens, indicating these fibers were called upon to contract on a routine basis. These results are a nice corroboration from a metabolic perspective of Henneman's Size Principle of motor unit recruitment (125).

Phosphorus NMR spectroscopy becomes an important tool in bioenergetics

A majority of the enlightening experiments mentioned in the previous subsection all had a major drawback. In most cases these experiments were conducted under *in vitro* conditions in which the muscle was excised and then placed in a bathing medium (ΔQO_2 and force measurements) or frozen and fixated for serial sectioning (quantitative histochemistry) or ground into a cellular slurry with a homogenizer (enzymatic assays). It would be preferable if bioenergeticists had an experimental technique which allowed *in vivo* or *in situ* measurements, to complement *in vitro* findings.

Fortunately, steady technological improvements since the 1940s allowed the development and application of biological phosphorous nuclear magnetic resonance spectroscopy (NMRS) to fill this role by the late 1970s. The intricate details of the quantum physics, electronic instrumentation, and digital signal processing principles required to execute an NMR experiment are more competently reviewed by others (2, 5, 31, 107, 212, 299, 300). The following

paragraphs serve as a historical summary and will survey the basic phenomena for readers who desire to understand NMRS from an end–user's perspective.

Although the quantum theory of NMRS had been documented by the mid–1940s (27, 247), until the 1970s, its application remained largely confined, to physicists and chemists measuring magnetic moments of nuclei found in crystalline salt structures and aqueous media. There were a few biological applications in the 1950s in which NMRS was used to assess plant water content (269), mouse blood flow (273) and the proton resonance amplitude in human red blood cells (231), but widespread use among biologists was retarded. This was primarily due to low field strengths of the electromagnets (≈ 0.1 Tesla) and cumbersome signal acquisition and processing methods, which conspired to give unacceptably low signal resolution and low signal–to–noise ratios. Improvements in signal resolution were aided by material science research in the early 1960s, which led to the development of niobium–titanium wire that superconducts at liquid helium temperatures (179, 271). New generation, higher field strength (>1.0–10 Tesla) superconducting magnets were constructed using the niobium–titanium wire embedded in concentric lamellae of copper. Stronger magnets allowed experimenters to more clearly discern among individual resonances.

Improvements in the signal–to–noise ratio were substantially aided by computer numerical methods research during the golden era of mainframe computing in mid–1960s. Cooley and Tukey (59, 224) left an indelible mark in the field of signal processing by resurrecting the algorithm for calculating a complex Fourier transform, the so–called Fast Fourier Transform (FFT). Although they were not to the first to derive the FFT (Carl Friedrich Gauss derived it around 100 years earlier (224)) their unique approach increased the computational efficiency by reducing the number of operations on an N–term complex Fourier series from N^2 to Nlog(N). For example, if N = 100, the number of operations is reduced from 100^2

= 10,000 to 100log100 = 200 –a 50–fold decrease. Application of the FFT to biological NMRS allowed experimenters to add time–dependent signals in computer memory and then simultaneously determine all of the frequency resonances in the spectrum using the FFT algorithm. As an approximation, if the number of signals added in memory doubles, the signal–to–noise improves about 41%. Prior to this time, a single frequency spectrum was obtained by continuously varying the magnet's field and noting where individual resonances occurred on an analog oscilloscope (92, 107). This approach did not allow for the signals to be digitally accumulated in memory and takes to acquire a single spectrum than using the FFT approach. These technological improvements allowed biological NMRS to flourish starting in the mid 1970s.

The fundamental piece of information any NMRS experiment provides is a continuous frequency distribution of quasi–Lorentzian shaped "peaks" of the specific nuclei under investigation (e.g. ^{31}P, ^{1}H, ^{13}C, ^{15}N, or ^{19}F). Each peak in a spectrum can be characterized by its area, linewidth, and resonant frequency. All of these characteristics can change as function of time during a biological experiment by perturbing the metabolic networks through step changes in energy demand, substrate supply, or hormonal activation. The numerically integrated area under any single peak is directly proportional to the total number of freely tumbling nuclei found in similar local electronic environments. Consequently, peak area measures the relative concentration of a species containing the nuclei of interest. The observed resonance linewidth of the nuclei within a given molecule decreases with increasing molecular mobility, increases with increasing magnetic field inhomogeneities, and can be influenced by the rate of chemical exchange with other molecules. The specific frequency at which nuclei resonate depends upon the interaction between the nuclei nucleons and their local electronic environment. The local electronic environment depends upon the presence of electron donating

ups e.g. ur

m amino

n carbonyl

ifferent mole

ample in a

up of creat

ysiurus n

ll reso

n electroni

ne molecul

example .

frequency

ent in a st

dissertati

earth's ma

ntum mec

ents the

clear spins

ses which

ntribution a

ked in the

ns will pre

agnetizatio

agnitude of

Next, a wi

illiseconc

roughly an

groups (e.g. unshared electron pairs of the oxygen atom in water or the nitrogen atom in amino groups) and electron withdrawing groups (e.g. free protons, metal ions, carbonyl carbon atoms). The small differences in resonant frequencies allow different molecules containing these nuclei to be resolved in a spectrum. For example, in a ^{31}P–NMR spectrum the phosphorus nucleus bonded to the amino group of creatine in PCr will resonate at a different frequency than the phosphorus nucleus of a free phosphate molecule. The three phosphorus nuclei in ATP will resonate at different frequencies because each is in a slightly different local electronic environment due to different bonding configurations within the same molecule. (See Figure 22: Sample high signal–to–noise $^{31P–NMR}$ spectra for an example).

Frequency resonance is achieved in the following manner. When nuclei are placed in a strong external magnetic field (e.g. the superconducting magnet used in this dissertation has a field strength (Bo) approximately 100,000–fold greater than the earth's magnetic field), they behave like tiny bar magnets designated by the quantum mechanical property called "spin". Furthermore, quantum mechanics restricts the nuclear spin states to only two levels: a low energy state in which the nuclear spins are aligned parallel to the external magnetic field and a high energy state in which they are aligned antiparallel (180). Based upon the Boltzmann distribution at physiological temperatures, there are only about 0.01% more nuclei found in the low energy state than the high energy state. Nuclei in either energy state will precess around the longitudinal axis of Bo, and, in aggregate, form a net magnetization vector ($\boldsymbol{M}$) that is parallel to the external magnetic field. The magnitude of $\boldsymbol{M}$ is proportional to the number of ^{31}P nuclei in the sample.

Next, a wire coil transmits a very short–duration, broadband pulse (on the order of microseconds) of magnetic energy to the biological sample (2, 143). This process is roughly analogous to striking a polytonal tuning fork with a sharp blow. With

the appropriate selection of pulse duration and power, this causes ***M*** to rotate 90° into a plane perpendicular to the longitudinal axis of the magnet. As ***M*** spins around in the plane it induces a time–varying voltage in the wire coil resembling an exponentially damped sinusoid decaying to zero as time increases. This analog voltage waveform is called the Free Induction Decay (FID). The FID is then digitally sampled into discrete time points and stored in computer memory. After a predetermined number of signals have been accumulated (16 or 32 in this dissertation) to improve the signal–to–noise ratio, the time domain data is converted into frequency domain data by the FFT algorithm. A continuous frequency distribution of peaks is the end result.

The major advantage of ^{31}P–NMRS is it can *non–invasively* and simultaneously monitor relative changes in concentrations of the key bioenergetic metabolites (PCr, ATP, Pi, ICF pH– (144, 222)) over extended periods of time in the same animal. In *vitro* based chemical assays require homogenizing one muscle per time point or per workload intensity level or both. This necessarily increases the variability and cost of the measurement since significantly more animals must be used.

Compared to *in vitro* methods, the major disadvantage of ^{31}P–NMRS is its relative insensitivity since an exceedingly small fraction (≈ 0.01%) of the population of available nuclei undergo transitions between energy levels. This necessitates using large tissue sample sizes and signal averaging techniques to increase the signal–to–noise ratio. Consequently, ^{31}P–NMRS is unable to reliably measure concentrations below the 100μM level (72, 107, 208, 212). As currently practiced, however, this is not a serious limitation since most of the energetically important, freely–tumbling metabolites (e.g. ATP, Pi, PCr) have intracellular concentrations greater than 1mM.

In 1973, the first published account of a biological application of phosphorous

NMRS illustrated that intracellular pH can be non–invasively monitored in red blood cells by tracking the resonance frequency separation (i.e. chemical shift) between the two phosphoryl moieties of 2,3–bisphosphoglycerate (222). Building on this observation a few years later, it was shown over a physiological pH range in frog muscle, that the chemical shift of Pi, but not ATP or PCr, is a sigmoidal function of pH (39). Therefore, muscle intracellular pH can easily be determined by measuring the chemical shift of Pi with respect to PCr and then converting it to a pH value using a titration curve.

Several of the papers published in the formative years (1973–1982) of biological ^{31}P–NMRS might be characterized as prosperous "fishing expeditions" evidenced by the relatively generic article titles, copious amounts of data, and nonspecific hypotheses by recent standards (3, 39, 66, 108, 144, 248). The following paragraph highlights a few observations from this period relevant to this dissertation, and illustrates a small fraction of the bioenergetic parameters readily obtainable from ^{31}P–NMRS experiments.

The non–invasive nature of ^{31}P–NMRS allowed investigators to confirm and refine many key *in vitro* studies done in the previous two decades. Hoult et al. (144) were the first to use NMR to verify PCr buffers ATP in accordance with Lohmann's and Lipmann's assertion 40 years earlier. In an unperfused excised rat leg preparation, ATP levels were maintained for nearly two hours while PCr declined, Pi increased, and hexose phosphates accumulated and then leveled off as anaerobic glycolysis ground to a halt. These authors were also the first to suggest the linewidth broadening of the Pi resonance may be due to spatial distribution of pH in the muscle as a result of an unspecified compartmentation process. Dawson et al. (66) found oxygenating a 4°C frog muscle preparation resulted in a significantly higher [PCr/Pi] ratio at rest than previous anoxic studies–confirming oxidative metabolism supports PCr synthesis. They also obtained a PCr recovery

time constant of around 14.5 minutes–only a minute longer than Kushmerick obtained using an *in vitro* approach (178), and found the Pi linewidth broadened during recovery. In a later series of papers Dawson showed isometric force is positively correlated with the free energy of ATP hydrolysis, $\Delta G_{ATP,}$ (67) and the relaxation rate is inversely correlated with ΔG_{ATP} (68). ΔG_{ATP} is the maximum available work per mole of ATP hydrolyzed ($\Delta G=\Delta G°'+RT\ln[ADP][Pi]/[ATP]$), whose variables are easily estimated from ^{31}P–NMR spectra. Meyer et al. showed the NMR–measured concentration of free Pi was over 6–fold lower in resting mammalian fast–twitch muscle than measured by chemical assay methods (212). This was meaningful since it placed the true [Pi] near the K_I of AMP deaminase (312) and phosphofructokinase (282), and moved it significantly lower than the K_m of glycogen phosphorylase (54). This suggested that the allosteric effector role of Pi should be reexamined in contracting skeletal muscle (207). For example, Connett suggested the Pi released from net PCr hydrolysis during a rest–to–work transition may play an important role in regulating the second, transient, 100–fold burst in glycolytic rate that occurs around t= 1 minute during a 4Hz isometric contraction (57) . Meyer et al. also showed the creatine kinase reaction was indeed at equilibrium *in vivo*, supporting the earlier works of Kuby and Noda in the 1950s (171, 230). Confirming that the creatine kinase reaction was at equilibrium *in vivo* is an essential prerequisite to calculating *in vivo* values of free [ADP] (185), phosphorylation potential (305) and the above resting oxygen consumption level during or after contractions (192, 203, 234).

Transient and steady–state analysis of PCr kinetics

Numerous *in vitro* studies in the late 1960s and 1970s documented the kinetic behavior of PCr during exercise and recovery in frog, rat, dog, and human skeletal muscle (73, 84, 120, 146, 177, 178, 244, 245, 259). The major observations were lactic acid was the primary cause of decreased ICF pH during contractions, PCr

recovery required oxidative metabolism and PCr recovery time–courses tended to represent monoexponentials after mild exercise. Additionally, it was shown intense exercise decreased the ICF pH resulting in slower PCr resynthesis and a biexponential PCr recovery time course. It was commonly argued that the lowered pH shifts the creatine kinase equilibrium away from PCr thereby slowing the recovery kinetics (120, 146, 257, 258).

Toward the mid 1980s, exercise and recovery PCr kinetics underwent additional scrutiny facilitated by continual improvements in the time resolution of ^{31}P–NMRS and signal gating techniques. From the current vantage point, two approaches evolved which guided investigators examining the nuances of PCr time courses: transient analysis and steady–state analysis. The focus of transient analysis is on quantifying the time constant, τ, of PCr during a rest–to–work or work–to–rest step transition. Variations of the kinetic parameter, τ, abound in the exercise literature. Two common examples include: the rate constant, k (= 1/ τ) and the half–time, $t_{1/2}$ (= τ ln(2)).

The primary focus of steady–state analysis is on quantifying the steady–state value of PCr after the transient phase has died out. Despite the fact in the late 1960s DiPrampero demonstrated kinetic data can be used to calculate steady–state values (73, 74), these two approaches simultaneously flourished in the 1980s without widespread realization in the bioenergetic community that they were really complementary perspectives of the same approximate first–order phenomenon.

Britton Chance and his colleagues advocated the steady–state ("work–cost") approach in which they found a positive linear relationship between the work rate of wrist flexion and the Pi/PCr ratio in the wrist flexor muscles of humans (48, 49, 223). In the steady–state, the macroscopic work rate (i.e. external power output in watts) is proportional to the cytoplasmic ATP demand rate which, necessarily, is

equal to the mitochondrial ATP synthesis rate and hence is proportional to oxygen consumption rate assuming a constant ATP/O_2 ratio (61, 142). Chance's group also demonstrated this steady–state behavior in isolated rat heart mitochondria and in *in vivo* rat leg using ^{31}P–NMRS. In the isolated heart mitochondria they mimicked increased ATP demand rate by adding a potato enzyme, apyrase A, that hydrolyzes ATP in the suspension and found a linear dependence between ATPase rate and the Pi/PCr ratio (115). In the rat leg they observed a linear dependence between isometric stimulation rate from 0.25Hz to 2.0Hz and Pi/PCr (7). In their human studies, they went on to show one month of aerobic training increased the slope or "system gain" of this work–cost relationship (49, 51). The increased slope signified that a given absolute change in the Pi/PCr ratio from rest–to–work will result in a larger change in the steady–state power output and hence oxygen consumption– perfectly consistent with the 1970s research showing increased oxidative capacity in trained skeletal muscle and the 1960s research on comparative fiber types.

The transient analysis approach toward PCr kinetics was formalized by Meyer (203) in a first–order analog electric circuit model (parallel RC) based upon earlier experiments by Kushmerick (175, 178) and Mahler (192). (*Digression*: The author's curiosity has revealed, perhaps, the earliest application of first–order electrical analog circuit models to *cellular* phenomena occurred in 1905 when Hermann modeled the passive spread of a transmembrane potential down an axon as a transmission cable (126). Sixty years later, Odum used a first–order model describing the diurnal variation in carbon flow between the competing processes of photorespiration and photosynthesis in plankton (232).)

The impetus for the Meyer model was to provide a conceptual framework for understanding the control of cellular respiration by changes in cytoplasmic phosphorylation potential as an alternative to Britton Chance's model based upon the kinetic limitation of mitochondrial oxygen consumption by ADP (49, 50, 53).

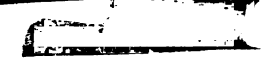

The essential feature of Meyer's model (cf. 165, 210, 211, 266) is that step changes in work rate within the aerobic ATP production capacity of the muscle fiber will change the oxygen consumption rate proportional to the change in cytoplasmic ΔG_{ATP}. The linearity of this relationship between oxygen consumption and ΔG_{ATP}, the "error signal", gives rise to the first–order monoexponential behavior of PCr kinetics seen in rest–to–work or work–to–rest step transitions (106, 165, 192). Furthermore, it is well appreciated PCr acts as a metabolic capacitor, spatially and temporally buffering ATP through the creatine kinase reaction (188, 213, 318), and muscle fiber oxidative capacity (hence capacity to support aerobic ATP production) is largely dependent upon mitochondrial volume density (65, 77, 78, 261). As a consequence of these characteristics, Meyer et al. asserted, and then experimentally verified, that the time constant describing the first–order behavior of PCr kinetics (τ_{PCr}) should be independent of workload, depend linearly on total creatine content (204), and depend inversely on fiber oxidative capacity (234). These assertions illustrate an inherent experimental convenience of PCr transient analysis in that oxidative capacity can be estimated from the time constant of a single work–rest transition rather than the slope of the steady–state work–cost relationship which requires quantifying several workload intensities for linear regression. Recently, Kemp has shown the steady–state analysis and transient analysis are equivalent constructs, but concluded the steady–state approach is much more sensitive to small pH changes compared to the more robust transient approach (165, 166, 167).

There have been numerous ^{31}P–NMRS studies over the past 15 years using transient analysis, and variations on the theme, toward understanding muscle bioenergetics. Two papers around 1984 out of George Radda's group from Oxford indicated the time course of PCr recovery from a work–rest transition becomes biexponential if the work intensity exceeds the aerobic ATP production capacity of

the muscle (9, 290). Their explanation is that during the work phase, anaerobic glycolysis was required to help meet the ATP demand and subsequently produced lactate which lowered the ICF pH. The lower ICF pH was correlated with longer PCr recovery times and biexponential behavior. These papers also showed the recovery rates of ADP >> PCr >> pHi.

Blei found the variations in τ_{PCr}, as measured by ^{31}P–NMRS within a given muscle, are much greater between individuals than between repeated measurements within one individual (26). He reported only a 9% variation for repeated measurements on a single subject, yet nearly a 1.8–fold variation across eight average humans (4 male, 4 female). This intersubject variability nicely corroborated decades of histochemical fiber typing which showed, on average, a 2–fold variation in oxidative capacity in average human skeletal muscle (261).

Achten et al. used recovery kinetics of Pi, rather than PCr, as a measure of oxidative capacity in human mixed calf muscle (1). They based their premise upon Pi exhibiting a 1:1 stoichiometry with PCr during PCr resynthesis (205), and the cause of Pi linewidth broadening being due to intercellular pH inhomogeneity as a result of different fiber type populations having different oxidative capacities (208). In their experiment, the Pi peak in spectra of five of seven volunteers split–not just broadened–into two discernible peaks. This permitted them to track two different rates of Pi recovery presumably corresponding to the Type I (more oxidative, faster recovery rate) and Type II (less oxidative, slower recovery rate) fiber populations. Routine estimation of oxidative capacity by multi–peak Pi recovery kinetics in lieu of PCr kinetics is limited, however. High intensity workloads which incur acidosis and fatigue are required to increase the likelihood of Pi peak splitting. This may not be tolerated well by patient populations with cardiorespiratory or neuromuscular diseases. Furthermore, even among normal human subjects, as relative workload intensity increases there will be increased variability of motor

unit recruitment and psychological motivation. This will significantly complicate the necessary correspondence between the actual working skeletal muscle fiber population and the volume of muscle tissue interrogated by the NMR transceiver coil (26). (Personal note: In the author's experience using a magnet with over six times the field strength in the Achten study (hence better spectral frequency resolution), and attempting to integrate the recovery Pi peak in the *more* heterogeneous rat mixed calf muscle (8, 261, 319), it has been found the Pi peak often has very low signal–to–noise and does not reliably split even in the same animal over repeated cycles of work and rest on the same experiment day.)

Interestingly, McCully and Chance have realized the benefits of using transient analysis rather than their steady–state analysis (200). In this human cross–sectional study they found a statistically significant positive correlation between τ_{PCr} of the calf muscle (hence decreasing oxidative capacity) and age. They also showed for elderly (≥ 80 y/o) volunteers there was no significant effect of gender or use of medication for common chronic illnesses (diabetes, hypertension, hypothyroidism) on τ_{PCr}. Elderly patients with peripheral vascular disease, however, had over a 66% longer τ_{PCr} as compared to the "normal" elderly. The loss in muscle oxidative capacity is likely due to the cumulative effects of decreased active lifestyle with increased age plus decreased peripheral blood flow capacity (56).

Lastly, the energetic cost of contraction is another useful parameter that can be extracted from analysis of ^{31}P–NMRS PCr kinetics. The conceptual basis allowing ATP cost measurements is summarized next. As mentioned before, the first–order electric analog model dictates that PCr acts as a metabolic capacitor. This implies that during a rest–to–work transition the intracellular pool of PCr "discharges" and supplies a "current" of phosphoryl groups to the myosin ATPase and SR Ca^{2+} ATPase. As steady–state is approached, the phosphoryl current from the

discharging metabolic capacitor monoexponentially decays to a lower value at the same time the phosphoryl current from the mitochondrial conductance is monoexponentially increasing. At a steady–state workload intensity within the oxidative capacity of the muscle fiber, the cytosolic ATP demand is met by the mitochondrial ATP supply current with no change in phosphoryl current supplied by PCr. The significance of this is that taking the time zero derivative of the [PCr] time course (i.e. the capacitive phosphoryl–charge time course) will provide the initial rate of change of PCr which reflects the initial energetic cost of contraction (104). That is $dPCr(t)/dt\,|_{t=0} = -1/\tau(PCr_0 - PCr_{ss})$ where τ= first order rate constant, PCr_0 = resting [PCr] and PCr_{ss} = steady–state [PCr]. Within the first several seconds of the transition to work from rest, net PCr hydrolysis must be supplying all of the phosphoryl current since glycolytic flux does not reach a maximum for at least 5–15 seconds (58) and oxidative metabolism has a time constant of at least 30–70 seconds depending on fiber type, species, and temperature (26, 178, 204, 234). Foley et al. used this time–zero derivative technique and amazingly showed that acute but not chronic depletion of ATP by 40–50% will decrease the cost of isometric twitch and tetanic contractions in rat fast–twitch muscle (102, 103). It was speculated the acute decrease in ATP favors more IMP production by the near–equilbrium adenylate kinase reaction during stimulation, and the increased IMP allosterically affects cross–bridge cycling kinetics such that maximal velocity of shorting is reduced, leading to the observed decreased in energetic cost of contraction. Since a gradual 9–week reduction in ATP did not alter the cost of contraction it was concluded low ATP, per se, was not the cause of the reduced energy cost (102).

In summary, the role of phosphocreatine in skeletal muscle energy metabolism is to serve as a phosphagen capacitor to temporally and spatially buffer changes in ATP thereby preserving a favorable cytosolic ΔG_{ATP} throughout large swings in

workload. The utility of analyzing steady–state and transient behavior of phosphocreatine kinetics in skeletal muscle is that it permits assessment of energetic costs of contraction and calcium handling, quantifies economy and efficiency of contraction, estimates oxygen consumption, and can measure relative oxidative capacity.

Measuring oxidative capacity via *in vivo* ^{31}P–NMRS has recently been proposed as a non–invasive alternative for estimating muscle fiber type distributions. The promise of ^{31}P–NMRS is it offers real–time tracking of energetically important intracellular metabolites (PCr, ATP, Pi, pH) within the same muscle. Not only does this greatly increase time resolution, it also increases statistical power over the one–muscle–one–time–point (and/or one–geographic–location) limitation of the muscle biopsy method.

Consequently, a necessary prerequisite would be to correlate a ^{31}P–NMRS derived parameter to an energy supply or energy demand fiber type parameter. Previous theoretical and empirical studies have shown that the steady–state PCr level during stimulation scales with oxygen consumption, and the time constant of PCr recovery after submaximal stimulation should be directly proportional to total creatine content and inversely proportional to oxidative capacity (192, 203, 208). Chapter 3 of this dissertation tests the hypothesis that the rate constant ($k = 1/\tau$) for PCr recovery is linearly dependent on muscle oxidative capacity in a relatively homogeneous fiber population.

Chapter 4 of this dissertation examines the following question: If the PCr recovery rate constant scales with oxidative capacity in a relatively homogeneous population, can the underlying distribution of fiber types in a heterogeneous muscle be determined based upon decomposing a global, multicomponent PCr recovery?

CHAPTER 3
Linear dependence of phosphocreatine kinetics on skeletal muscle oxidative capacity

Introduction

The changes in phosphocreatine (PCr) that occur in skeletal muscle during transitions between rest and moderate stimulation or exercise follow a monoexponential time course (192, 203, 296). This behavior can be explained by a linear metabolic model in which respiration rate is proportional to the cytoplasmic free energy of ATP hydrolysis (ΔG_{ATP}), and the creatine kinase reaction acts as an ATP buffer or phosphagen capacitance (203, 213). According to this linear model, the time constant for PCr changes (τ) should be independent of stimulation rate over submaximal workloads, i.e. workloads that can be maintained in the steady–state by oxidative ATP production. In addition, the model predicted that τ should depend linearly on total creatine content and inversely on muscle mitochondrial content or oxidative capacity. Previous studies of rat fast–twitch muscle confirmed that τ was independent of stimulation rate over a threefold range of submaximal rates (203) and directly proportional on total creatine content (204). The purpose of this study was to test the hypothesis that the rate constant for PCr recovery ($k=1/\tau$) is linearly dependent on muscle oxidative capacity. Also, the effect of intracellular acidosis on the PCr recovery rate after stimulation is examined. These results provide a framework for the practical application of ^{31}P nuclear magnetic resonance spectroscopy (^{31}P–NMRS) data for noninvasive estimation of relative skeletal muscle oxidative capacity.

Methods

Animal care and feeding

Adult male Sprague–Dawley rats (initially 250–350g); Harlan Sprague Dawley Inc., Indianapolis, IN) were housed three per cage in a temperature (≈22°C) and

humidity (≈35%rh) controlled room on a 12:12 hour light–dark cycle. Rats were provided Purina Rat Chow and tap water *ad libitum* except for one treatment group noted below. All experiments were performed during the rat's nocturnal cycle.

Treatment groups

Muscle mitochondrial content was decreased in one group of rats ("MMI") by treatment with methimazole (1–methyl–2–mercaptoimidazole, MMI; Ref. (60)) administered in the drinking water (0.025% w/v) for 8–10 weeks. In brief, the pharmacological mechanism of MMI involves inhibiting the peroxidase enzyme–which oxidizes dietary iodide into iodine–thereby preventing iodine incorporation into tyrosine within the thyroid follicular cell (122), schematic shown in Appendix E– Methimazole Inhibition). This drastically reduces thyroid hormone (T_4 and T_3) synthesis by the follicular cells resulting in systemic hypothyroidism. Chronically low serum [T_3] reduces the nuclear transcription of many structural and enzymatic proteins found within the mitochondria resulting in decreased mitochondrial volume percent within skeletal muscle tissue (41, 263). A treatment period of 8–10 weeks was chosen since it has been shown that rat skeletal muscle cytochrome C content monoexponentially decreased with a time constant of 11 days after surgical thyroidectomy (293). Cytochrome C is an electron–carrying, heme–protein found within inner mitochondrial membrane. Because methimazole treatment reduced body mass, the food supply to a second group of rats ("Control–MMI") was moderately restricted to 35 $g \bullet day^{-1} \bullet cage^{-1}$. Rats in both groups were handled at least twice per week to monitor changes in body mass (Appendix H– MMI Effects).

Muscle mitochondrial content was increased in a third group of rats ("Trained") by a ten week interval training program using a computer controlled running–wheel apparatus (311). This interval training program was progressively increased until reaching a final regimen of 37 m/minute for 60 minutes/day by the start of

week nine (Appendix F– Intensity–Duration Protocol). Shepherd has shown the common laboratory rat running at 35–40m/minute has a whole–body oxygen consumption of 85–90%VO_{2max} (270). The running wheel apparatus provided a mild constant current electric shock (approximately 0.5 mAmp) if the rat did not run at the expected velocity. As a group, the rats met or greatly exceeded the required number of wheel revolutions per day except during week seven when the incremental duration change was greater than previous weeks. (Appendix G– Training Compliance). All rats were trained under dim red light Monday through Friday within six hours of the start of their nocturnal ("awake") cycle. Similar training regimens using a treadmill nearly doubled the mitochondrial content in rat white muscle (127, 294). A fourth group of rats ("Control–trained") was handled daily for 10 weeks but not run on the wheels. A rat was not trained on the day of its experiment.

Muscle surgical protocol

Rats were anesthetized with sodium pentobarbital (ip: 50 mg/kg body mass), and an intraperitoneal catheter was inserted for administering additional anesthetic (5mg/kg) at approximately 30 minute intervals. The rats were prepared for *in situ* stimulation of the right leg on a custom built ^{31}P–NMR probe as previously described (204) (see also photograph in Appendix A– ^{31}P–NMR Probe). In brief, the right sciatic nerve of the supine rat was cut and placed in a bipolar platinum electrode, and the right knee was fixed between two brass posts using a 18G needle bored through the distal head of the femur. A 20lb–test braided filament fishing line was threaded through the space between the Achilles tendon and the distal fibulo–tibular symphysis and then tied to a half–bridge microfoil strain gauge force transducer mounted on an adjustable support in the probe. Adjustment of this mount placed the right posterior leg 1–2 mm directly above a 1.2 cm diameter, flat, circular surface coil similar to that shown in Appendix B– Leg

Cross–Section. Muscle length was optimized to give a maximal, isometric twitch in response to a supramaximal square–wave pulse (10–20V amplitude, 2ms duration, Grass stimulator model S48). Passive tension averaged 200–300 grams. Steady–state isometric twitch force from the entire leg was recorded (Gould recorder model 2200S) at 1 mm/sec chart speed and 500 grams/cm sensitivity. The probe was ventilated with 100% oxygen and body temperature was continuously monitored via a rectal thermistor (YSI probe model 402A). Body temperature was maintained between 37°–39°C by modulating the magnet bore air temperature with a warm–air blower using a feedback–controller (YSI controller model 73A). This method of maintaining body–temperature homeostasis was shown to satisfactorily maintain the posterior leg intra–muscle temperature around 37°C in a separate supplemental experiment summarized in Appendix C– Temperature Homeostasis. At the end of each experiment (detailed in next paragraph) the superficial 2–3 mm sections of the stimulated and contralateral unstimulated gastrocnemius muscles were excised and immediately clamp–frozen in liquid nitrogen and stored at –80°C. After all NMR experiments were completed, spectrophotometric assays of citrate synthase activity (277), cytochrome C content (75), ATP content (22) and total creatine content (PCr + creatine: Ref. (22)) were performed. The spectrophotometer was calibrated each day prior to running any assay. Relative myosin heavy chain isoform distribution was determined by polyacrylamide–gel slab–electrophoresis of the purified, denatured protein (289, 116). The superficial 2–3 mm of the gastrocnemius represents the volume of muscle that is most effectively sampled by the 1.2cm diameter flat surface coil (175). The remaining portion of the stimulated posterior leg muscle group was removed and weighed so force measurements could be expressed as gram force per gram wet muscle.

Spectral acquisition parameters and muscle stimulation protocol

^{31}Phosphorus–NMRS of the right posterior leg was acquired at 162MHz in a 89mm diameter, vertical–bore, Bruker AM400, 9.4 tesla spectrometer. The transceiver coil was tuned to resonate at 162MHz and impedance matched to 50 Ω for maximum power transfer immediately prior to placing the probe in the magnet bore. Rat's head was down. The B_0 field was shimmed on the proton signal from muscle water to a line width of 50–75 Hz. The B_1 radio frequency pulse width was set to 15–20 μsecond to optimize the signal–to–noise ratio for the 1.76 second interpulse interval (TR) used during stimulation. (Note: The B_0 field is the constant magnetic field of the superconducting 9.4T magnet; the B_1 field is the magnetic component of the electromagnetic wave emitted by the radiofrequency transmitter coil.) Before muscle stimulation, a fully relaxed control spectrum (TR = 15 seconds, 16 scans) was acquired. Partially saturated spectra (TR = 1.76 seconds, 16 spectra+1 dummy scan) were then continuously acquired in 30–second blocks before (2 spectra), during (16 spectra), and after (16 spectra) eight minutes of submaximal isometric twitch stimulation at 0.33Hz (MMI study) or 0.75Hz (Trained study). These stimulation rates where chosen on the basis of previous studies (142, 203, 204) and pilot experiments, which demonstrated they could be maintained for eight minutes without substantial muscle fatigue or acidification. After a 30 minute rest period which was sufficient time for PCr and pH to recover to resting steady–state values, another series of spectra were acquired before, during, and after eight minutes of 2.0Hz isometric twitch stimulation for all four treatment groups. This stimulation rate exceeds the maximum rate that can be maintained in the steady–state by oxidative metabolism in superficial gastrocnemius muscle of control rats (142).

Spectral analysis

The summed free induction decays (FIDs) were zero–filled to 2K complex data and multiplied by (i.e. convolved with) a monotonically decreasing exponential

function in the time domain before Fourier transformation. This results in a 20Hz linewidth broadening in the frequency domain. Relative changes in PCr were determined by the Method of Natural Lineshapes (MNL) (124). This method computes the integral of the peaks in each spectrum relative to the area of the same peaks in a high signal–to–noise spectrum obtained by adding all 34 spectra in each stimulation–recovery cycle. (See also Chapter 3–Methods–Spectral Analysis for additional discussion on the MNL.) Results were expressed as percent of initial PCr/ΣATP. The initial PCr/ΣATP and Pi/ΣATP were computed by integration of the fully relaxed control spectrum acquired prior to the start of each experiment. Intracellular pH was determined by the chemical shift (δ) of Pi relative to PCr at –2.52ppm using the formula: $pH=6.77+\log[(0.89-\delta)/(\delta-3.19)]$ (175). Changes in PCr during stimulation and recovery were fit to a monoexponential function by an iterative least–squares algorithm that minimized χ^2 using two–parameters (τ and steady–state PCr level). The initial rates of PCr hydrolysis at the onset of stimulation were computed from these fits as previously described (104)

Statistical analysis

All data are reported as means±SEM. Comparisons of means (treatment versus corresponding control) were made by Student's t–test or Tukey's Honestly Significant Difference test, at the $P<0.05$ level of significance. SigmaPlot 4.0 for Windows was used for simple linear regression to examine the relationship between phosphocreatine recovery rate constant and oxidative capacity or end–stimulation pH. SigmaPlot uses the Cholesky decomposition to invert the *X'Y* matrix.

Results

Treatment effects

Citrate synthase activity of the superficial gastrocnemius muscle was decreased by 71% in the MMI group and increased 1.8 fold in the Trained group, compared to

their corresponding control groups (Table 2). Citrate synthase is a key flux–regulating Krebs cycle enzyme found in the mitochondrial matrix and has been shown to be a reliable estimator of mitochondrial content in isolated mammalian skeletal muscle fibers (151). Taken together, the treatments resulted in a 6.7 fold range of nominal mitochondrial content, as indicated by this particular mitochondrial marker enzyme.

Table 2: *Treatment groups and effects*

	Control–MMI	MMI	Control–trained	Trained
N	10	9	7	11
Body mass (g)	299±2	301±4	391±11	338±8*
Stimulated muscle mass (g)	2.3±0.1	2.3±0.1	3.1±0.1	2.7±0.1
Initial peak isometric twitch force (g/g)	240±13	235±24	145±7	263±20*
Citrate synthase activity (μmole/minute/g)	14.7±1.6	4.2±0.6*	15.7±1.7	28.1±1.5*
Cytochrome C content (nmole/g)	3.8±0.5	? (< ≈2)	3.3±0.4	10.6±0.1*

Values are mean±SEM; N, number of rats. MMI, methimazole. The Control–MMI rats had a moderately restricted food supply. The Control–trained were fed *ad libitum*. Force values are expressed per gram wet weight of stimulated muscle. *Significant effect of treatment versus corresponding control group (P<0.05).

Similarly, cytochrome C, another mitochondrial marker, was over threefold higher in the trained compared with its corresponding control group. Cytochrome C in the MMI group was below the level (approximately 2 nmole/g) that could be reliable measured using our spectrophotometric assay procedure. Neither treatment resulted in a significant change in the relative myosin heavy chain homodimer isoform distribution of the superficial gastrocnemius sections (overall mean 50±2% Type IIa, balance Type IIb, with Type I not detected).

There was a significant difference between initial peak isometric twitch force in the Trained group compared to its corresponding Control–trained group (free fed) during 0.75Hz stimulation (Table 2). Force in the Trained group, however, was

similar to the MMI group and the corresponding Control–MMI group (restricted food intake). This suggested the force was anomalously low in the Control–trained group potentially due to a reason related to their larger body mass compared to the other three groups (Table 2). To resolve this issue, we ordered another group of rats and interval trained some of them as previously described above in Methods–Treatment Groups. As before, both of the new (') groups (Trained', Control–trained') were handled on a daily basis and fed *ad libitium*. Mechanical measurements we made using a standard horizontal bench apparatus for *in situ* stimulation (214). In this case, there was no significant difference in any mechanical characteristic between the Trained' versus Control–trained' (free fed) rats (Table 3). Furthermore, peak isometric twitch force was similar to the MMI, Control–MMI, and Trained groups obtained in the NMR study (Table 2). Consequently, it is probable the lower peak isometric twitch force in the Control–trained rats during the NMR study reflects difficulty in maintaining optimal muscle length for larger rats within the confined space of the NMR probe (see also photograph in Appendix A– ^{31}P–NMR Probe).

Table 3: ***Mechanical characteristics–Bench experiment***

	Control–trained'	Trained'
N	10	7
Body mass (g)	406±5	351±10*
Stimulated muscle mass (g)	3.4±0.2	3.1±0.2
Initial peak isometric twitch force (g/g)	261±24	237±18
Time to peak twitch force (ms)	23±4	21±2
Twitch half–relaxation time (ms)	18±3	18±2
Peak isometric 20 Hz tetanic force (g/g)	387±36	356±47
Peak isometric 40 Hz tetanic force (g/g)	603±101	711±84
Peak isometric 60 Hz tetanic force (g/g)	1068±99	1085±139
Peak isometric 80 Hz tetanic force (g/g)	1320±108	1249±154
Peak isometric 100 Hz tetanic force (g/g)	1465±116	1366±158
Peak isometric 150 Hz tetanic force (g/g)	1518±126	1428±167
Peak isometric twitch force after 20 minutes of continuous 2Hz twitch stimulation (g/g)	236±24	225±13

Values are mean±SEM; N, number of rats. Both groups were fed *ad libitium*. All force values are expressed per gram wet weight of stimulated muscle.
*Significant effect of treatment versus corresponding control group ($P<0.05$).

Initial resting values of pH, PCr/ΣATP, and Pi/ΣATP were similar to those reported previously (175, 203), although the Pi/ΣATP was significantly higher in the Control–MMI group compared with the other three groups (Table 4). There was also a small but significant increase in total creatine content in the MMI treated group (Table 4).

Table 4: *Metabolites in resting superficial gastrocnemius*

	Control-MMI	MMI	Control-trained	Trained
N	10	9	7	11
Intracellular pH	7.09±0.03	7.06±0.01	7.15±0.03	7.09±0.02*
PCr/∑ATP	3.34±0.16	3.77±0.16	3.53±0.12	3.50±0.07
Pi/∑ATP	0.14±0.01	0.08±0.02*	0.09±0.01	0.09±0.01
ATP content (μmole/g)	7.37±0.12	6.83±0.26	7.04±0.16	7.16±0.12
Total creatine content (μmole/g)	38.4±0.8	41.1±0.8*	33.1±0.6	33.4±1.1

Values are mean±SEM; N, number of rats. pH, PCr, Pi, and ∑ATP are measured in fully relaxed spectrum (TR = 15 seconds) where ∑ATP is the sum of the peak areas of the α–, β–, and γ–ATP resonances. ATP and total creatine content were measured by chemical assay of contralateral (unstimulated) superficial gastrocnemius. *Significant effect of treatment versus corresponding control group ($P<0.05$).

Effect of submaximal stimulation

Figure 1 shows sample spectra acquired before, during, and after stimulation at the submaximal rates. Figure 2 shows the time course of PCr changes in the four groups during and after the submaximal stimulation. As expected, PCr decreased at the onset of stimulation and recovered exponentially afterward. In all groups, there was a transient alkalinization at the onset of stimulation and transient acidification at the onset of recovery (data not shown). These transient pH changes can be attributed to proton consumption and release by net PCr hydrolysis and resynthesis, respectively (4). If these transients are ignored, there were only minor changes in intracellular pH by the end of submaximal stimulation (Table 5). There was no significant decrease in peak twitch force by the end of the eight minute submaximal stimulation in any treatment group (data not shown).

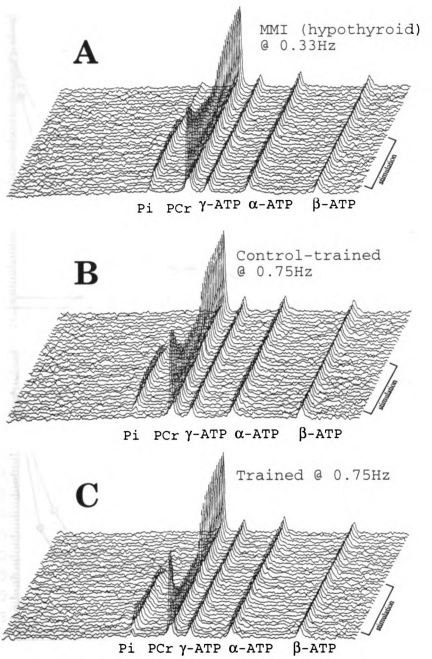

Figure 1: Sample ^{31}P-NMR spectra stackplots

Sample spectra acquired before (bottom two spectra in each series), during (next 16 spectra), and after (top 16 spectra) eight minutes of submaximal stimulation. A single spectrum represents the time–averaged behavior of phosphorus metabolites over a period of 29.9 seconds (16 FIDs+1dummy scan, TR = 1.76 seconds). X–axis is resonance frequency in parts–per–million (arbitrary scale). Y–axis is resonance amplitude which is proportion to the number of nuclei in a given local electronic environment. Z–axis is increasing experiment time.

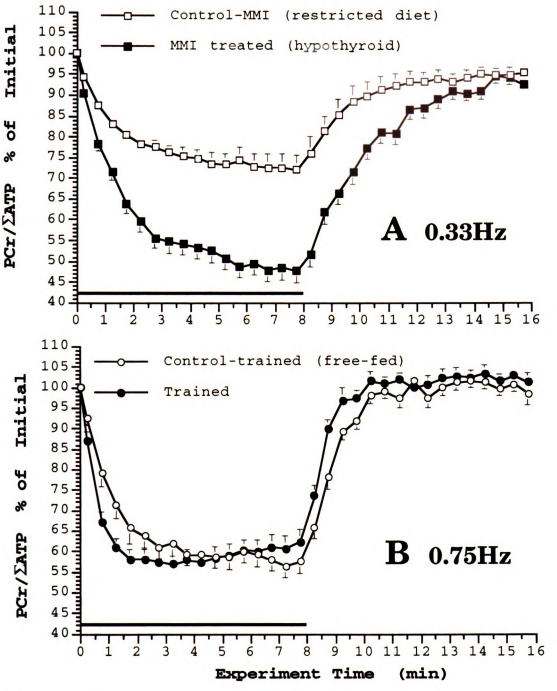

Figure 2: Time course of PCr changes (submaximal stim.)

Mean±SEM, Number of rats as in Table 2. Time course of PCr/ΣATP during and after submaximal stimulation.

Table 5: *PCr kinetics and pH during submax. stimulation*

	Control–MMI	MMI	Control–trained	Trained
N	10	9	7	11
Stimulation rate (Hz)	0.33	0.33	0.75	0.75
PCr monoexponential time constant, τ: Onset of stimulation (minute)	1.32±0.29	1.69±0.15	1.17±0.16	0.52±0.08*
PCr monoexponential time constant, τ: Onset of recovery (minute)	1.57±0.19	2.65±0.27*†	1.01±0.08	0.69±0.07*
Steady–state PCr/ΣATP during stimulation (% of initial)	73±4	48±3*	58±3	61±3
Initial rate of PCr hydrolysis, μmole/g/twitch	0.38±0.05	0.48±0.05	0.27±0.05	0.56±0.06*
Intracellular pH at end of stimulation	6.97±0.02	6.94±0.02	6.95±0.02	6.90±.0.02

Values are mean±SEM; N, number of rats. *Significant effect of treatment versus corresponding control group ($P<0.05$). † Significant difference between τ at onset of stimulation versus τ at onset of recovery corresponding control group ($P<0.05$).

The time constant for PCr recovery after submaximal stimulation was significantly shorter in the Trained group, and significantly longer in the MMI group, compared with their corresponding control groups (Table 5). There was no significant difference in the time constant for PCr changes at the onset of stimulation versus the onset of recovery in the Control–trained or Trained groups. In the MMI group, however, the τ at the onset of stimulation was significantly shorter than the τ at the onset of recovery. Also shown in Table 5 are the steady–state PCr levels approached during stimulation and the initial rate of PCr hydrolysis, both estimated by extrapolation from monoexponential fits. A previous study showed that the initial rate of PCr hydrolysis is a good estimate of the ATP cost of isometric twitch contractions (104). Consequently, the lower initial rate of PCr hydrolysis in the free–fed Control–trained group is consistent with their anomalously lower initial peak isometric twitch force in the NMR study (Table 2).

When the data were pooled from all four treatment groups during submaximal stimulation, there was a good linear correlation ($r = 0.84$, $n=37$, $P< 0.01$) between the rate constant of PCr recovery (i.e. $k = 1/\tau$) and citrate synthase activity, normalized to total creatine content (Figure 3). Normalization to total creatine content is formally required because τ for PCr recovery also depends on total creatine as stipulated by the linear metabolic control model of skeletal muscle oxidative phosphorylation (203); however, the correction is minor in this case. The correlation coefficient between $1/\tau$ and citrate synthase activity without this normalization was 0.82 (graph not shown). From a different vantage point, it has been argued that normalization of metabolite content and enzyme activities to total creatine (as opposed to expressing on a per dry weight or per wet weight or per gram of protein basis) minimizes inter–muscle differences, which aids in identifying true metabolic differences among different muscles (164).

There were no significant correlations in any treatment group between end–stimulation pH after a submaximal workload and citrate synthase activity normalized to total creatine content (data not shown).

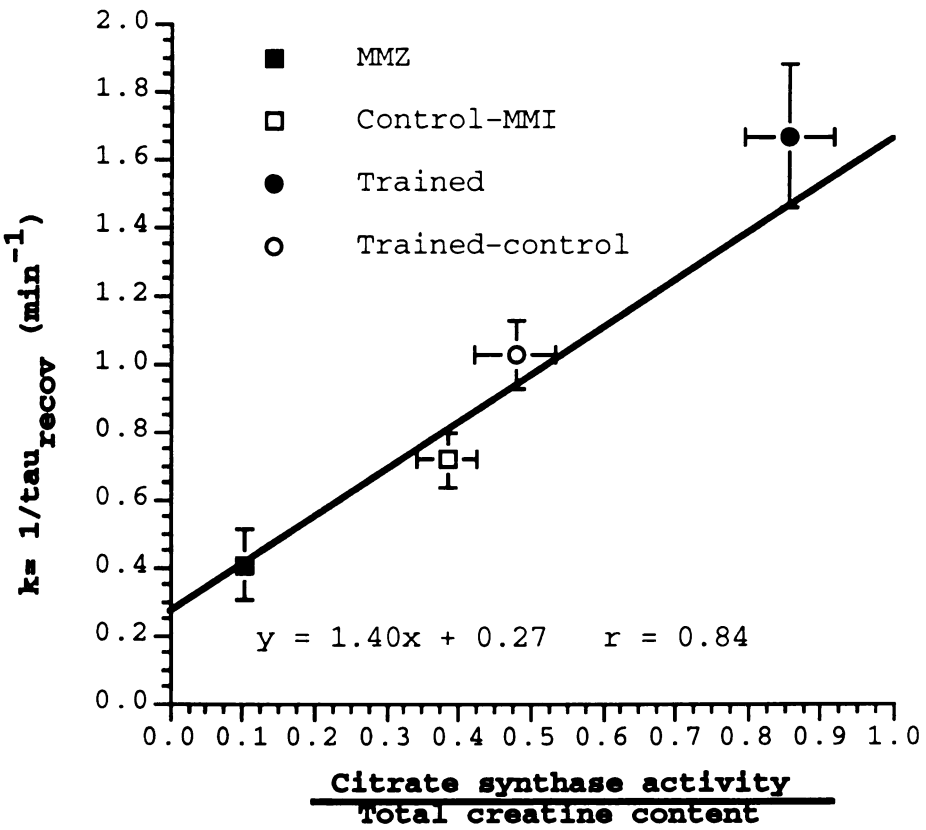

Figure 3: PCr recovery rate constant v. oxidative capacity

Correlation between the rate constant (k= 1/τ) for PCr recovery after submaximal stimulation and citrate synthase activity, normalized to muscle total creatine content. Plotted points are means±SEM for the four treatment groups. Linear regression was calculated from individual muscle data points (n=37).

Effect of 2.0Hz Stimulation

Figure 4 shows the time course of changes in isometric twitch force, PCr/∑ATP, and ICF pH during 2.0Hz stimulation in the four treatment groups. This stimulation rate is known to be beyond the maximum rate that can be maintained in the steady–state by oxidative metabolism in the least–oxidative fibers in gastrocnemius muscle of sedentary rats (142). Consequently, PCr decreased more rapidly at the onset of stimulation, and the muscles became more acidic than during submaximal stimulation. On the other hand, less acidification occurred in the Trained rats compared to the other groups, as expected from the higher muscle oxidative capacity (Figure 4C).

Although the PCr changes at the onset of 2.0Hz stimulation were not markedly different between the four groups (Figure 4B), the recovery of PCr after stimulation was clearly faster in the Trained group, and slower in the MMI group, compared with controls (Figure 5). There was a significant correlation between $1/\tau$ for PCr recovery after 2.0Hz stimulation and normalized citrate synthase activity, but the correlation was weaker ($r= 0.70$, $n=37$; graph not shown) than for the same relationship after submaximal stimulation. This increased variance is in part due to an independent effect of pH, since there was a significant correlation ($r=0.73$, $n=53$, $P<0.01$) between $1/\tau$ for PCr recovery and ICF pH at the end of the 2.0Hz stimulation for the two control groups (Figure 6).

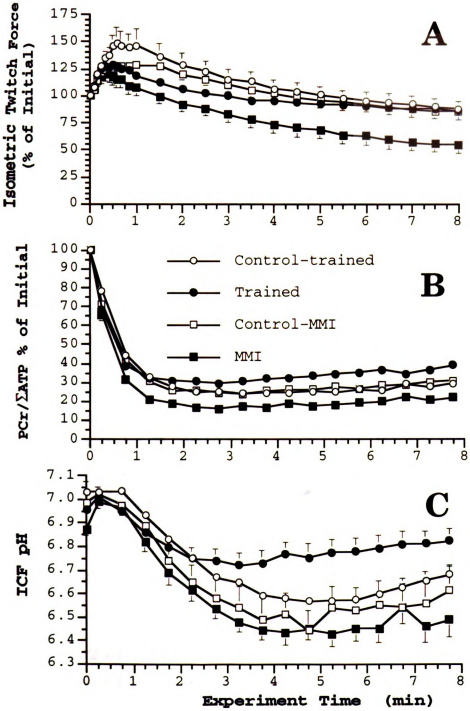

Figure 4: 2.0Hz Stimulation time courses

Peak isometric twitch force (A), PCr/ΣATP (B), and ICF pH (C) during 2.0Hz stimulation. Values are means±SEM; number of rats as in Table 2.

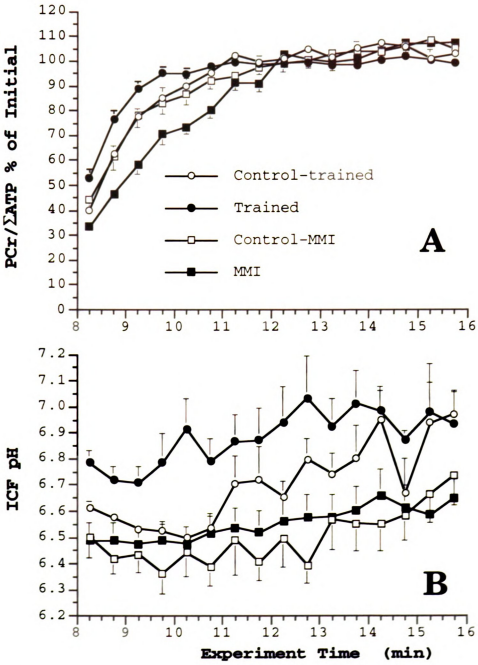

Figure 5: 2.0Hz Recovery time courses

PCr/ΣATP (A) and ICF pH (B) during recovery after eight minute 2.0Hz stimulation. Values are means±SEM; number of rats is as in Table 2.

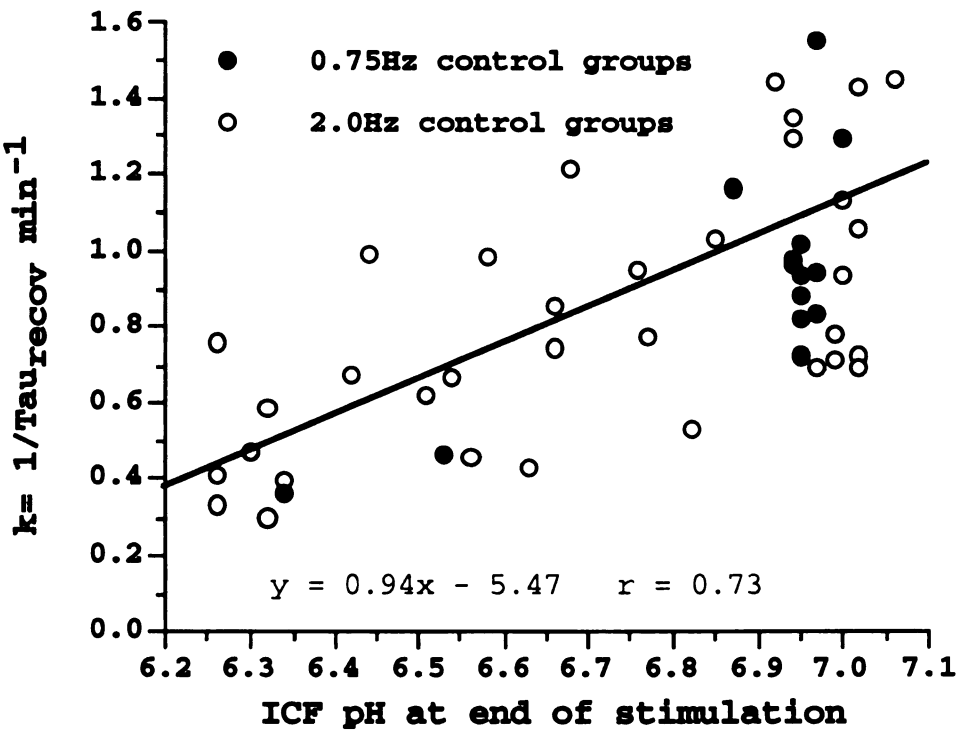

Figure 6: Rate constant v. pH (supramaximal stim.)

Correlation between rate constant for PCr recovery after eight minutes of isometric stimulation versus ICF pH at end of stimulation in control muscles stimulated at 0.75Hz or 2.0Hz.

Discussion

The main result of this study is that there is a linear relationship between the global NMR–derived rate constant for PCr recovery ($k = 1/\tau$) and muscle oxidative capacity, as indicated by citrate synthase activity. Taylor et al. were among the first to explicitly suggest this correlation over 15 years ago (290) and since then analogous results have been reported by others in rat (296) and human muscle (individual fibers: (153, 274); whole muscle: (26, 200, 217, 308). This is the first study, however, to cover over a 6–fold range of citrate synthase activity. The practical implication of this result is that noninvasive ^{31}P–NMRS of PCr recovery transients can be used as an index of oxidative capacity in skeletal muscle.

It should be emphasized that this correlative method is strongly dependent upon the choice of mitochondrial marker, which is complicated by several factors. First, the intrinsic constituents of the electron transport system within the inner mitochondrial membrane (i.e. any cytochrome) are a somewhat better measure of true oxidative capacity (65, 198, 254) than Krebs cycle enzymes (e.g. citrate synthase, α–ketoglutarate dehydrogenase) which may have anaplerotic and amphibolic functions in addition to oxidizing di– and tri–carboxylic acids (28). On the other hand, compared to Krebs cycle enzymes solubilized in the gel–like matrix, most electron transport system constituents are tightly integrated within the inner mitochondrial membrane making them more challenging to routinely isolate and purify intact with sufficient yield. Second, the various markers of mitochondrial content do not change proportionally during muscle adaptation (30, 256) or across fiber types (151). For example, the slope of Figure 3 would have increased if cytochrome C content were used in lieu of citrate synthase activity since cytochrome C underwent a 3.2–fold increase whereas citrate synthase increased by only 1.8–fold in the Trained versus Control–trained groups.

The relationship between the PCr recovery rate constant and muscle oxidative capacity was previously derived from a first–order analog RC circuit model of muscle respiration (203). This circuit model assumes **1)** the cytoplasmic creatine kinase reaction is in instantaneous and spatially uniform equilibrium (213, 318); **2)** oxygen and substrate supply are not limiting during recovery (259); **3)** anaerobic ATP production is negligible during recovery (62, 178); **4)** the mitochondrial ATP/O_2 and basal rate of muscle QO_2 are constant (119, 25); and **5)** PCr resynthesis accounts for all but a negligible fraction of the extra ATP consumed during recovery (120, 290).

In the context of the circuit model, the use of PCr recovery rate constants to estimate oxidative capacity depends on four assumptions in addition to the five

listed above: **1)** total creatine content (Tc) must be known because τ also depends linearly on total creatine (204); **2)** the PCr measurements must be made over the range in which the PCr/Tc ratio is directly proportional to ΔG_{ATP}, i.e., from approximately 0.2 to 0.7 (203); **3)** the model assumes that the cytoplasmic ATPase rate (almost entirely due to the myosin ATPase (250)) is a step function of the motorneuron stimulation rate (set by the experimenter or central nervous system), both at the onset of stimulation and at the onset of recovery; **4)** the circuit model assumes a constant intracellular pH.

With these additional assumptions, the circuit model predicted that $1/\tau$ for PCr decline at the onset of stimulation should equal $1/\tau$ during recovery and, therefore, might also be used to estimate oxidative capacity. In practice, however, the recovery rate constant is likely to be more reliable than the onset of stimulation rate constant for several reasons. First, the onset and recovery rate constants are expected to be equal only for submaximal stimulation, which can be maintained in a steady–state without fatigue by oxidative metabolism. Consequently, during the supramaximal 2.0Hz stimulation in this study, PCr depletion was faster than PCr recovery in all groups (Figure 4B versus Figure 5A). In the MMI group, the onset τ was significantly shorter than recovery τ for 0.33Hz stimulation (Table 5), suggesting that even this low rate exceeded the oxidative capacity of some fibers in these muscles. Second, the confounding contribution of anaerobic glycolysis to total ATP production during stimulation can be substantial, particularly in fast–twitch muscles. Conversely, PCr recovery is thought to depend almost entirely on oxidative metabolism in mammalian muscle (120, 166, 259). Third, the assumption that ATPase rate is a crisp step–function of stimulation rate is not satisfied if force is not constant, because the ATP cost of contraction is directly proportional to force within a muscle (26, 104, 118). For example, in this study there was a pronounced staircase effect during the 2.0Hz twitch stimulation. This would cause variations in

the ATPase rate and result in deviations from the ideal monoexponential time course of PCr depletion at the onset of stimulation.

Analysis of PCr recovery transients (i.e. τ) after submaximal workloads (24, 195, 200) is more preferable than analyzing the slope of steady–state PCr/Pi versus workload, the "work–cost" relationship (7, 49, 223), to estimate oxidative capacity. In contrast to the PCr recovery rate constant which depends only on oxidative capacity (under the reasonable assumption total creatine does not change on an acute basis), the steady–state PCr approached during stimulation also depends on ATPase rate. This is nicely illustrated in Figure 2B in which both the Trained and Control–trained groups had comparable steady–state PCr levels during submaximal stimulation despite the higher oxidative capacity of the Trained group. This is the result of the lower isometric twitch force (Table 2) and hence lower ATPase rate of the Control–trained (free fed) group. Furthermore, measuring τ is independent of the given single submaximal workload chosen (23, 106, 203). By definition, constructing a "work–cost" relationship, however, requires several workloads ($\geq$3) over a large enough dynamic range to give different steady–state PCr/Pi ratios to calculate a slope from linear regression. Consequently, the τ method maybe more preferable for patients with cardiovascular disease (296) or renal disease (235) in which the submaximal workload range may be small and ill–defined and supramaximal workloads are contraindicated.

The strong correlation between the PCr recovery rate constant and end–stimulation ICF pH (Figure 6) suggests workload intensities resulting in significant intracellular acidosis can potentially confound attempts to estimate relative oxidative capacity. Decreased PCr recovery rates due to lower ICF pH has been shown in healthy human mixed limb muscle (287, 308), malignant hyperthermia–susceptible humans (221), rat mixed muscle (168), and hypercapnic cat soleus (119) and is probably related to a non–specific global pH effect on the

mitochondrial oxidative machinery and/or on substrate delivery to the mitochondrial matrix from the cytosol.

In summary, the results of this study confirm the rate constant for PCr recovery in skeletal muscle after submaximal stimulation is linearly dependent on oxidative capacity as indicated by mitochondrial marker enzymes. These results are consistent with predictions based upon the linear thermodynamic model of respiratory control by ΔG_{ATP} (203). The practical implication is that relative oxidative capacity (depending on the chosen mitochondrial marker) can be estimated in muscles of human subjects from ^{31}P–NMRS measurements of PCr recovery. Extrapolating from our results, we suggest clinical measurements be made after brief exercise of sufficient intensity and duration to cause a 50–60% decrease in PCr without incurring significant intracellular acidosis.

CHAPTER 4
Estimation of skeletal muscle fiber distributions by phosphocreatine transient analysis

Introduction

Numerous parameters derived from *in vivo* phosphorus nuclear magnetic resonance spectroscopy or proton magnetic resonance imaging have been proposed to non–invasively estimate mammalian muscle fiber–type distributions. For example, it has been long recognized inter–fiber pH heterogeneity best explains the line broadening of the inorganic phosphate (Pi) peak in a ^{31}P–NMR spectrum (66, 208, 290). This phenomenon has been exploited in several studies whereby Pi peak splitting is observed to occur after intense exercise and has been interpreted as a differential pH response due to differential recruitment of at least two distinct fiber type populations in human mixed muscle (1, 236, 302, 303). In other studies, Pi peak splitting has not been documented in a majority of subjects studied (21, 149), especially if the subjects are endurance athletes (236, 324). It would appear reliable and repeatable estimation of fiber type distributions in diverse subject populations based upon Pi peak splitting is questionable.

It has also been proposed that fiber type distribution be non–invasively estimated by examining steady–state ratios of ^{31}P–NMRS metabolites at rest or during exercise. Blei et al. has shown a negative correlation between the global NMR–derived ATPase rate–presumably mirroring a global histochemically determined ATPase rate–and resting Pi/ATP in human forearm muscle. They did not find a correlation between ATPase rate and resting PCr/ATP (26). Using spatial localization in rat leg muscle it has been shown that superficial regions (high ATPase activity, low oxidative capacity) have a lower resting Pi/ATP ratio than deep regions (lower ATPase activity, higher oxidative capacity). There was no superficial—to–deep gradient observed for the resting PCr/ATP ratio (46). In

contrast to these studies, Takahashi et al. found a much stronger positive correlation between resting PCr/ATP and % Type II fibers than between resting Pi/ATP and % Type II fibers (288). These findings were indirectly supported by an earlier study which showed sprinters–with presumably higher percentages Type II fiber population–had higher PCr/ATP ratios in their gastrocnemius than sedentary controls or an endurance athlete (29).

Results from ^{1}H–MRI studies have also been generally equivocal. While some investigators have shown a correlation between % Type I fibers and the longitudinal relaxation time, T_1, (145) and no correlation between % Type I and the transverse relaxation time, T_2, (145, 288), others have shown no dependence of T_1 on fiber type yet observed slow–twitch fibers have longer T_2 values than fast–twitch fibers (89).

Since the time constant of the exponential PCr recovery after a single work–to–rest step–change is proportional to the relative oxidative capacity of the working muscle (153, 203, 234, 290) examining PCr transient behavior has been another popular approach toward non–invasive estimation of fiber type distribution (26, 200, 217, 296, 308). Unlike the previously mentioned techniques above, there has been generally consistent agreement among different investigators, including those who assay muscle biopsies (274), regarding the accuracy and reproducibility of this method. An interesting corollary to this approach is it may be possible to identify the proportion and relative oxidative capacity of two or more fiber populations in mixed muscle by extracting the amplitude and duration of the exponential components comprising the global NMR–derived PCr recovery time constant. In theory, these components should roughly correspond to the widely–cited histochemical fiber type categories of Type I versus Type II or Fast–Oxidative–Glycolytic versus Fast–Glycolytic versus Slow–Oxidative.

It has been well established that rat leg musculature has considerably more

intra–muscle (i.e. fiber type) and inter–muscle heterogeneity with respect to metabolic capacity (8) and mechanical performance (319) than human muscle (83, 261, 272). Given these observations, the primary objective of this study is to decompose the components of high signal–to–noise exponential PCr recovery transients in an attempt to unambiguously identify the distribution of distinct fiber populations based upon relative oxidative capacity in the rat leg. A secondary objective of this study is to document the pattern of temporal changes in PCr, pH, and isometric force during a prolonged bout series of stimulation–recovery cycles. This is done to determine whether the cyclic temporal changes are sufficiently disparate to compromise the interpretation of gated–NMR experiments in which increased signal–to–noise is achieved by adding spectra acquired at identical time points during repeated stimulation cycles. Lastly, the results of this study are unique in that they illustrate the utility of Principal Component Analysis for routine processing of very large NMR datasets.

Methods

Animal care and feeding

Adult male Sprague–Dawley rats (300–400g); Harlan Sprague Dawley Inc., Indianapolis, IN) were housed three per cage in a temperature (≈22°C) and humidity (≈35%rh) controlled room on a 12:12 hour light–dark cycle. Rats were provided Purina Rat Chow and tap water *ad libitum*. All experiments were performed during the rat's nocturnal cycle.

Muscle surgical protocol

Rats were anesthetized with sodium pentobarbital (ip: 50 mg/kg body mass), and an intraperitoneal catheter was inserted for administering additional anesthetic (5mg/kg) at approximately 30 minute intervals. The rats were prepared for *in situ* stimulation of the right leg on a custom built ^{31}P–NMR probe as previously described (204). A photograph is provided in Appendix A– ^{31}P–NMR Probe. In

brief, the right sciatic nerve of the supine rat was cut and placed in a bipolar platinum electrode, and the right knee was fixed between two brass posts using an 18G needle bored through the distal head of the femur. A 20lb–test braided filament fishing line was threaded through the space between the Achilles tendon and the distal fibulo–tibular symphysis and then tied to a half–bridge microfoil strain gauge force transducer mounted on an adjustable support in the probe. Adjustment of this mount nestled the right posterior leg within a 2.0 cm diameter saddle–shaped surface coil as shown in Appendix B– Leg Cross–Section. Muscle length was optimized to give a maximal isometric twitch in response to a supramaximal square–wave pulse (10–20V amplitude, 2ms duration, Grass stimulator model S48). Passive tension averaged 200–300 grams. Steady–state isometric twitch force of the hindlimb was recorded (Gould recorder model 2200S) at 1 mm/sec chart speed and 500 grams/cm sensitivity. The probe was ventilated with 100% oxygen. Since the experiments lasted between 1–10 hours, depending on stimulation protocol, the body temperature was continuously monitored via a rectal thermistor (YSI probe model 402A) and maintained between 37°–39°C by modulating the magnet bore air temperature with a warm–air blower using a feedback–controller (YSI controller model 73A). This method of maintaining body–temperature homeostasis was shown to satisfactorily maintain the posterior leg intra–muscle temperature around 37°C in a separate supplemental experiment summarized in Appendix C–Temperature Homeostasis. At the end of the experiment the stimulated posterior leg muscle group was immediately removed and weighed so force measurements could be expressed as gram force per gram wet muscle.

Stimulation–Recovery protocol

Rats were divided into three "treatment" groups based upon stimulation frequency (Table 6). The stimulation frequencies chosen are known to be well

within (0.75Hz) or above (2.0Hz and 5.0Hz) the aerobic capacity of rat leg muscle based upon measurements of steady–state oxygen consumption relative to maximum oxygen consumption (142). Data from pilot experiments permitted the recovery duration to be chosen to ensure intracellular pH reliably recovered to a resting value of approximately 7 prior to the next stimulation period. Note the number of rats and number of cycles reported in Table 6 was chosen based on the convenience obtained from analyzing a balanced statistical design and the fact all rats were able to endure at least eight cycles without equipment malfunctions, computer memory limitations, or other anomalies. A complete portrayal of the number of rats per cycle number can be found in Appendix D–N vrs. Cycle Number.

Table 6: *Treatment groups*

Stimulation frequency (twitches/second)	**0.75Hz**	**2.0Hz**	**5.0Hz**
Number of rats	7	7	7
Minimum number of contiguous stimulation–recovery cycles per rat	8	8	8
Stimulation duration in one cycle (minutes)	5.7	5.3	2.1
Recovery duration in one cycle (minutes)	5.7	16.0	29.9

Spectral acquisition parameters

^{31}Phosphorus–NMR spectra of the right posterior leg were acquired at 162MHz on a 89mm diameter, vertical–bore, Bruker AM400, 9.4 tesla spectrometer as previously described (234), except a 2cm saddle–shaped surface coil was used to sample a larger population of fibers (Appendix B– Leg Cross–Section). The transceiver coil was tuned to resonate at 162MHz and impedance matched to 50 Ω for maximum power transfer immediately prior to placing the probe (with the rat head–down) in the magnet bore. Rat's head was down. The B_0 field was shimmed on the proton signal from muscle water to a line width of 50–75Hz. The B_1 radio frequency pulse width was set to 20–25μseconds to optimize the signal–to–noise

Table

ratio for the given interpulse interval (Table 7). (Note: The B_0 field is the constant magnetic field of the superconducting 9.4T magnet; the B_1 field is the magnetic component of the electromagnetic wave emitted by the radiofrequency transmitter coil.) The total seconds per block in Table 7 represents the time over which the partially saturated phosphorus spectra were continuously acquired and averaged to generate individual time points during and after the isometric twitch stimulation periods.

Table 7: *NMRS Acquisition parameters*

Stimulation frequency (twitches/second)	**0.75Hz**	**2.0Hz**	**5.0Hz**
NS–number of spectra in one block = number of spectra signal averaged together per single time point	16	32	16
TR– interpulse interval (sec.) = total seconds required to acquire a single spectrum = relaxation delay+pulse width+acquisition time	1.33	1.00	1.00
Total seconds per block (NS x TR)	21.33	32.00	16.00
Number of blocks acquired during one stimulation period in one cycle	16	10	8
Number of blocks acquired during one recovery period in one cycle	16	30	116

Pulse acquisition (8064Hz sweep width, 1K complex data) was gated to periods immediately before or at least 100 milliseconds after a twitch contraction in order to minimize motion artifacts. Before the start of each experiment a single fully relaxed control spectrum of the resting muscle was acquired (TR = 15 seconds, 16 scans).

Spectral processing

The summed free induction decays (FIDs) were zero–filled to 2K complex data and multiplied by (i.e. convolved with) a monotonically decreasing exponential function in the time domain before Fourier transformation. This results in a 20Hz linewidth broadening in the frequency domain. Each spectrum (approximately

17,000 in total) was phase corrected and frequency corrected based upon the Principal Component Analysis (PCA) method of Brown and Stoyanova (33, 281).

> What is Principal Component Analysis? (*from discussions with R. Stoyanova, Fox Chase Cancer Center, May 1998*)
>
> PCA is a multivariate data analysis technique for decomposing large datasets along the axes of its largest variations. These axes are estimated as the eigenvectors of the data–covariance matrix and are called principal components (PCs). The PCs are ranked by their contribution to the total variance in the dataset. If there are N variables of interest in an experiment, each PC represents a linear combination of the degrees of freedom of the N–dimensional data set. The first principal component, PC1, explains the largest amount of variance. The second principal component, PC2, is orthogonal to PC1 and explains the second largest amount of variance. That is, PC2 is related to the maximum amount of residual variability left over after identifying PC1. For example, in NMR spectral analysis, suppose we have a set of spectra, containing a single peak whose amplitude varies as a function of time. Then PC1 reflects the overall lineshape and amplitude of this peak whereas the rest of the PCs will be noise–related and are ignored. If in this dataset, besides the amplitude variations, there are differences in the peak position and phase, then PC2 and the higher order PCs can be used to estimate the amount of the frequency shift and phase shift in each spectrum.
>
> In this study, PCA was utilized to preprocess NMR spectral data by correcting both frequency shifts and phase shifts of each NMR spectrum prior to Fourier Transformation. This preprocessing makes subsequent determination of peak areas and peak shifts much less sensitive to drifting of the B_0–field (rats were typically in the magnet approximately 1–10 hours), fluctuations in the electrical power grid at 5 PM, or systematic operator error in integrating peak areas. The latter has been shown to be a significant source of variability in the *in vivo* NMR literature (209).

Baseline correction was also performed on every spectrum. For each rat in each stimulation protocol, the spectra were added across cycles beginning with cycle #3 to obtain a single high signal–to–noise stimulation–recovery time course of spectra. Cycles #1 and #2 were not included since the PCr and pH time courses were visibly different than the other cycles as shown in the Results. The number of spectra in

the high signal–to–noise stimulation–recovery time courses are 32, 40, and 124 for the 0.75Hz, 2.0Hz, and 5.0Hz frequencies, respectively.

Spectral analysis

For each high signal–to–noise spectrum the relative peak areas were determined using the Method of Natural Lineshapes (MNL) (25, 26, 124). The MNL performs a point by point summation of all the spectra (in this case, all the high signal–to–noise spectra) in a stimulation–recovery series. This generates a single reference spectrum with a natural lineshape unique to each experimental subject. The numerically integrated peak areas of the individual lower signal–to–noise spectra are expressed relative to the single reference spectrum, which in this case has a *very* high signal–to–noise. The advantage of MNL over the more common Lorentzian or Gaussian curve–fitting methods is that it largely removes operator bias in determining the best lineshape to be integrated, is faster, and is at least as accurate. The disadvantage of MNL is that it is not suitable for any resonance peak undergoing significant chemical shifting e.g. inorganic phosphate (124). Intracellular pH was determined by the chemical shift (δ) of Pi relative to PCr at –2.52ppm: pH=6.77+log[(0.89–δ)/(δ–3.19)] (175).

We then applied the Non–Negative Least Squares algorithm (no minimum energy constraint, 200 points within the 1–>500 second time–window) to the PCr time course data. The NNLS algorithm generates a "spectrum" of recovery PCr time constants (i.e. relative amplitude vrs. duration) (112, 184, 313). The height of each peak in the "spectrum" represents the i^{th} ΔPCr term at its corresponding time constant, τ_i. $\Delta PCr_{t=0}$ is the PCr value at the onset of recovery (end–stimulation).

$$PCr(t) = \Delta PCr_{t=0} + \sum(\Delta PCr_i(1-e^{-t/\tau_i}))$$

Equation 1: Multicomponent PCr recovery

(i = 1 to n, where n is determined by the algorithm)

What is NNLS?

In simplistic terms, Non–negative Least Squares analysis is a regression technique conceptually similar to the traditional Least Squares method in that both iterative techniques seek to minimize the collective deviations of individual observations from a user–supplied function (e.g. exponential) between a dependent and independent random variable. In the traditional Least Squares technique the algorithm determines the function's parameters (e.g. time constant duration) for a predetermined number of terms specified by the user. In contrast, the NNLS algorithm does not specify a fixed number of function parameters *a priori* thereby eliminating user bias.

Statistical analysis

All results are reported or plotted as mean±SEM. Prior to comparing means, data (in 24 stimulation frequency (8) x cycle number (3) of "cells") was verified for normality using the Shapiro–Wilks' test and verified for homogeneity of variance with Cochran's *C* test. In virtually all of the 24 cells, both normality and homogeneity of variance were satisfactory. This was based upon the Shapiro–Wilks' or Cochran's *C* test–statistic not reaching the $P < 0.05$ level of significance. The statistical design for comparing means is a balanced two–factor experiment (stimulation frequency x cycle number) with repeated measures on cycle number. In other words, rats–the random effect–are nested in stimulation frequency and repeated in cycle number levels. All pair–wise comparisons of group means for the main effect of stimulation frequency or cycle number were made by Tukey's Honestly Significant Difference test at the $P < 0.05$ level of significance using SPSS v6.1 for Windows.

Results

Cyclic changes in metabolites and force

Figure 7 shows sample ^{31}P–NMR spectra of numerous contiguous stimulation–recovery cycles of individual rats at 2.0Hz or 0.75Hz. The stimulation–recovery protocol and NMR acquisition parameters are detailed in Table 6 and Table 7.

Figure 8, Figure 9, and Figure 10 show the time course of relative PCr changes during the first eight cycles for the 0.75Hz, 2.0Hz, and 5.0Hz rats, respectively. All values in Figure 8 through Figure 10 are reported as percent of initial PCr, where "initial" refers to the resting PCr level at the start of the experiment. Literature values report the range of [PCr] from chemical assays to be approximately 25–30 μmole/g (175). As predicted by a first–order model for the control of oxidative metabolism for submaximal (i.e. 0.75Hz) workloads (203), the PCr exponentially decreased to a new steady–state during stimulation and exponentially increased back to resting levels during recovery. The 2Hz and 5Hz cycles follow a qualitatively similar time course but with visibly higher–order PCr kinetics.

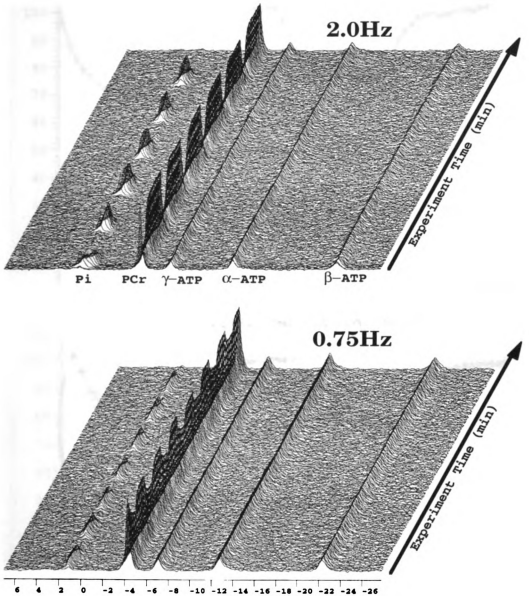

Figure 7: Sample ^{31}P-NMR spectra stackplots

A single spectrum represents the time-averaged behavior of phosphorus metabolites over a period of 32.0 seconds (32 FIDs) for the 2.0Hz rat or 21.3 seconds (16 FIDs) for the 0.75Hz rat. A 5Hz rat, not shown, looks qualitatively similar, but has a much longer recovery and each spectrum represents 16.0 seconds (16 FIDs). X-axis is resonance frequency in parts-per-million (arbitrary scale). Y-axis is resonance amplitude which is proportion to the number of nuclei in a given local electronic environment. Z-axis is increasing experiment time.

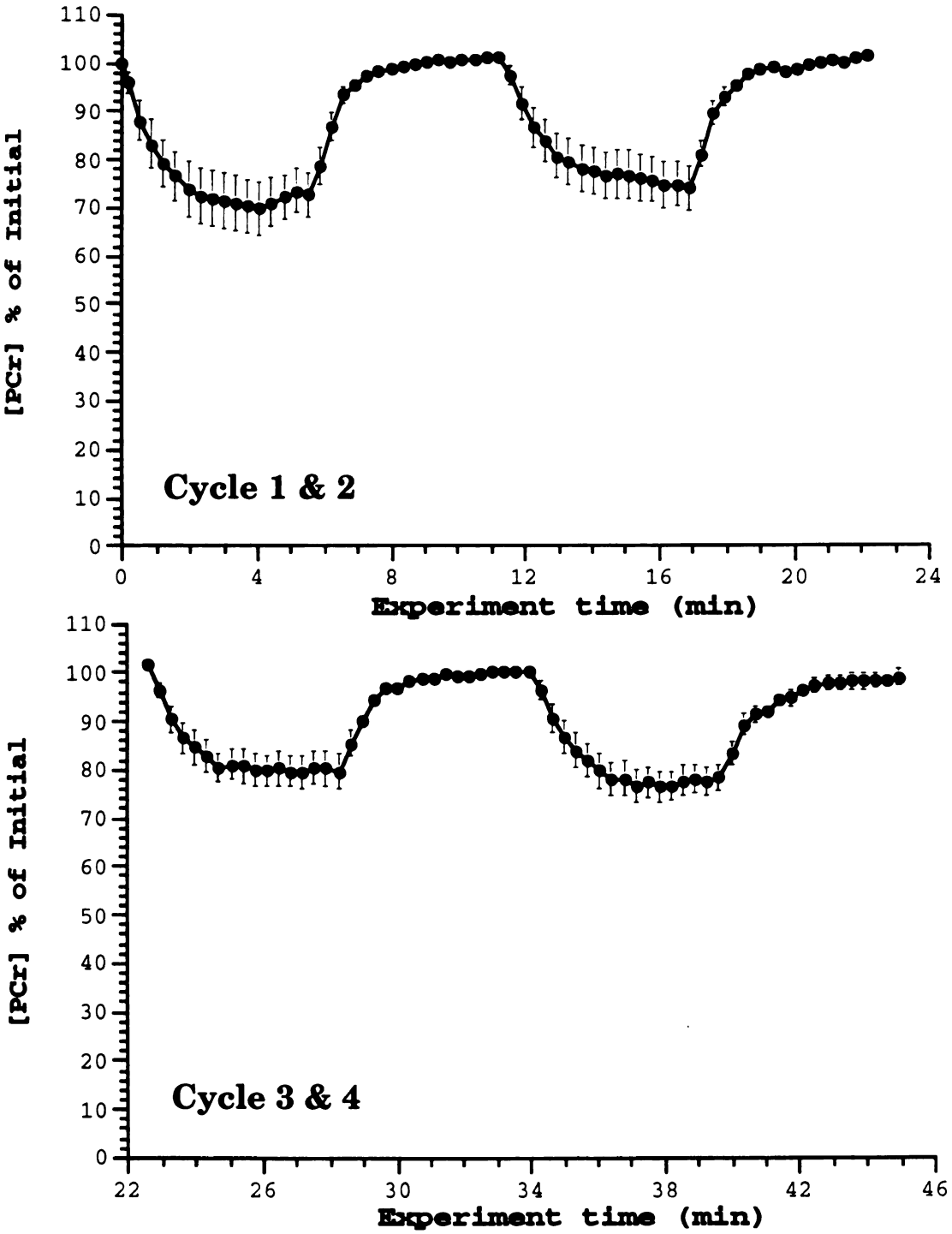

Figure 8: Time course of PCr changes (0.75Hz)

Means±SEM (N=7), one cycle = 5.7 minute stimulation, 5.7 minute recovery

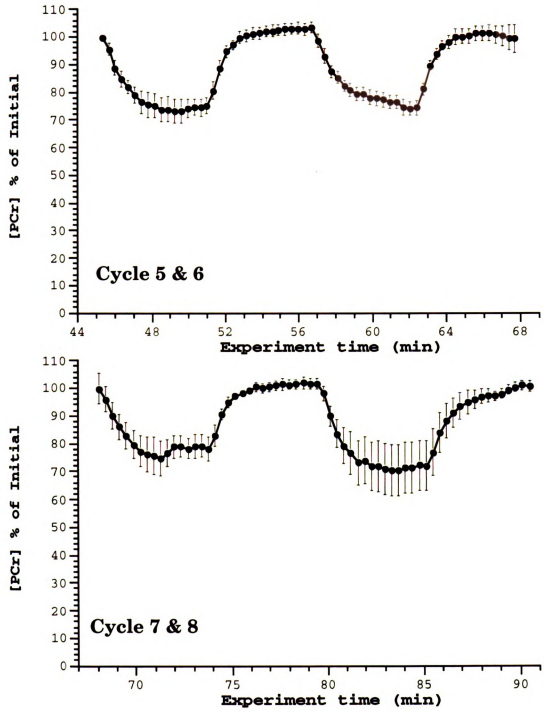

Figure 8 (cont'd): Time course of PCr changes (0.75Hz)

Means±SEM (N=7), one cycle = 5.7 minute stimulation, 5.7 minute recovery

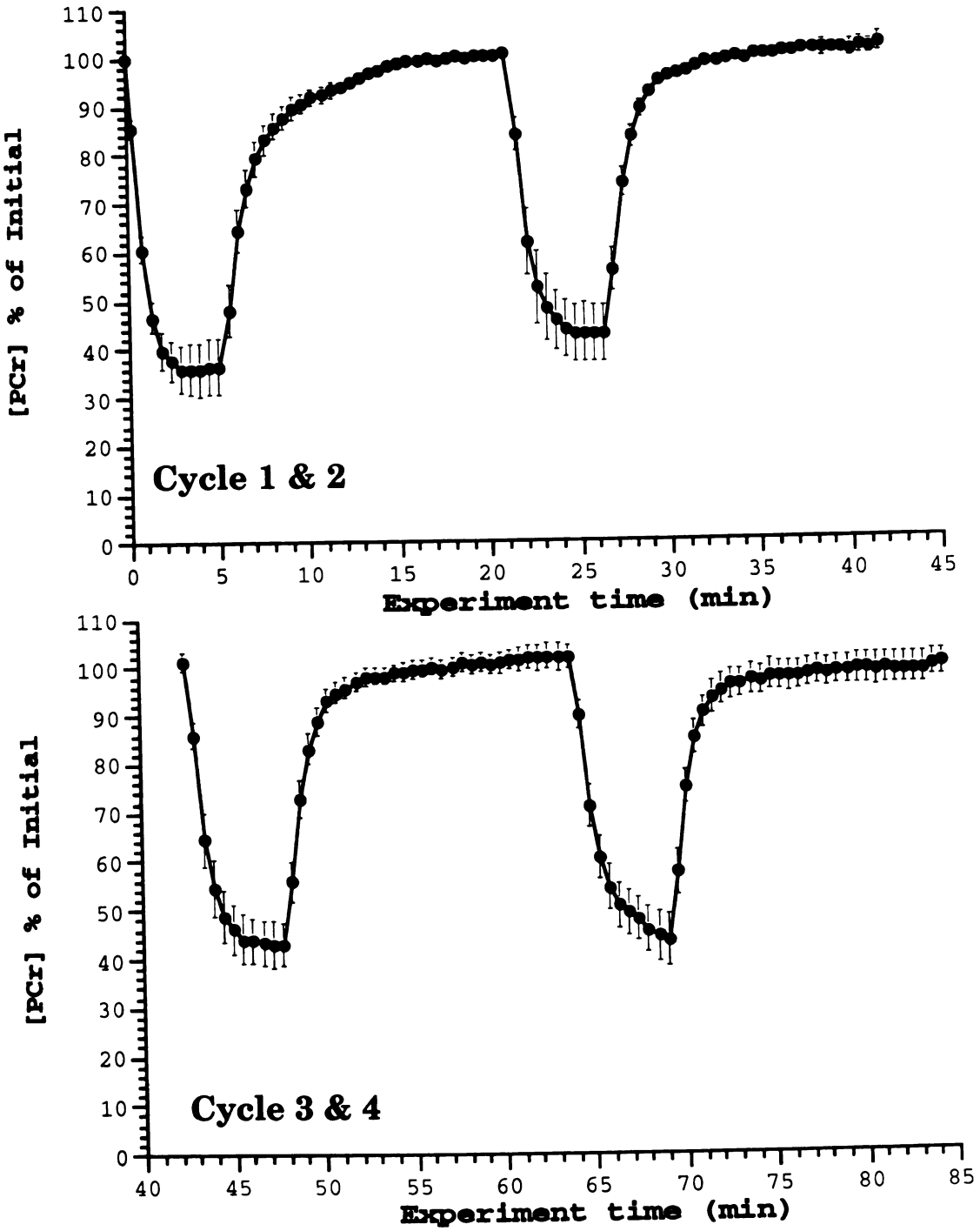

Figure 9: Time course of PCr changes (2.0Hz)

Means±SEM (N=7), one cycle = 5.3 minute stimulation, 16.0 minute recovery

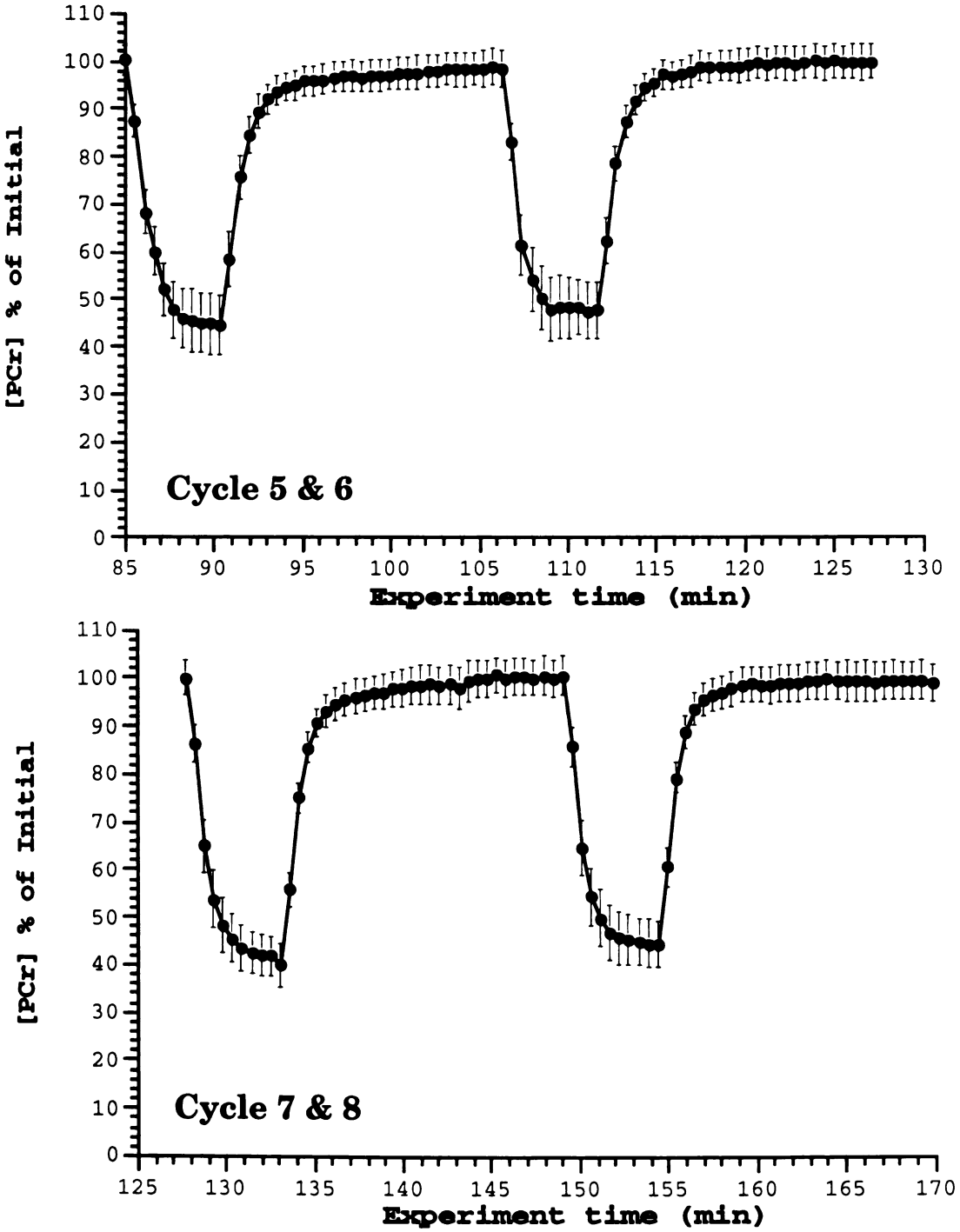

Figure 9 (cont'd): Time course of PCr changes (2.0Hz)

Means±SEM (N=7), one cycle = 5.3 minute stimulation, 16.0 minute recovery

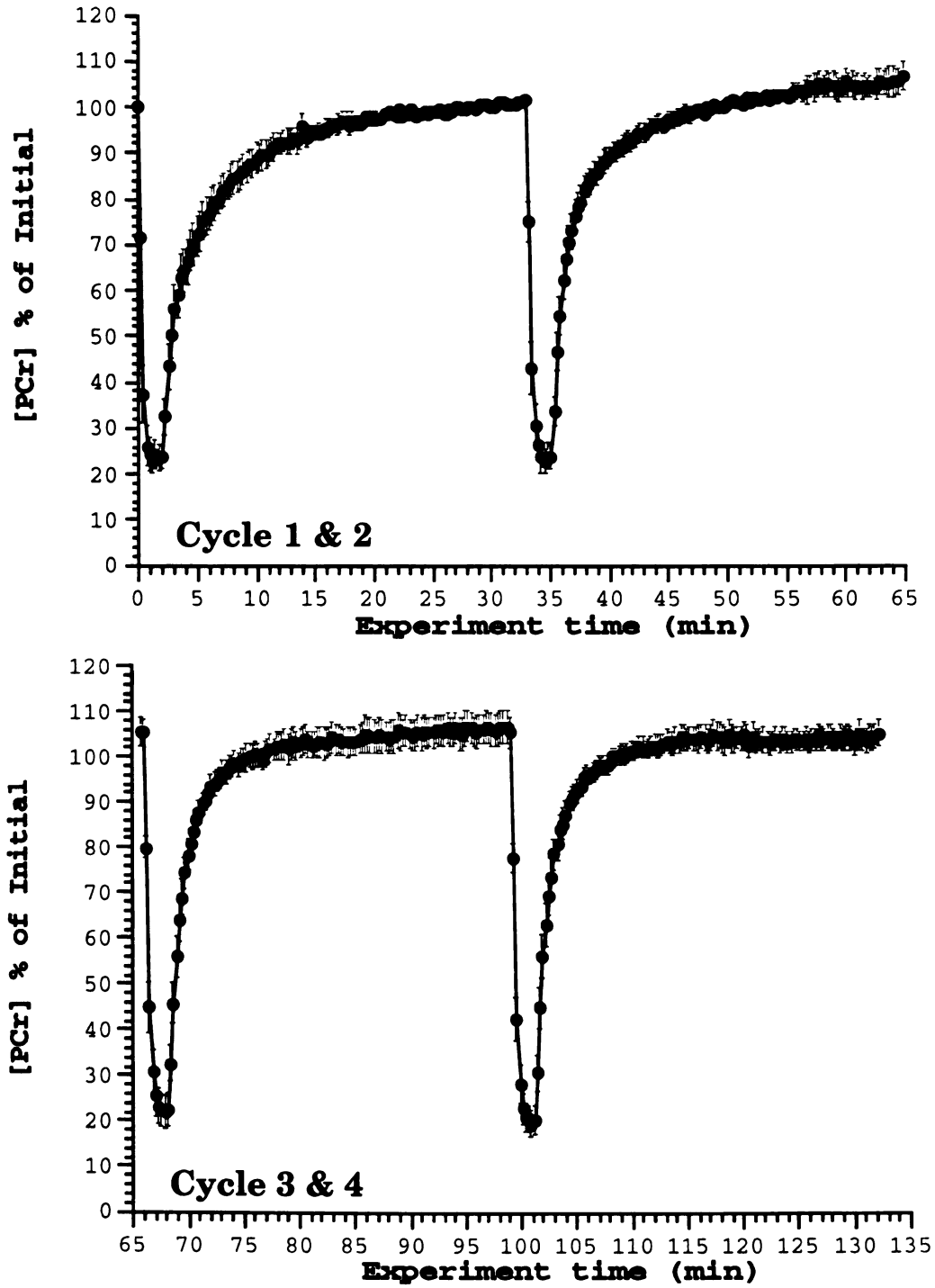

Figure 10: Time course of PCr changes (5.0Hz)

Means±SEM (N=7), one cycle = 2.1 minute stimulation, 29.9 minute recovery

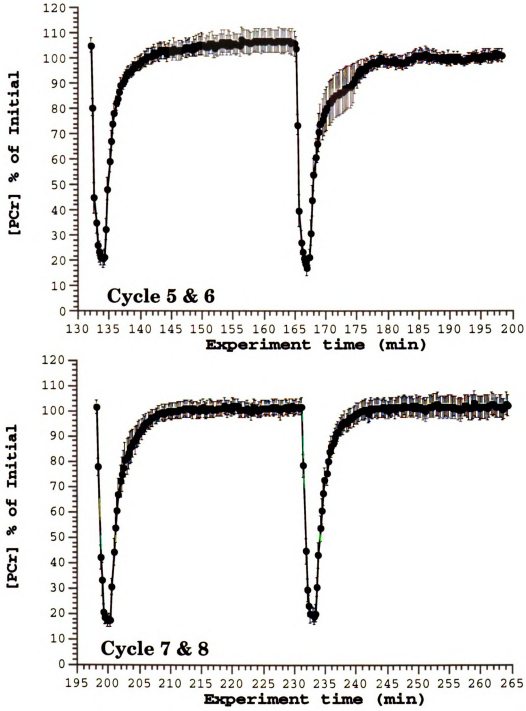

Figure 10 (cont'd): Time course of PCr changes (5.0Hz)

Means±SEM (N=7), one cycle = 2.1 minute stimulation, 29.9 minute recovery

Figure 11A shows the steady–state PCr level (PCr_{ss}) attained during stimulation is proportional to the isometric twitch rate (see also Figure 7). This is consistent with previous studies showing that steady–state mitochondrial oxygen consumption scales with workload (192, 203). (Steady–state during stimulation was taken as the mean PCr level of the last two time points just prior to the onset of recovery for each rat. I considered the last two time points the minimum number of points necessary to attain a quasi–steady–state during stimulation. It is acknowledged that a true steady–state may not have been attained during the 5Hz stimulation.) PCr_{ss} was significantly different ($P < 0.05$) across stimulation rates but not across cycles #1–8. Figure 11B suggests the recovery duration chosen for each stimulation rate was sufficient for complete resynthesis of PCr prior to the start of the next cycle since recovery PCr_{ss} re–attained a value around 100%. (Steady–state during recovery was taken as the mean PCr level of the last four time points just prior to the onset of the next stimulation period for each rat. After visual inspection of each rat's recovery time course, the last four time points during recovery appeared to consistently differ the least from one another. This was taken as evidence of a steady–state.) There were no significant differences across stimulation rate or across cycles #1–8 for recovery PCr_{ss}. For the two or three rats in the 0.75Hz or 2.0Hz groups that successfully completed all 25 cycles (taking five or nine hours, respectively) there was approximately a 10% decline in the recovery PCrss value, independent of the stimulation rate, over the course of the experiment (Figure 11B).

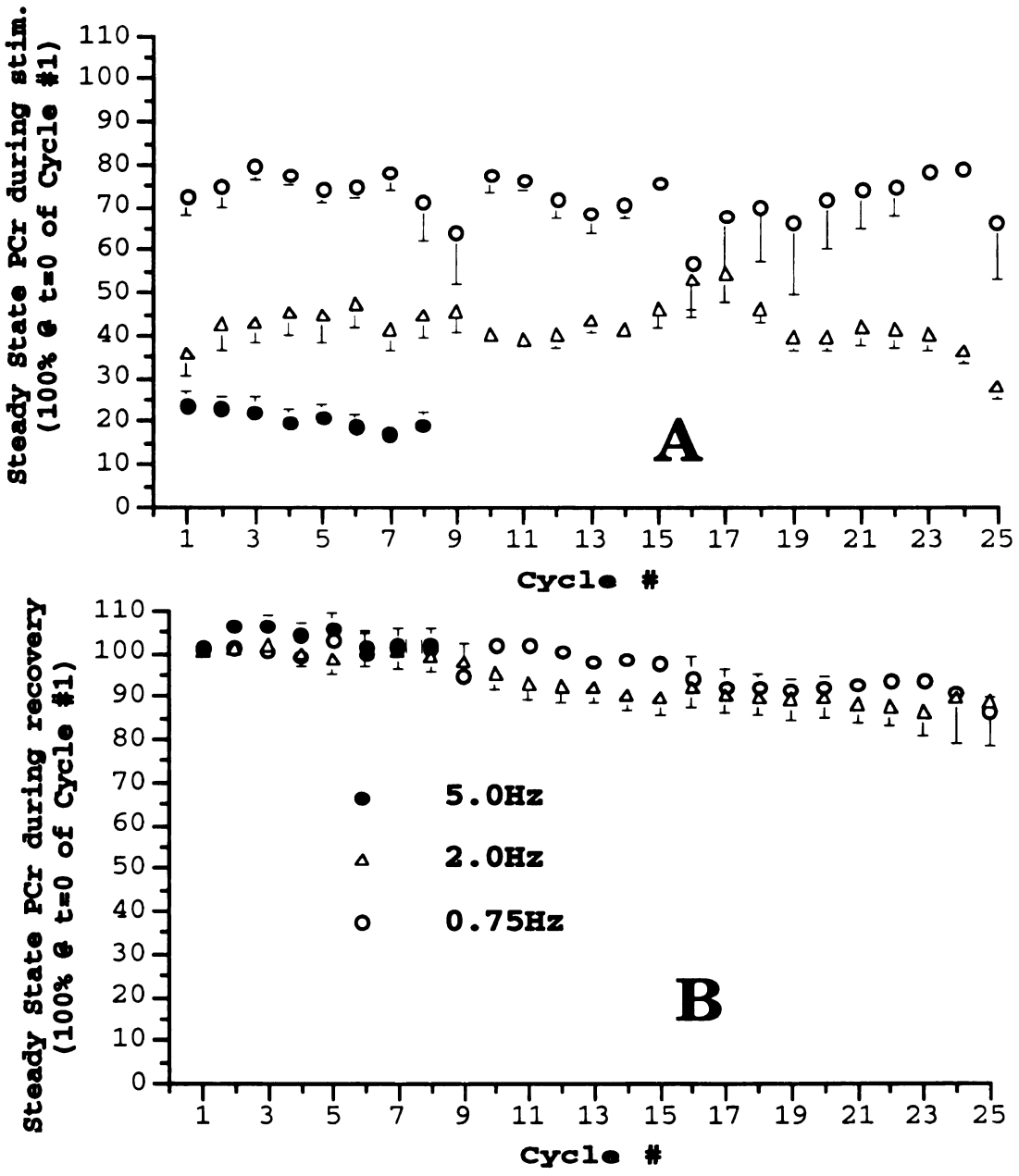

Figure 11: Steady-state PCr characteristics vrs. cycle

Mean±SEM(N=7 through cycle #8–see Appendix D for N vrs. cycle #). Analysis of the first eight cycles showed a statistically significant effect ($P < 0.05$) of stimulation frequency on PCrss during stimulation but not during recovery. There was no effect of cycle number or interaction between cycle number and stimulation frequency on PCrss during stimulation or during recovery.

Figure 12, Figure 13, and Figure 14 show the time course of intracellular (ICF) pH changes during the first eight cycles of the 0.75Hz, 2.0Hz, and 5.0Hz rats, respectively. As best viewed in the 0.75Hz and 2.0Hz rats, there was a transient intracellular alkalinization at the start of the stimulation and a transient acidification at the start of recovery. This transient pH behavior is attributed to net proton consumption by PCr hydrolysis during stimulation or net proton production by PCr resynthesis during recovery (4). Relative to the stimulation time course, the generally larger variance of ICF pH in all recovery time courses is due to operator difficulty in localizing and hence integrating the Pi peak in the NMR spectrum.

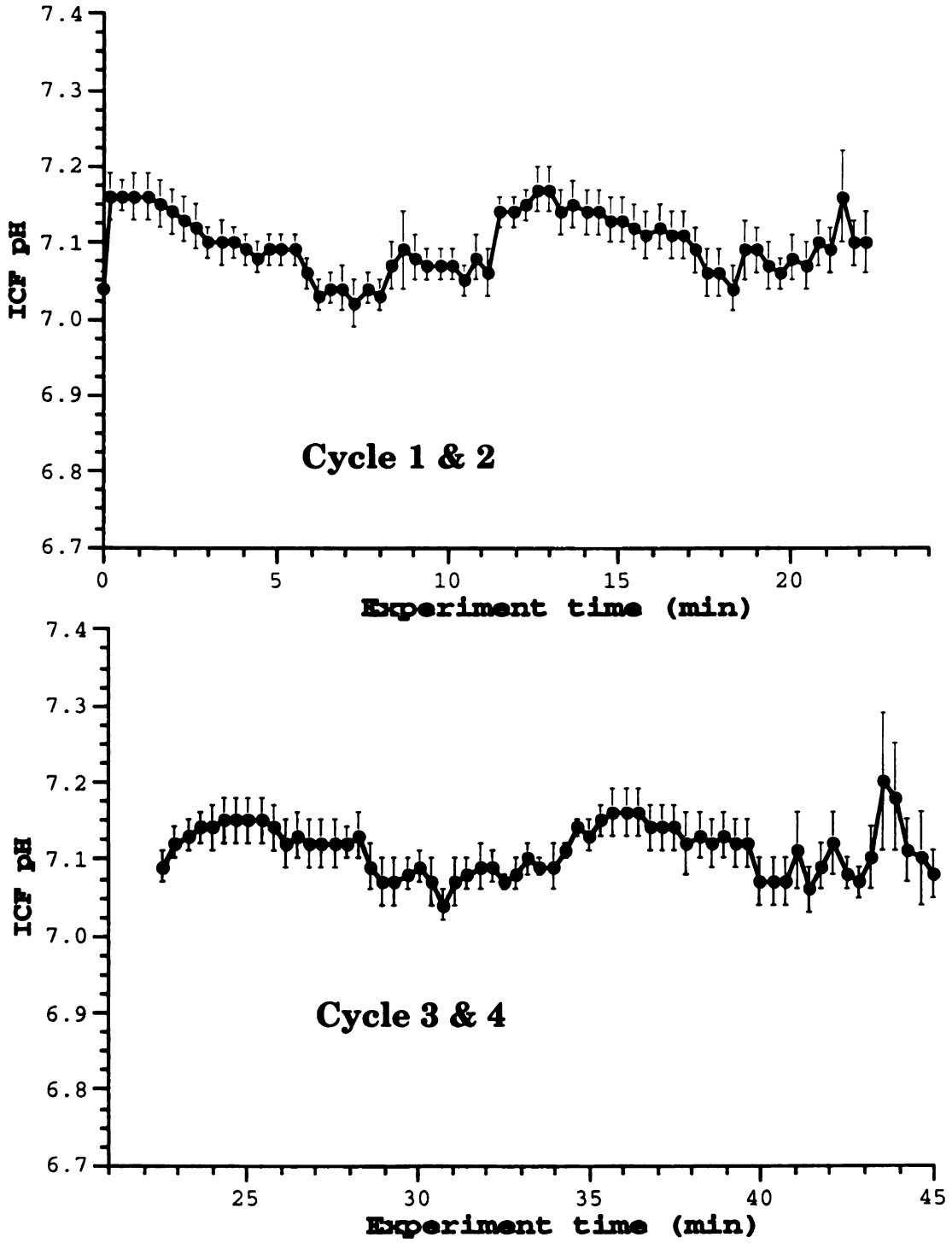

Figure 12: Time course of ICF pH changes (0.75Hz)

Means±SEM (N=7), one cycle = 5.7 minute stimulation, 5.7 minute recovery.

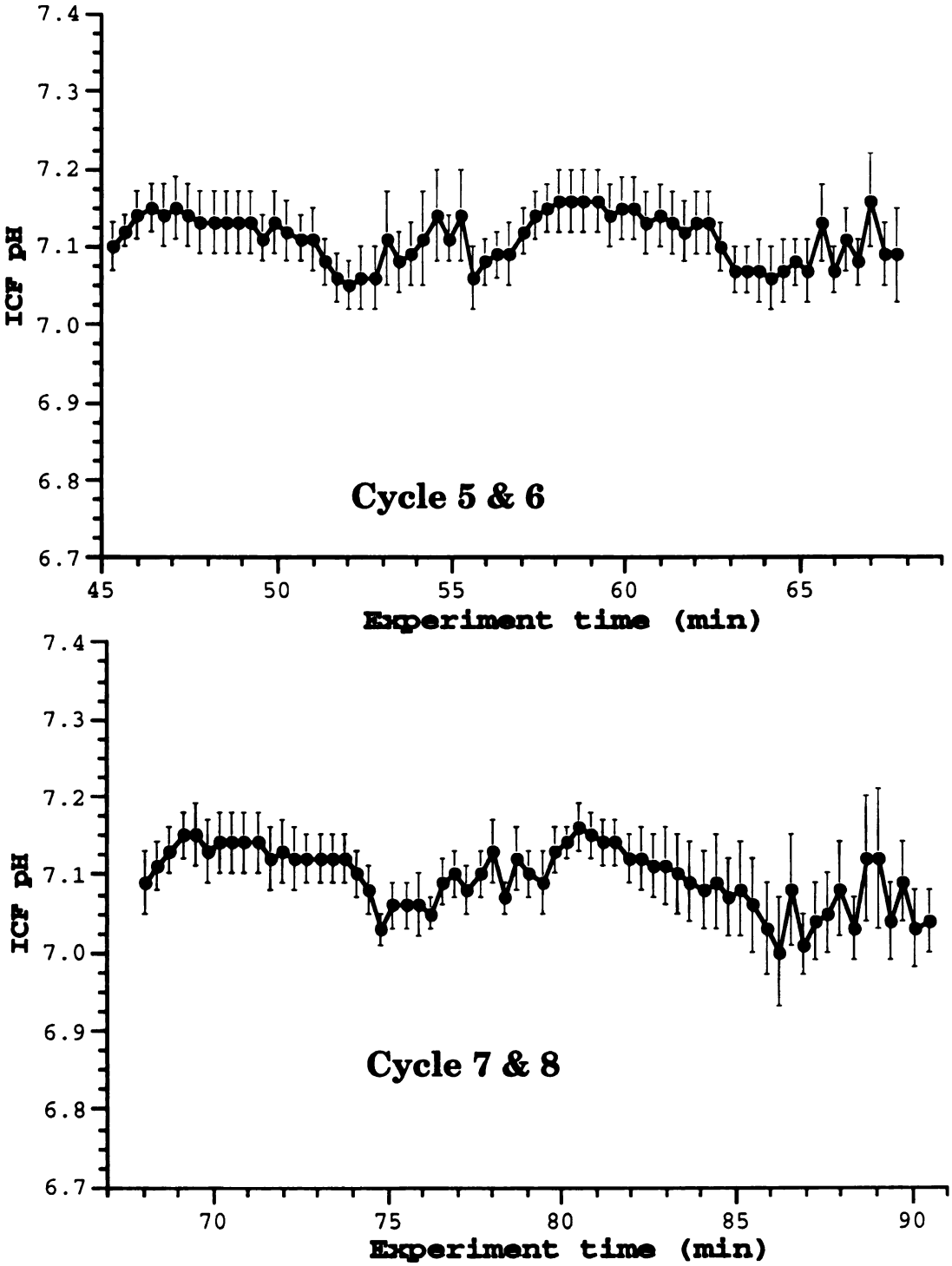

Figure 12 (cont'd): Time course of ICF pH changes (0.75Hz)

Means±SEM (N=7), one cycle = 5.7 minute stimulation, 5.7 minute recovery

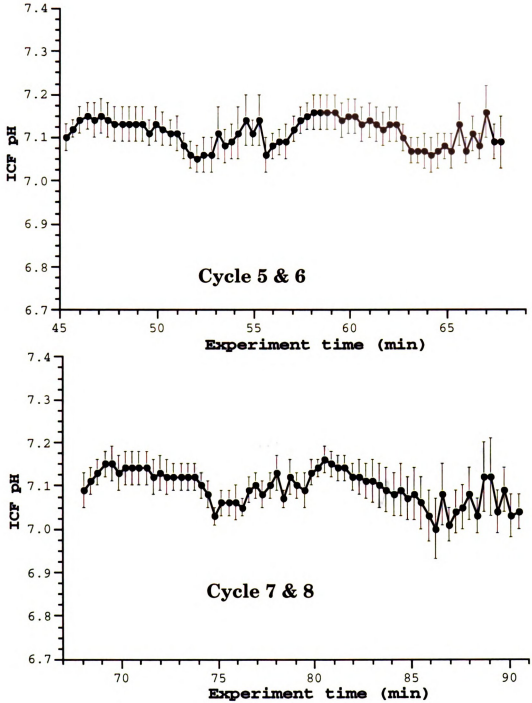

Figure 12 (cont'd): Time course of ICF pH changes (0.75Hz)

Means±SEM (N=7), one cycle = 5.7 minute stimulation, 5.7 minute recovery

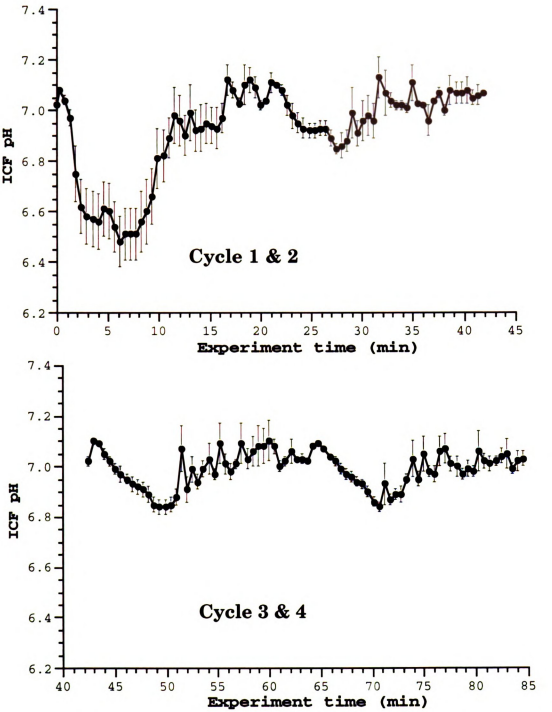

Figure 13: Time course of ICF pH changes (2.0Hz)

Means±SEM (N=7), one cycle = 5.3 minute stimulation, 16.0 minute recovery

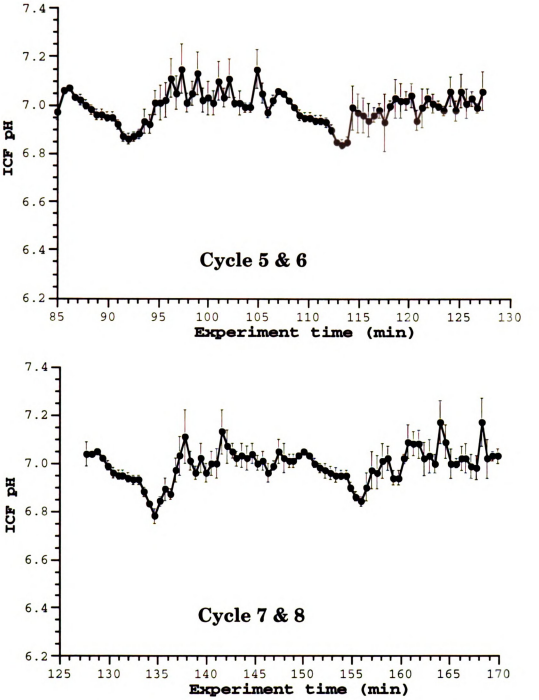

Figure 13 (cont'd): Time course of ICF pH changes (2.0Hz)

Means±SEM (N=7), one cycle = 5.3 minute stimulation, 16.0 minute recovery

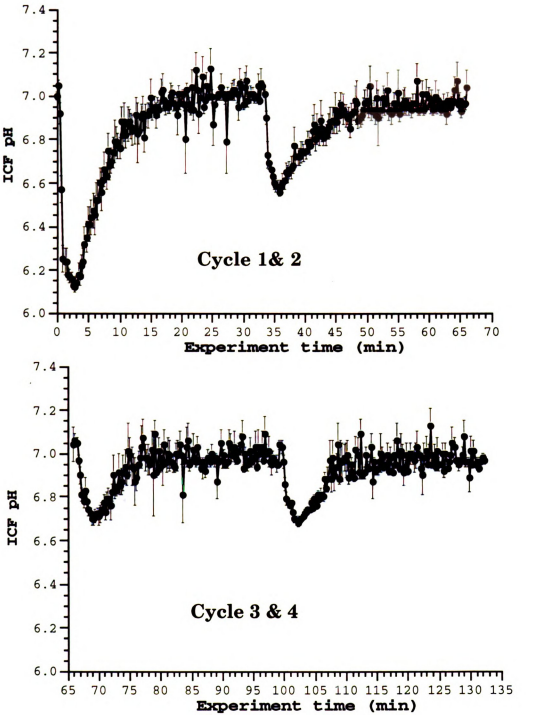

Figure 14: Time course of ICF pH changes (5.0Hz)

Means±SEM (N=7), one cycle = 2.1 minute stimulation, 29.9 minute recovery

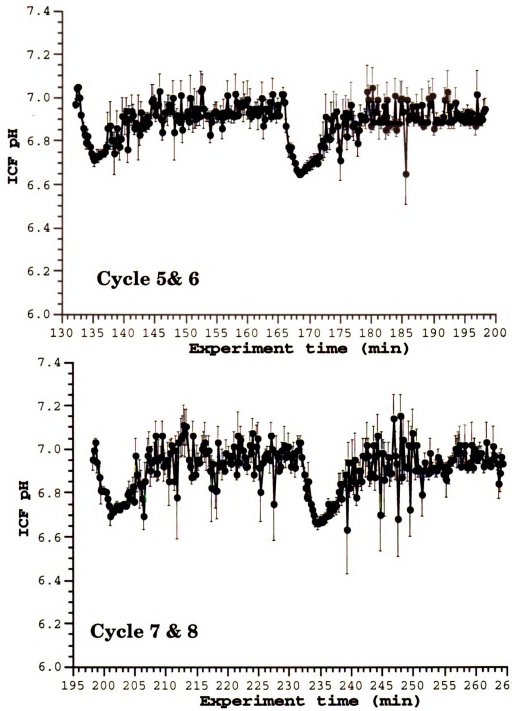

Figure 14 (cont'd): Time course of ICF pH changes (5.0Hz)

Means±SEM (N=7), one cycle = 2.1 minute stimulation, 29.9 minute recovery

Figure 15 shows end–stimulation pH is dependent not only upon stimulation frequency, as expected, but also cycle number. End–stimulation pH was determined from chemical shift between Pi and PCr in the last spectrum acquired before the onset of recovery. The higher stimulation frequencies resulted in lower ICF pH by the end of the stimulation period which is primarily due to increased glycolytic flux producing lactic acid (257, 260).

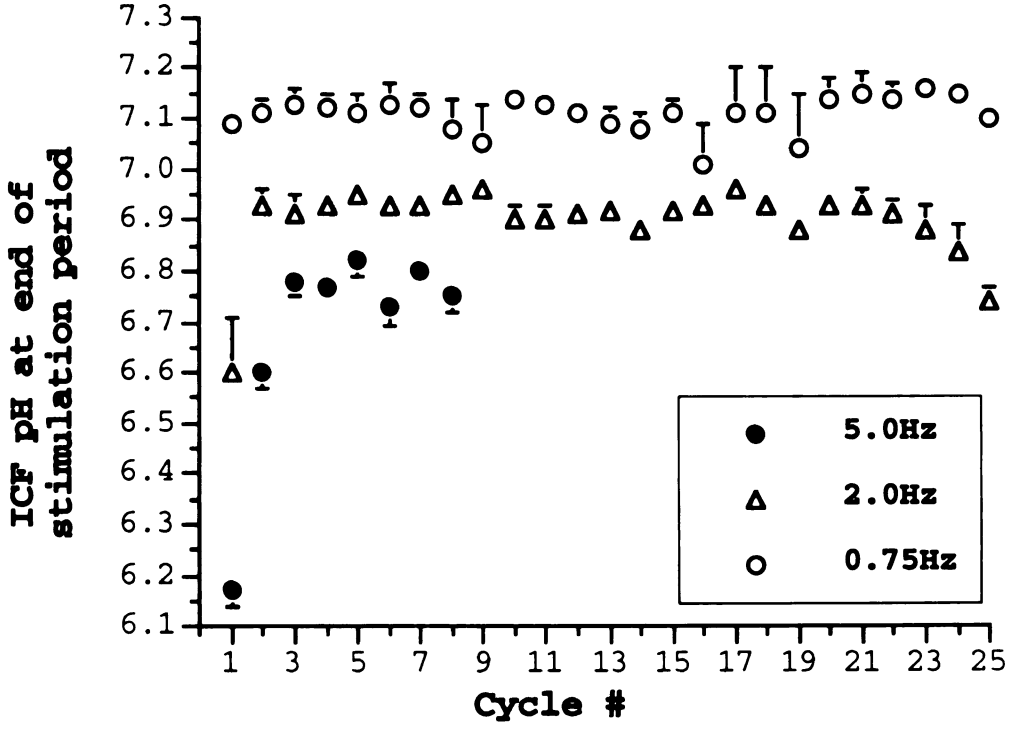

Figure 15: End–stimulation ICF pH vrs. cycle

Means±SEM (N=7 through cycle #8–see Appendix D for N vrs. cycle #). Analysis of the first eight cycles showed a statistically significant effect ($P < 0.05$) of stimulation frequency for a given cycle #. There was also a significant interaction between cycle number and stimulation frequency.

Isometric twitch force normalized per gram wet–weight of stimulated muscle (gastrocnemius–plantaris–soleus group) is shown in Figure 16, Figure 17, and Figure 18. All cycles exhibit a positive staircase phenomenon (the early potentiation of twitch force) which is currently thought to be due to modulation of the myosin regulatory light chain phosphorylation state by rising levels of calcium and/or changes in the microfilament lattice spacing (252). The ripples seen in the 5Hz twitch profiles are a result of brief delays (<5 seconds) in the spectrometer computer's pulse–acquisition sequence due to writing data to the hard disk prior to triggering the Grass stimulator.

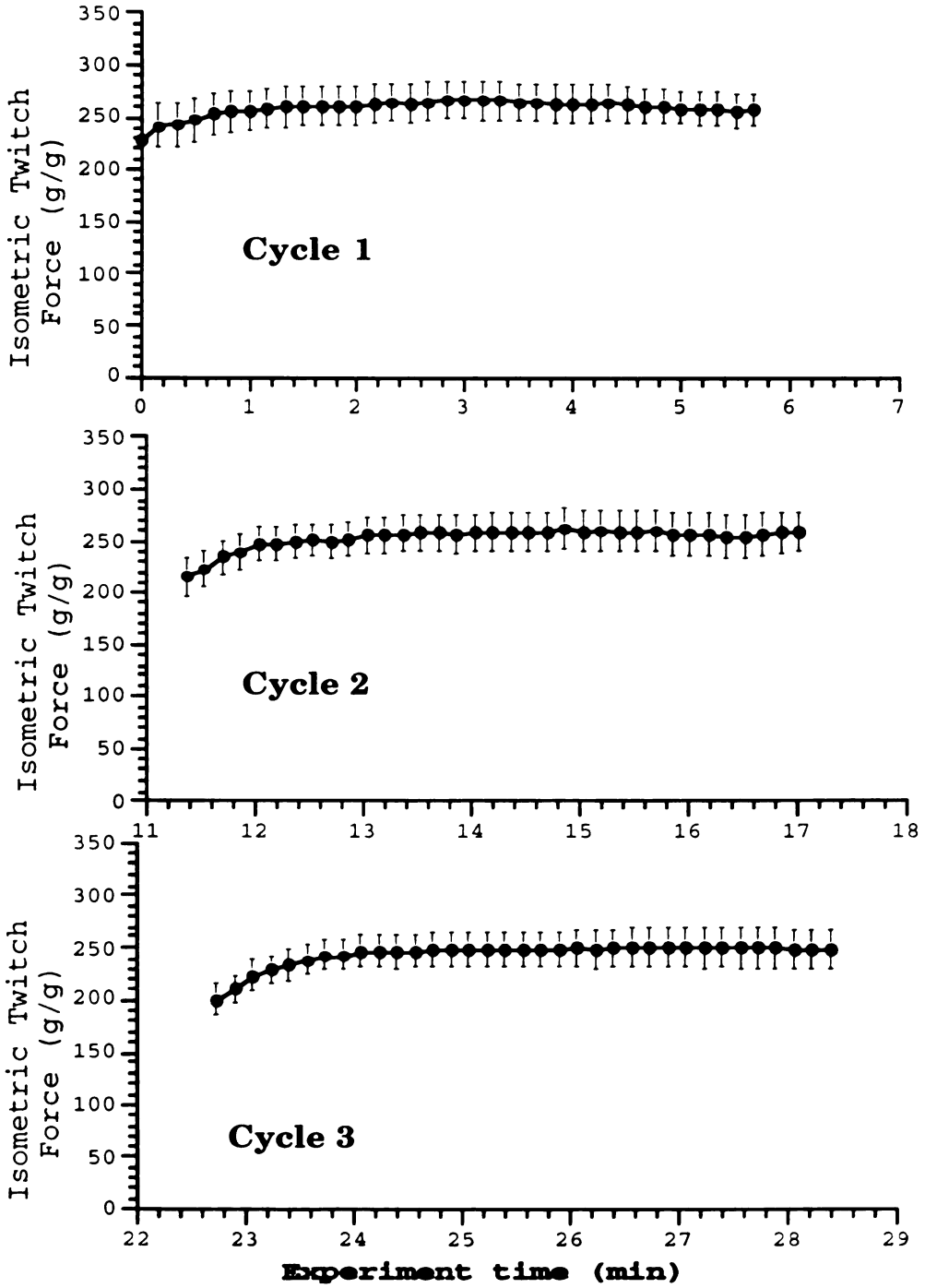

Figure 16: Time course of isometric twitch force (0.75Hz)

Means±SEM (N=7), one stimulation cycle = 5.7 minutes

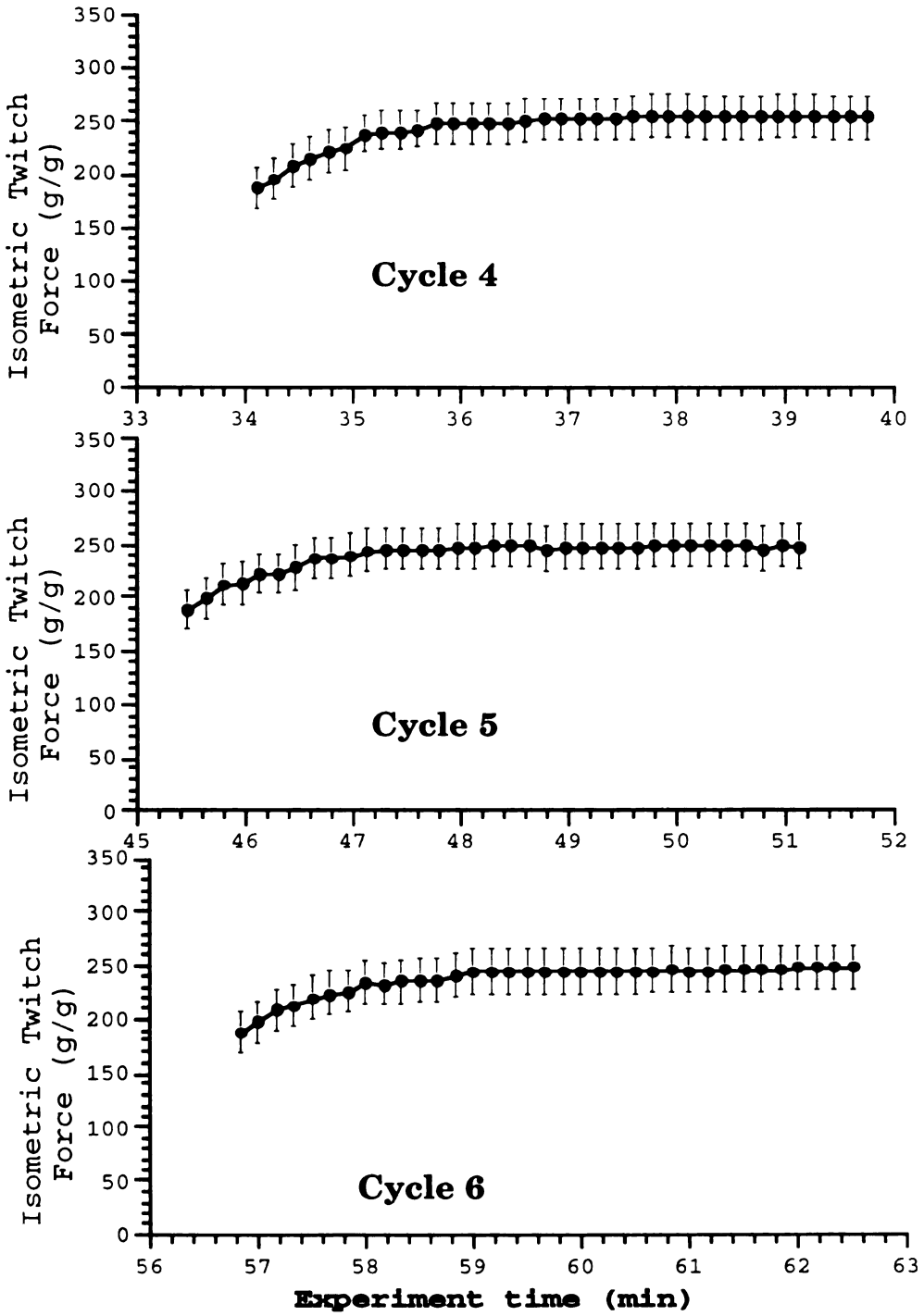

Figure 16 (cont'd): Time course of isometric twitch force (0.75Hz)

Means±SEM (N=7), one stimulation cycle = 5.7 minutes

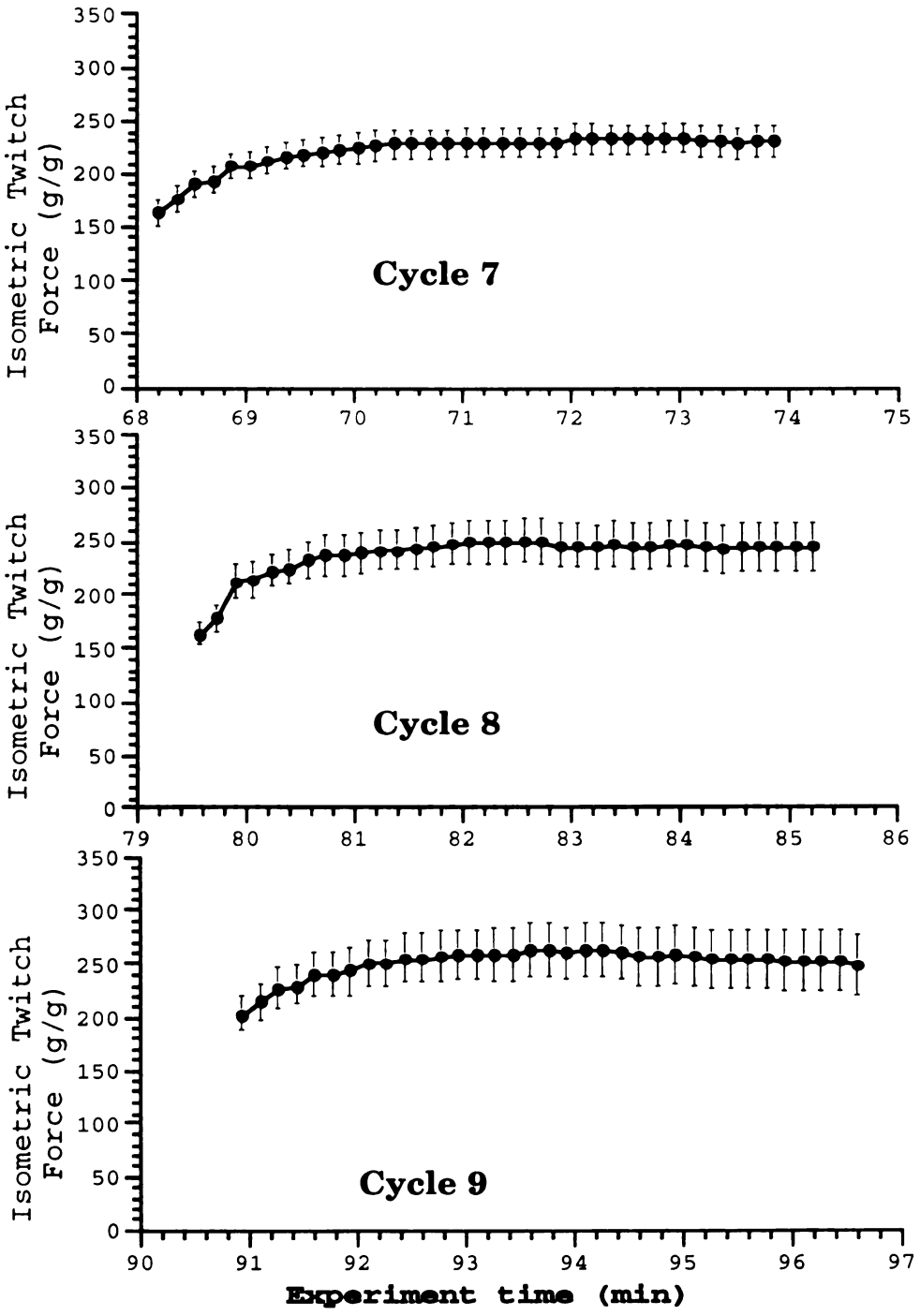

Figure 16 (cont'd): Time course of isometric twitch force (0.75Hz)

Means±SEM (N=7), one stimulation cycle = 5.7 minutes

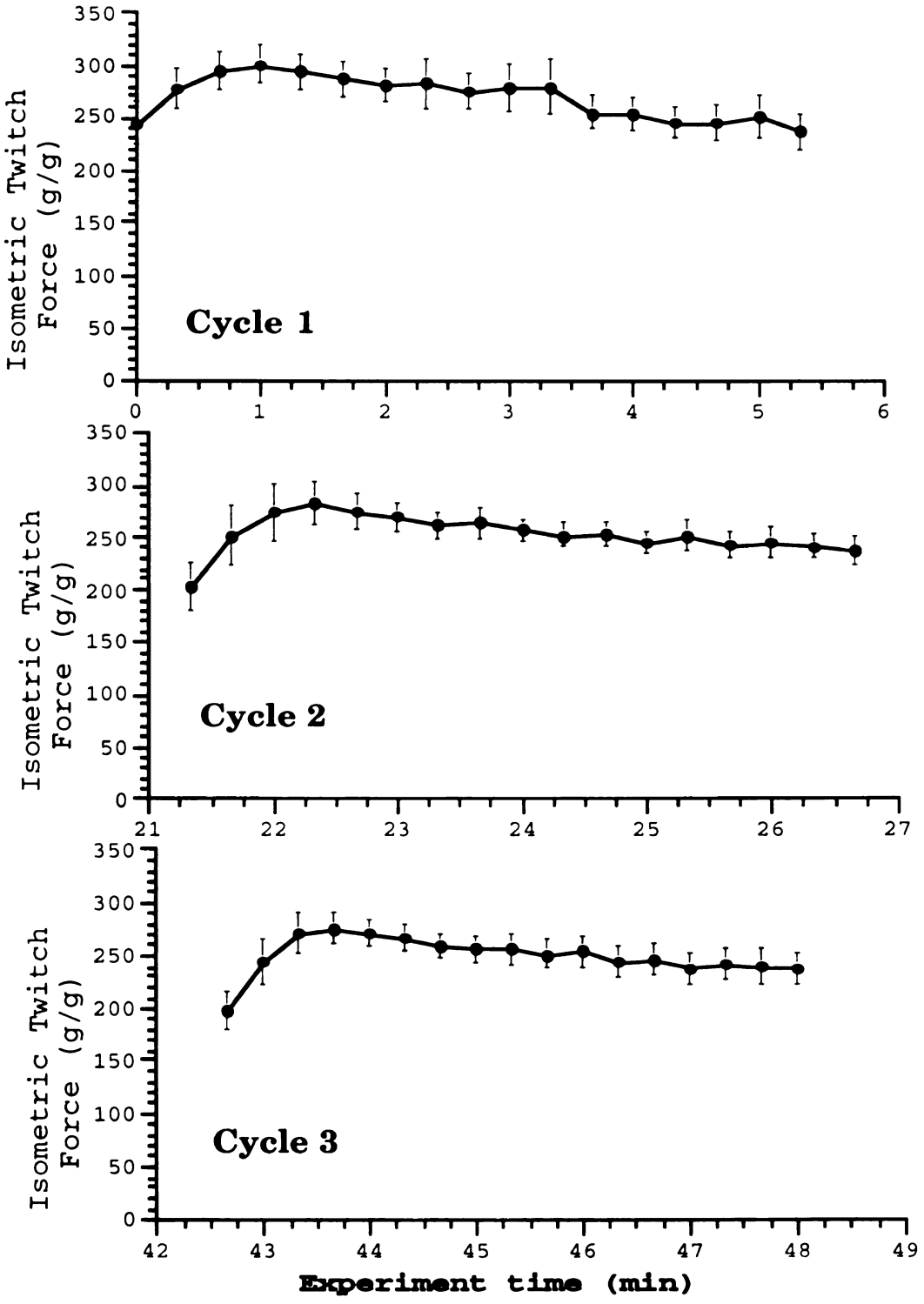

Figure 17: Time course of isometric twitch force (2.0Hz)

Means±SEM (N=7), one stimulation cycle = 5.3 minutes

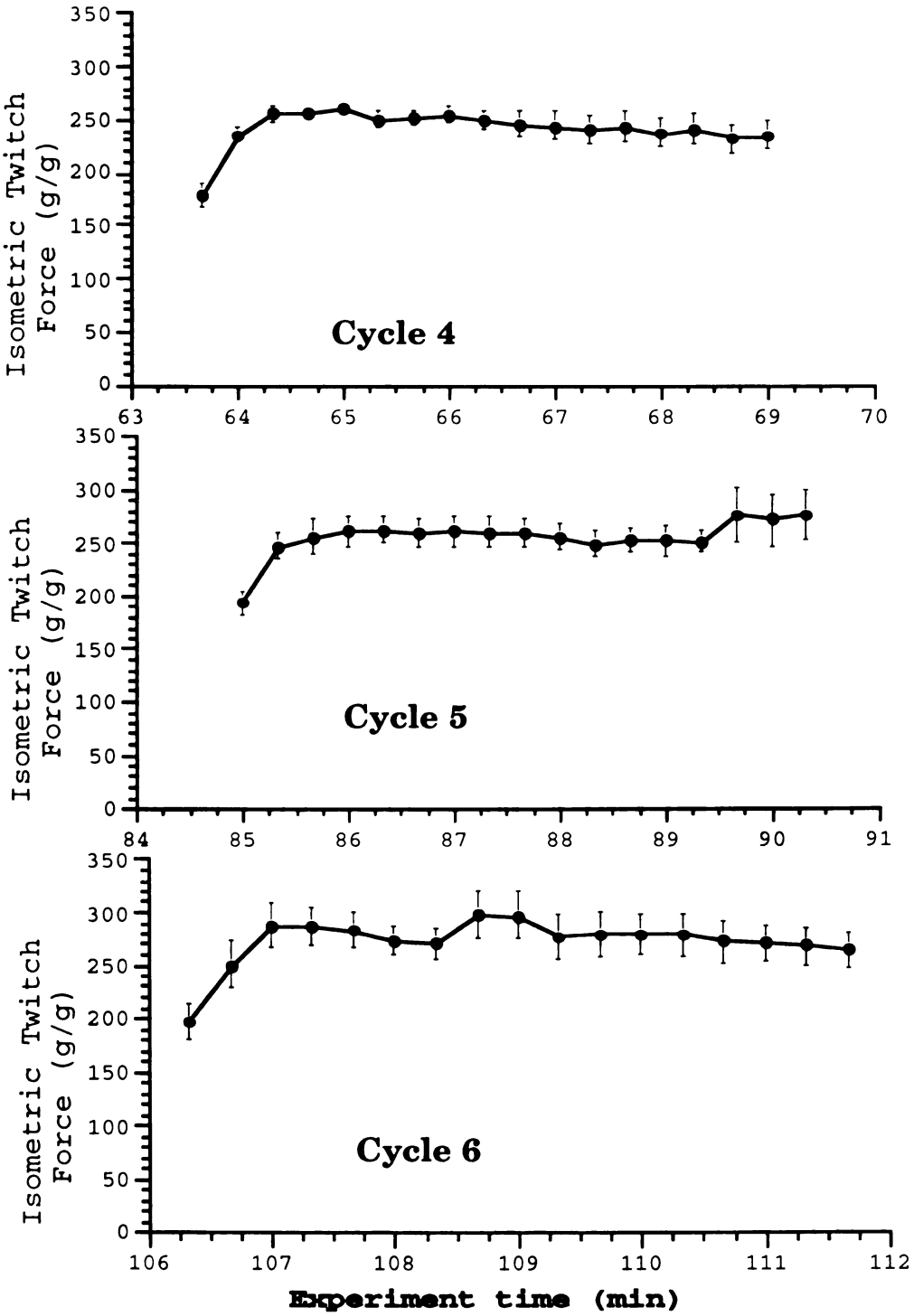

Figure 17 (cont'd): Time course of isometric twitch force (2.0Hz)

Means±SEM (N=7), one stimulation cycle = 5.3 minutes

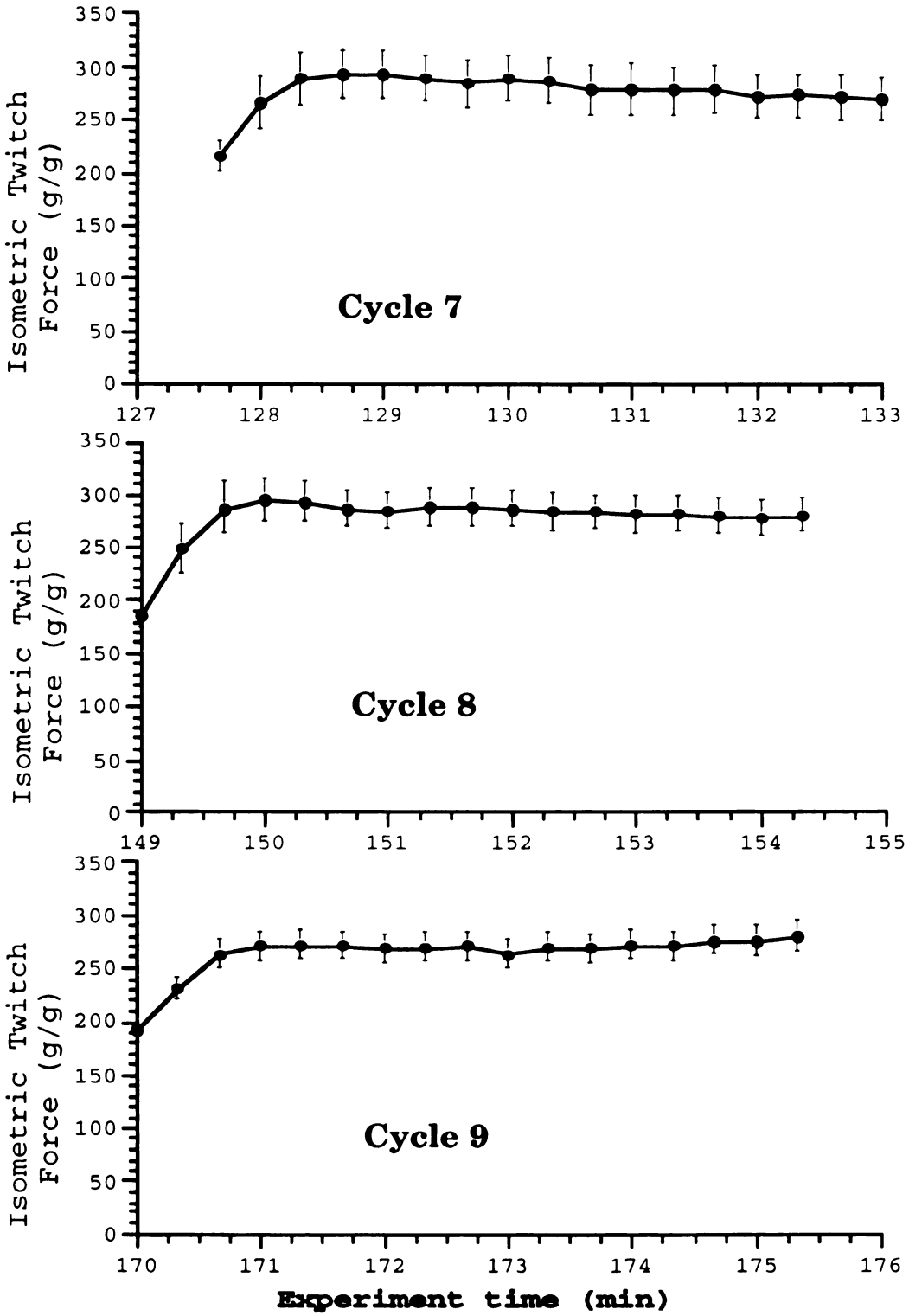

Figure 17 (cont'd): Time course of isometric twitch force (2.0Hz)

Means±SEM (N=7), one stimulation cycle = 5.3 minutes

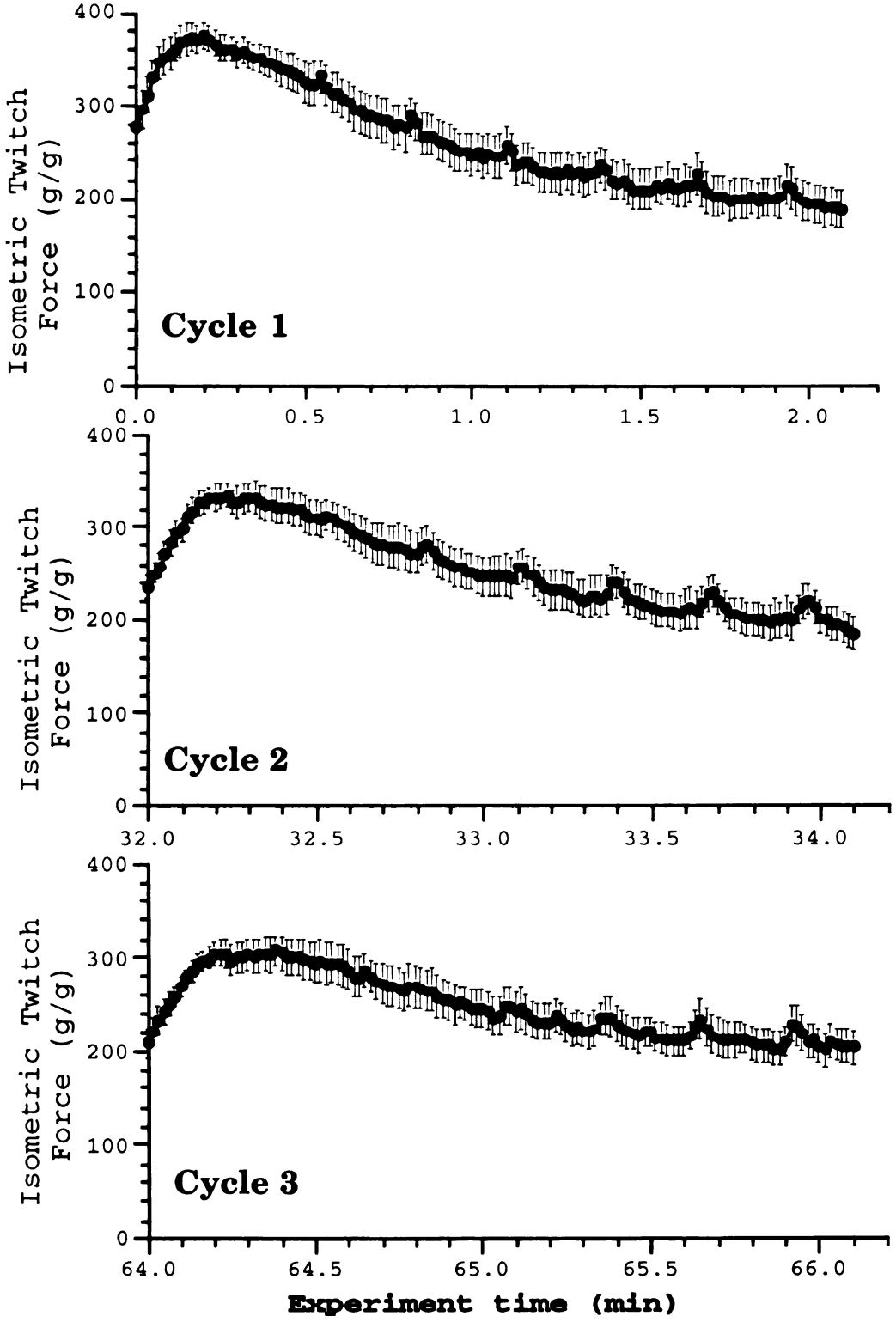

Figure 18: Time course of isometric twitch force (5.0Hz)

Means±SEM (N=7), one stimulation cycle = 2.1 minutes

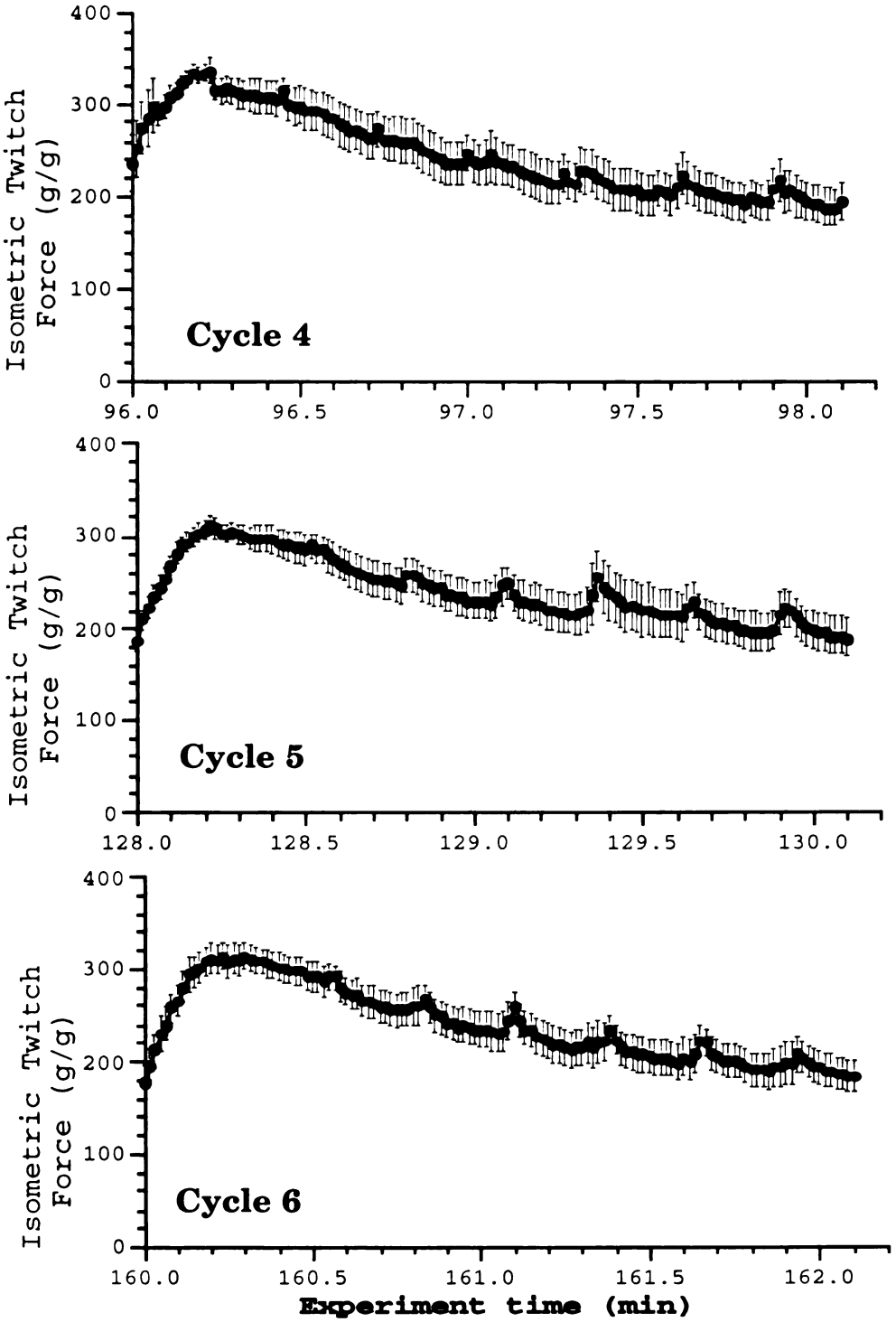

Figure 18 (cont'd): Time course of isometric twitch force (5.0Hz)

Means±SEM (N=7), one stimulation cycle = 2.1 minutes

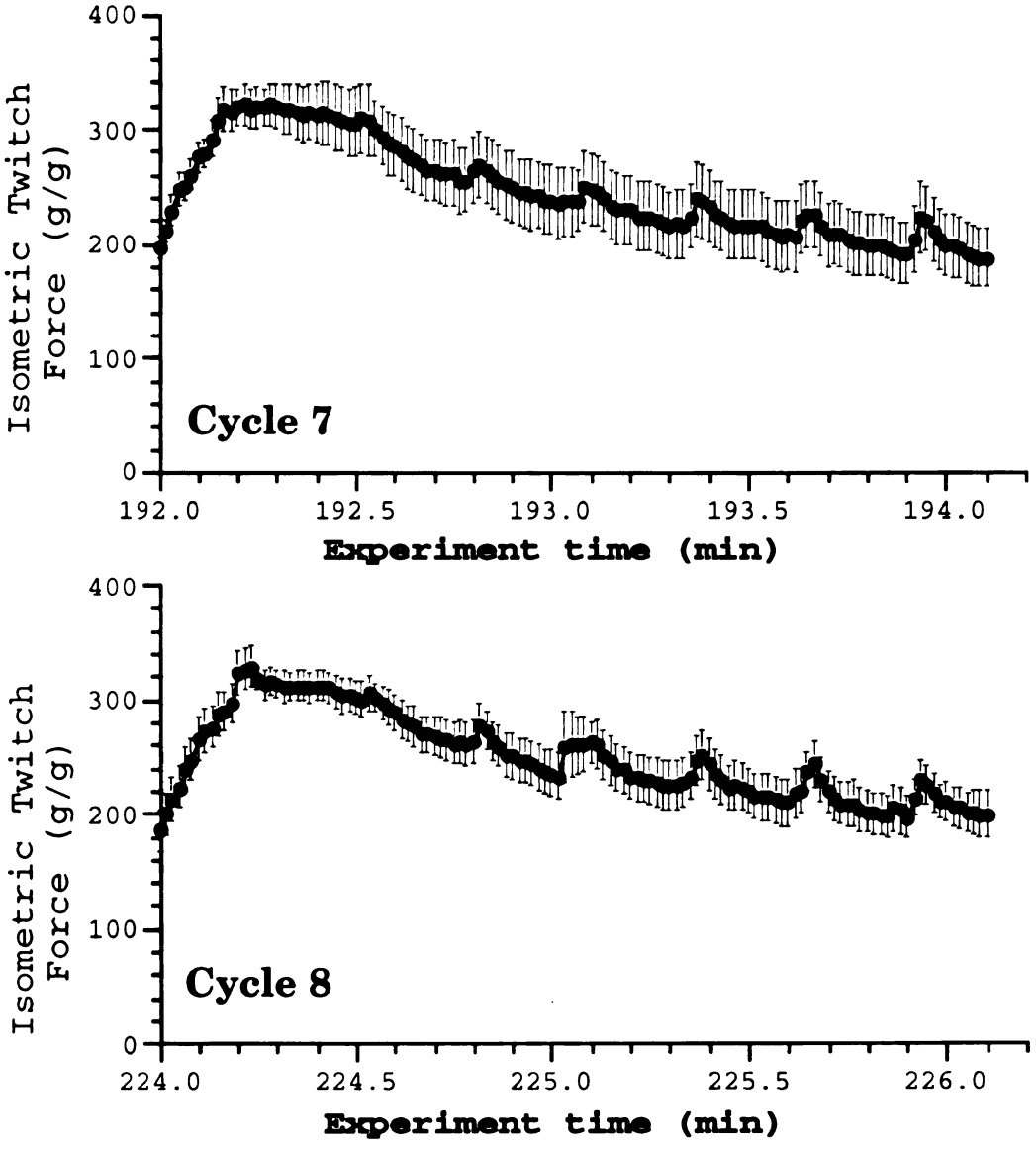

Figure 18 (cont'd): Time course of isometric twitch force (5.0Hz)

Means±SEM (N=7), one stimulation cycle = 2.1 minutes

Analysis of the first eight cycles showed no statistically significant effect ($P < 0.05$) of within–cycle stimulation frequency on initial peak twitch force (Figure 19A). There was an effect of stimulation frequency on end–stimulation peak twitch force within a cycle. (Figure 19B, initial peak twitch force was measured at the first time point for each cycle; end–stimulation peak twitch force was averaged over the last three time points.) There was a slightly significant effect of increasing cycle number within the 0.75Hz and 5.0Hz stimulation frequencies (Figure 19A); however, there was no effect of increasing cycle number on end–stimulation peak twitch force (Figure 19B). Lastly, there was no significant interaction between cycle number and stimulation frequency for either initial or end–stimulation peak twitch force.

During the recovery periods of each cycle for most rats, two or three supramaximal twitches were elicited for the purpose of determining the time–to–peak tension (TPT) and half–relaxation time (HRT) in milliseconds The TPT and HRT parameters give a rough global estimate of calcium release and uptake kinetics (hence activation and de–activation of the cross–bridge machinery), respectively. It is acknowledged the time required for energy storage and release in the series elastic components (SEC) of the muscle tissue can potentially confound the interpretations of TPT and HRT measurements. No attempt was made to quantify this SEC contribution. Analysis of the first eight cycles showed a statistically significant effect ($P < 0.05$) within cycles #2–#5 of stimulation frequency on twitch HRT when comparing the 2Hz and 5Hz groups (Figure 20A). There were no other significant effects of stimulation frequency on HRT or TPT within a given cycle (Figure 20A and B). Across cycles, TPT in cycle #1 was significantly different

than the remaining cycles for the 2.0Hz and 5.0Hz groups. Also, the 2.0Hz group had a significantly longer HRT during the first cycle compared to remaining cycles. There was no significant difference across cycles for HRT or TPT in the 0.75Hz group.

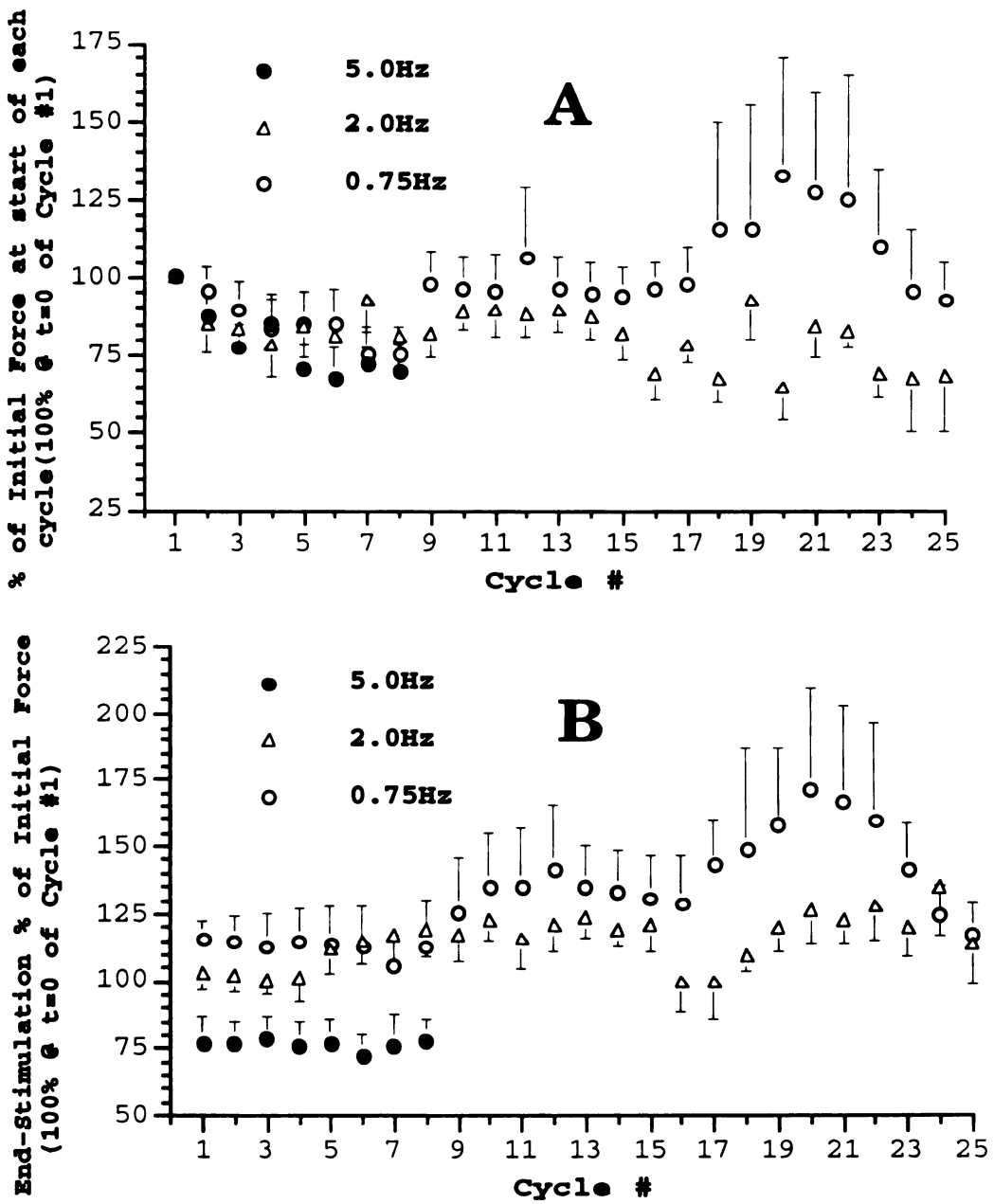

Figure 19: Initial and end-stimulation peak twitch force

Mean±SEM(N=7 through cycle #8–see Appendix D for N vrs. cycle #). All values are expressed relative to the force measured at t=0 of cycle #1 within given stimulation frequency.

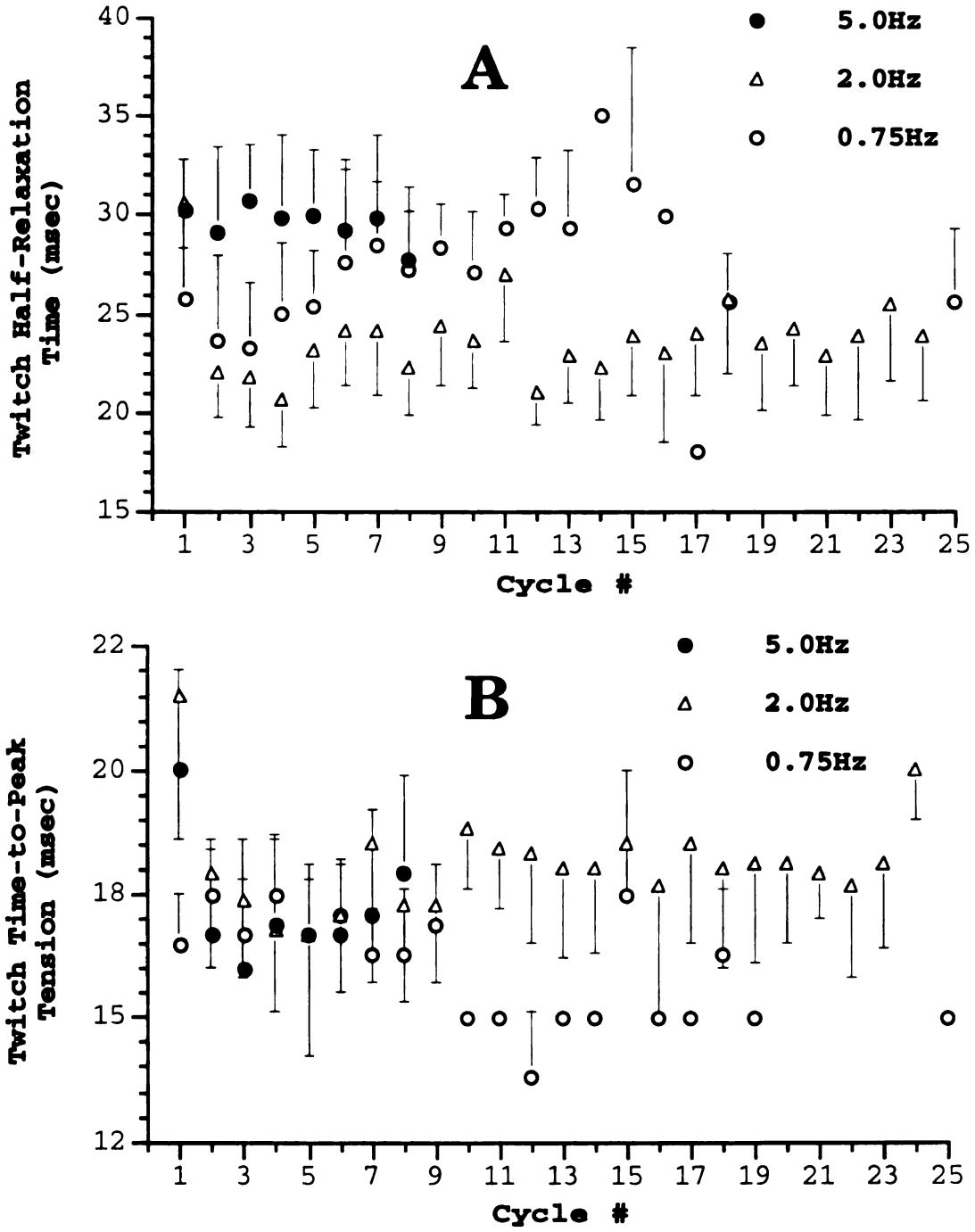

Figure 20 Force kinetics of single twitches vrs. cycle #

Mean±SEM(N=7 through cycle #8–see Appendix D for N vrs. cycle #).

Utility of Principal Component Analysis

Figure 21 shows a typical "before and after" output of the PCA method applied to a region of 129 points around the PCr peak for a single rat. The first four principal components roughly correspond to the overall lineshape (PC1), frequency shift (PC2), linewidth (PC3), and phase shift (PC4) of the PCr peak. The PC magnitude represents the relative amount of variance that can be explained by the given PC component. For example, Figure 21A illustrates PC1 in the original uncorrected NMR dataset, can explain approximately 89.6% of the variance in the PCr peak. After five iterations of phase and frequency correction, PC1 was able to explain 99.5% of the variance whereas the remaining PCs explained proportionally less variance in the PCr peak (Figure 21B). The robustness of the PCA spectral correction method is nicely shown in cycle #5. In this cycle there is an abrupt discontinuity in the resting steady–state PCr level as indicated in the PC1 (i.e. overall lineshape) time course in the original dataset (Figure 21A). This abrupt change in the resting PCr level appears to be largely due to a sudden frequency shift as shown in PC2. The exact cause of this discontinuity is mysterious since the muscle is at rest and presumably in a metabolic steady–state. A single isolated malfunction of the spectrometer computer, superconducting magnet, or Grass stimulator over the five hour experiment seems unlikely since events abruptly returned to their normal pattern. Interestingly, this discontinuity occurred around 5 PM, so one potential rational is that an abnormal fluctuation in the building or campus electrical power grid occurred as most people left their offices. Regardless of the cause, the PCA method was able to easily correct this abnormality (PC1 in Figure 21B).

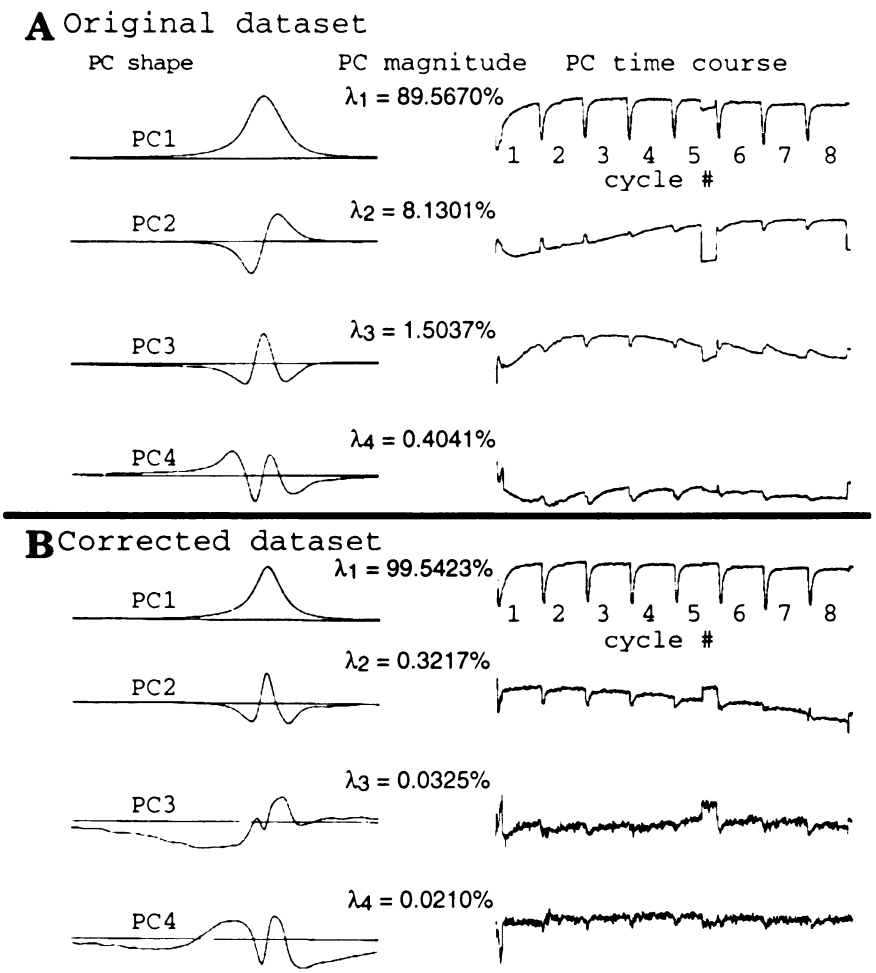

Figure 21: Spectral correction by PCA

The first four principal components (PCs) of the PCr peak from a single 5Hz rat before (A) and after (B) five corrections by the Principal Component Analysis method. PC1, PC2, PC3, and PC4 roughly correspond, respectively, to the overall lineshape, frequency shift, linewidth, and phase shift of the PCr peak. Lambdas are the eigenvalues of the data covariance matrix and represent the relative contribution of each principal component to the overall variance in the dataset.

Decomposition of global PCr time constants

After phase and frequency correction by the PCA method and then baseline correction, a high signal–to–noise ^{31}P–NMR time course was obtained by summing across cycles #3–#8 for each rat (Figure 22). Next, the NNLS algorithm was applied to each rat's PCr recovery time course data points (Figure 23A) thereby generating a "spectrum" of time constants (Figure 23B). The relative amplitude (ΔPCr_i) and time constant duration (τ_i) of the PCr transients are summarized in Table 8 for all rats. (ΔPCr_i and τ_i are the iterated parameters from Equation 1.) For convenience, all of the time constants were rank ordered and assigned to arbitrary bins based upon visually apparent groupings. Comparisons among means was performed on the four cells in Table 8 that had $N \geq 5$. There are two general trends which reached statistical significance ($P \leq 0.05$): within a given stimulation frequency, there was always one component that had a larger relative amplitude than the rest; and secondly, the duration of the 5Hz–Long, 5Hz–Short–Medium, 2.0Hz–Medium, and 0.75Hz–Medium were significantly different from one another.

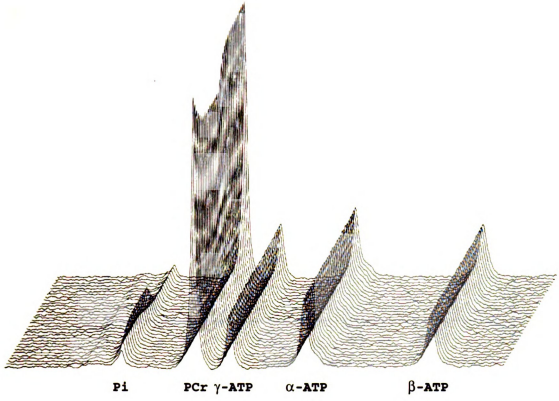

Figure 22: Sample high signal–to–noise ^{31}P–NMR spectra

Individual spectra (such as shown in Figure 7) were summed across cycles for a given rat to generate a single high signal–to–noise stimulation–recovery time course. The above 32 spectra are from a single 0.75Hz rat summed across #3–#8 cycles.

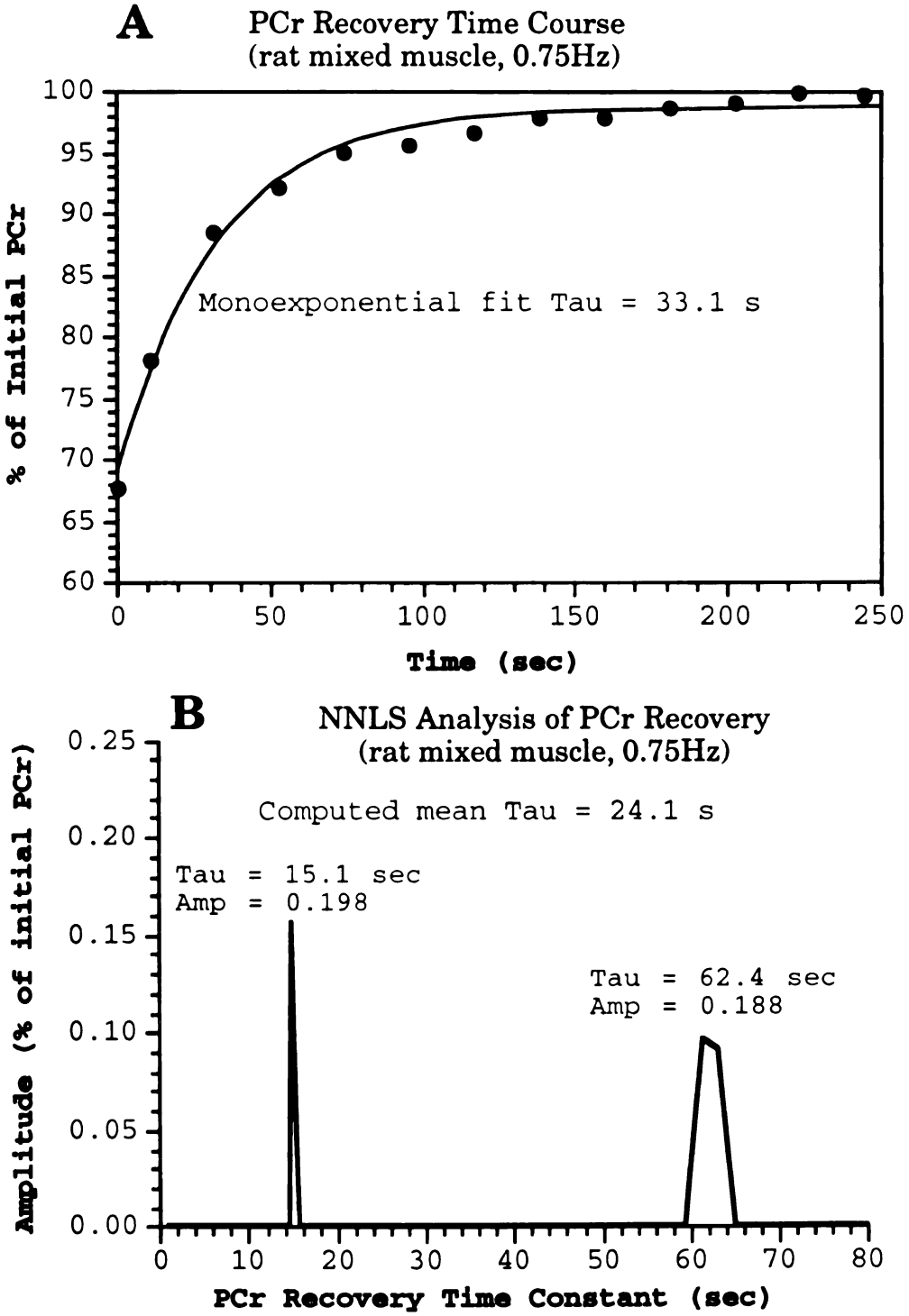

Figure 23: NNLS applied to a PCr recovery transient

A: The 5.7 minute PCr recovery time course of a single rat mixed muscle stimulated at 0.75Hz for 5.7 minutes. A monoexponential fit using the Marquardt–Levenberg algorithm (194) is superimposed.
B: The resulting "spectrum" of time constant values obtained by applying the NNLS algorithm to Figure 23A.

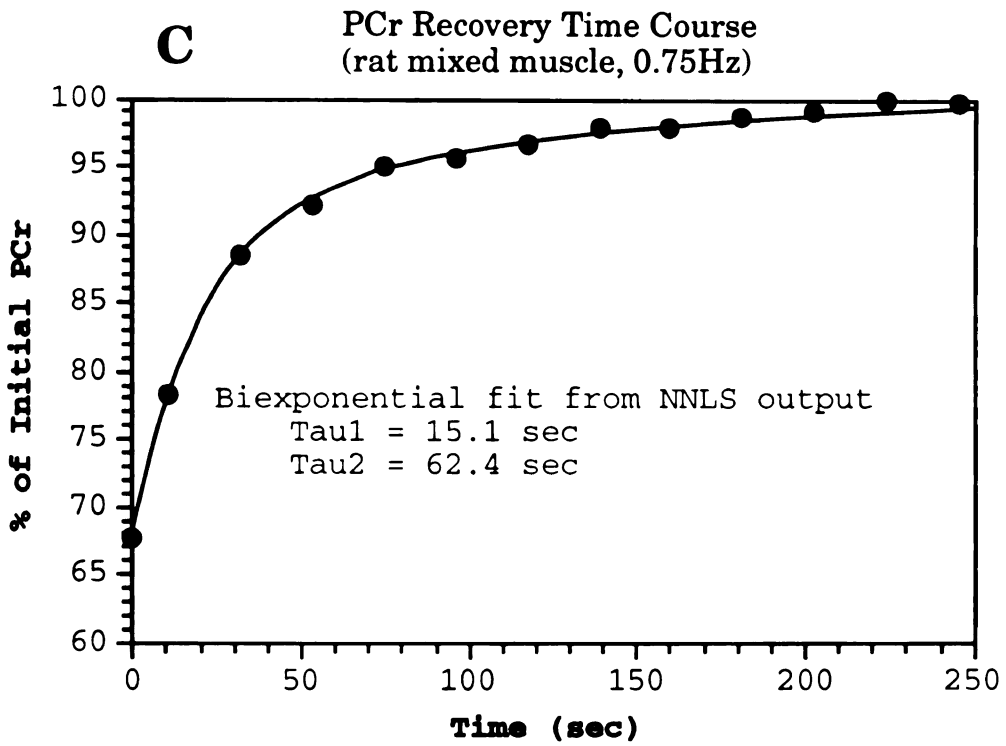

Figure 23 (cont'd) NNLS applied to PCr recovery transient

C: The 5.7 minute PCr recovery time course of a single rat mixed muscle stimulated at 0.75Hz for 5.7 minutes. A biexponential fit is superimposed using the tau and amplitude parameters from Figure 23B .

Table 8: *Time constants from NNLS output*

Twitch Stim. Rate	Very Short	Short	Short–Medium	Medium	Long	Very Long
0.75Hz (7)	1.0 *0.01* (2)	15.1 *0.20* (1)	30.0 *0.16* (2)	**51.1±3.43** ***0.27±0.06*** **(6)**	107.9 *0.06* (1)	186.5 *0.11* (1)
2.0Hz (7)	1.0±0.0 *0.01±0.00* (3)	14.4±2.1 *0.03±0.02* (3)	none observed in this range	**43.8±0.9** ***0.34±0.05*** **(7)**	none observed in this range	226.4 *0.02* (1)
5.0Hz (7)	2.3±1.3 *0.04±0.00* (3)	16.1±1.9 *0.14±0.02* (3)	**33.1±2.8** ***0.28±0.08*** **(5)**	none observed in this range	**83.5±4.9** ***0.53±0.10*** **(6)**	322.9 *0.89* (1)

All values are mean±SEM. For each table cell: top number is time constant duration (seconds), middle italic number is relative magnitude of time constant (% of initial PCr), bottom number is N. **Bold** indicates dominant time constants.

Modelling of fiber type distributions

The global time course of PCr recovery for a hypothetical mixed muscle was modeled using two diverse distributions of fiber oxidative capacities: discrete bimodal versus quasi–Gaussian. In the discrete bimodal model, the mixed muscle consisted of 1000 cells composed of 50% high–oxidative capacity fibers and 50% low–oxidative capacity fibers (Figure 24A). In the quasi–Gaussian model the mixed muscle consisted of 1000 cells with a broad normal distribution of oxidative capacities (Figure 24B). In both models the PCr recovery time course from individual muscle fibers was assumed to be monoexponential, rising from a steady–state end–stimulation level that is linearly dependent on tau, where tau is independent of submaximal workload (203). A four–minute global time course of PCr recovery after a submaximal workload for the whole mixed muscle was computed from the sum of the individual muscle fiber PCr recoveries for each hypothetical distribution (Figure 25). The resulting global PCr recovery transient was then decomposed using the NNLS algorithm thereby generating a "time constant spectrum" for each distribution (Figure 26).

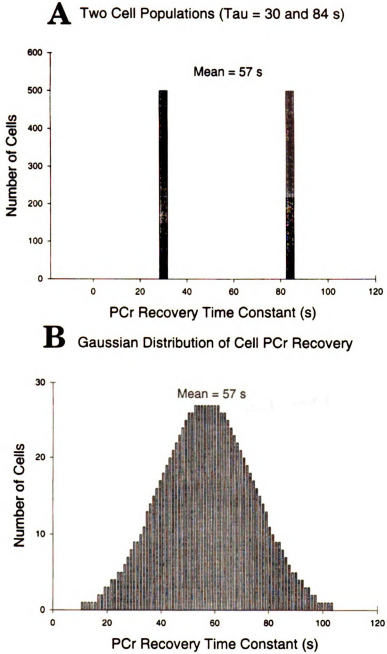

Figure 24: Hypothetical fiber type distributions

Discrete bimodal (A) and quasi–Gaussian (B) distributions of fibers were constructed with equal values of mean PCr recovery tau (57 seconds). The discrete bimodal model has 500 high–oxidative capacity muscle fibers with PCr tau = 30 seconds and 500 low–oxidative capacity muscle fibers with PCr tau = 84 seconds The quasi–Gaussian model has 1000 muscle fibers with 100 distinct PCr recovery taus (57±18 seconds, mean±SD).

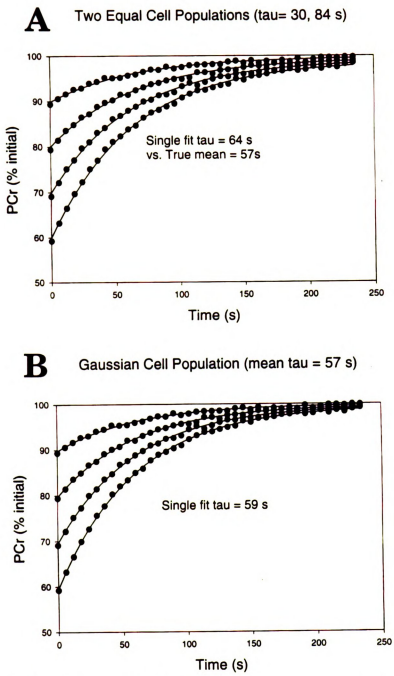

Figure 25: Synthesized global PCr recovery time–courses

Four–minute global PCr recovery time courses after four different submaximal workloads were calculated for the bimodal and Gaussian distribution. Artifical noise was added to all recovery time courses. In each distribution, a monoexponential curve fit is superimposed over the synthesized recovery time points along with the monoexponential tau value.

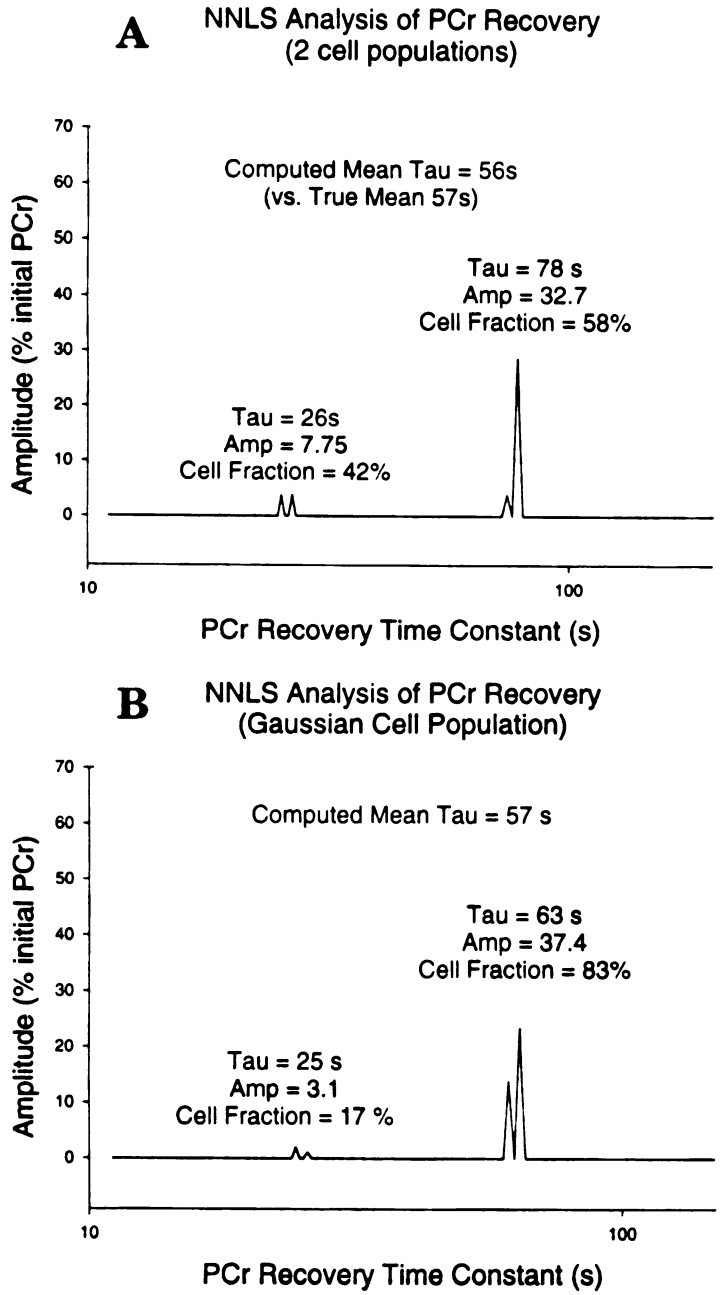

Figure 26: NNLS output of hypothetical distributions

The "spectrum" of time constant values was obtained by applying the NNLS algorithm to the synthesized global PCr recovery time course after the highest submaximal workload. Note both underlying hypothetical distributions have similar spectrums. The relative cell fraction for the fast and slow component was calculated for a given amplitude weighted by its tau value. This resulted in a computed mean tau virtually identical to the assumed true mean of 57 seconds.

Discussion

Decomposition of PCr recovery transients

This study has shown that application of the unbiased Non–Negative Least Squares algorithm to high signal–to–noise PCr recovery transients of rat mixed muscle yields multiple time constants for both submaximal (0.75Hz) and supramaximal (2.0 and 5.0Hz) workloads (Table 8). The general trend seen in Table 8 is that faster recovery time constants are recorded more often as stimulation frequency increases. Though not the central observation in other studies, this pattern does appear when results of these studies are considered in aggregate. For example, in studies using a single combination of stimulation intensity and duration which placed the workload in the submaximal domain, the PCr recovery time course was best fit by a monoexponential function in frog (192, 66), rat (203), cat (176), and human (149, 195, 323) muscle. In other studies using only supramaximal stimulation intensity and duration, the PCr recovery time course was best fit by a biexponential function in rat (214, 243) and human (120, 259, 274) muscle. Curiously, in a few reports, if the muscle contains a slow–oxidative fiber distribution it exhibits PCr recovery kinetics resembling a slightly underdamped second–order response after either submaximal stimulation (cat soleus (176); creatine–depleted rat gastrocnemius (204)) or supramaximal stimulation (isolated human Type I fibers (274)). Lastly, a few human studies using submaximal and then supramaximal workloads have noted monoexponential and then biexponential PCr recovery time courses, respectively (9, 287, 308).

Over twenty years ago an explanation for this stimulation–dependent pattern of time constants was put forward by Sahlin's group based upon human biopsy data (120, 258). They suggested that as workload intensity increases, the increase in anaerobic glycolytic flux produces an increased $[H^+]$ which shifts the creatine

kinase equilibrium reaction to the right (as written below) by the beginning of recovery.

$$PCr + ADP + H^+ <—> ATP + Cr$$

Throughout the subsequent recovery, this mass action effect of elevated but decreasing $[H^+]$ results in a lower $\Delta[PCr]/\Delta time$ which would explain any slow exponential components that may be observed. As mechanistic support for their explanation, they cited *in vitro* experiments in the mid–1950s which showed a strong dependence of the creatine kinase equilibrium constant and reaction velocity on pH. This is due to the adenine nucleotides' changing binding affinities since pH modulates the ionization states of their Mg^{2+} and/or K^+ complexes. More recently, this proton mass–action explanation for multicomponent PCr recovery kinetics has also been directly or implicitly stated in numerous human *in vivo* ^{31}P–NMRS studies (6, 9, 21, 217, 291, 308).

The above mass–action argument is somewhat weakened on two accounts. First, it is implicitly assumed the muscle is composed of a cellular homogenous population of fibers with regard to oxidative capacity and total creatine content such that pH effects are the sole modulator of the creatine kinase equilibrium and reaction velocity. But it is well documented humans and animals have significant intra–muscle and inter–muscle fiber type heterogeneity (261). Second, the argument assumes the creatine kinase reaction is acting as an isolated equilibrium system so that increases in $[H^+]$ lead to predictable stoichiometric decreases in [PCr]. Although it is established that the creatine kinase reaction is at equilibrium during all but the most severe workloads (165, 201, 213, 318), it is also well recognized this reaction is not isolated; it is functionally coupled by ATP and ADP to several non–equilibrium reactions (the Na^+/K^+–, Ca^{2+}–, and myosin–ATPases; mitochondrial ATP synthetase) (169, 172, 211). This implies, for example, that the net PCr resynthesis reaction occurring during recovery

creatine kinase reaction:	$ATP + Cr <---> PCr + ADP + H^+$
mitochondrial ATP synthetase:	$ADP + Pi \longrightarrow ATP$
Net reaction during recovery:	$Cr + Pi \longrightarrow PCr + H^+$

is also not at equilibrium. This complicates a simple and explicit mass action relationship between changes in $[H^+]$ and changes in [PCr]. Experimentally, data from *in situ* resting cat slow–twitch muscle, has shown hypercapnic acidosis to pH 6.5 increases, not decreases, the steady–state [PCr] by approximately 8–10% (206, 118, 119). Other studies have shown decreased pH, primarily due to increased lactic acidosis, prolongs the PCr recovery in rat (234) and human mixed muscle (287, 308) but not in dogfish white muscle (62). Taken together, these results suggest quantitatively or qualitatively forecasting the precise effect of changes in $[H^+]$ on [PCr] is extremely challenging and cannot be extrapolated from examining the creatine kinase reaction in isolation.

An alternative explanation for the global NMR–observed multicomponent behavior of PCr recovery kinetics is the well documented existence of intra–muscle and inter–muscle heterogeneity of fiber type distributions based upon muscle biopsy data (109, 261, 241). As commonly practiced, the non–invasive nature of ^{31}P–NMRS dictates that the PCr signal arising from a given volume of muscle represents the global average of individual muscle fiber PCr transients. Theoretically, it is possible for every muscle fiber to exhibit unique PCr kinetics since each cell may have slightly different total creatine content and mitochondrial volume density. In reality, the intra–muscle fiber type variability is somewhat reduced since muscle fibers within a given motor unit have essentially the same biochemical and mechanical characteristics (110, 123, 37).

Comparison of the 5.0Hz versus the 0.75Hz data in Table 8 reveals that the higher workload resulted in more frequent appearance of exponential components with significantly longer and shorter durations than the lower workload. Since the duration of the recovery PCr time constant is inversely proportional to

mitochondrial content (203, 234), these results suggest that the longer time constant (i.e. the "long" 83.5 seconds component) is due to the presence of fibers with low relative oxidative capacity. It is likely this fiber population has an attenuated PCr recovery rate due a lower ICF pH (234, 287, 308) since it has been shown in cat soleus that hypercapnic acidosis can increase the PCr recovery time constant by 2.7–fold (119). Harkema et al. speculated this attenuation was due to perturbations in cytoplasmic substrate delivery to the mitochondria and/or deviations from the mitochondrial enzymes' pH optima which thereby decreased mitochondrial ATP synthesis rate and hence decreased the PCr recovery rate (119).

The shorter time constants (i.e. the "short" 16.1 seconds, and "short–medium" 33.1 seconds components in Table 8) are more frequently observed at higher workloads and maybe explained by a preferential increase in blood flow (in both relative and absolute terms) to fibers with higher oxidative capacity. (191, 295, 182). The increased blood flow would enhance the rate of oxidative recovery metabolism and increase the PCr recovery rate resulting in shorter time constants.

The explanation of the occasionally observed "very short" PCr recovery time constant from is problematic but raises an intriguing possibility concerning glycolytic regulation. This very fast recovery component (approximately two seconds) would correspond to an unattainable mitochondrial ATP synthesis rate 5–15 times greater than the calculated ATP synthesis rate at maximal oxygen consumption in the rat hindlimb (QO_{2max} ≈6.6 mM/minute from Table 5 of Ref (234)). If oxidative metabolism cannot explain this very fast component, the only other quantitatively significant and high flux rate source of ATP during the initial phase of recovery is anaerobic glycolysis. In effect, the glycolytic flux would exhibit a "momentum" quality which would carry it into the early phases of recovery. This conjecture, of course, runs counter to the conventional wisdom, that states when stimulation stops, glycolytic flux will abruptly stop due to removal of allosteric

facilitation of phosphofructokinase and glycogen phosphorylase. Unfortunately, the spectral time resolution used in this study (see Table 7) was insufficient for us to conclude that the pH change during the first 40 seconds of recovery was due to continued lactic acidosis superimposed upon the expected transient acidification from net PCr resynthesis (4, 167, 276). Consequently, at this time, a cogent explanation for this very fast component remains elusive.

Lastly, as an independent test of the NNLS algorithm's ability to decompose PCr recovery transients, we digitally scanned in the raw data points (SigmaScan 2.0 for Windows) from a previously published human study by Walter et al. (Figure 3A of Ref (308)). They reported a monoexponential recovery time constant of approximately 34 seconds in the medial gastrocnemius after a submaximal workload (9 seconds of rapid plantar flexions at 30% maximal voluntary contraction which caused only a modest decrease in ICF pH to 6.8). Applying the NNLS algorithm to the scanned data points, a fast (22 seconds) and slow (90 seconds) component were resolved (i.e. biexponential recovery) suggesting two fiber populations with different oxidative capacities were contributing the global NMR–derived PCr time course. At a longer duration workload which resulted in significant intracellular acidosis to pH 6.2 they superimposed a biexponential curve on their recovery data points but did not report time constants. Applying the NNLS algorithm to their higher workload data confirmed their biexponential curve fit and showed that the two components were prolonged (39 seconds, 130 seconds).

Temporal metabolite patterns during prolonged intermittent exercise

This study documents the temporal pattern of PCr, pH, and isometric force during numerous, prolonged, intermittent stimulation–recovery cycles for submaximal and supramaximal workloads in the common laboratory rat. This type of stimulation protocol more closely mimics the cyclic work–rest locomotion

patterns of humans and many animals (123, 255, 283). To the knowledge of the author, there are only three other studies in the past 30 years of the muscle energetics literature that have used a remotely similar stimulation–recovery protocol (virtually all other studies employ a single bout or, more rarely, a second bout). Curtin et al. (62) measured heat and ^{31}P–NMR metabolites during nine cycles of an 18 second isometric tetanus plus two hour recovery in *ex vivo* dogfish white muscle. Edwards et al. (84) measured ATP, PCr, and lactate via muscle biopsy throughout five cycles of 15 second dynamic contractions at 66% maximum voluntary contraction followed by 20 second recovery in the human quadriceps. Finally, Marsh et al. (195) measured ^{31}P–NMR metabolites during six cycles of five minute submaximal dynamic wrist flexions with a five minute recovery in humans. This group did not record the temporal patterns of pH changes and chose to plot only the cyclic PCr and Pi data from one of six subjects.

A key finding in the current study is the end–stimulation pH during the first cycle was significantly lower (approximately 6.6 or 6.15) than the remaining cycles for the 2.0Hz and 5.0Hz but not 0.75Hz workloads (Figure 15). After the first cycle or two, the end–stimulation pH attained essentially same value (approximately 6.95 or 6.8) as cycle number increased. This pattern is similar to the one observed by Edwards et al. in human quadriceps (84), except they measured lactate, but not by Curtin et al. (62) in dogfish white muscle. In Curtin's paper the end–stimulation pH of the first cycle was higher than the remaining eight cycles. A possible explanation for this large initial deviation in our pH data is there may be a delay distributing the blood to the more oxidative fibers (182, 295) thereby requiring these fibers to use anaerobic glycolysis to a larger extent during the first two cycles. As the experiment continues, local metabolic factors (e.g. H^+, K^+, adenosine, acetylcholine spill over from synapses, (183) continue to accumulate and open dormant capillary anastomoses such that subsequent stimulation cycles begin with

better perfusion.

Regardless of the precise underlying mechanism of the pH deviation, these results have two practical implications. First, they indicate the importance of "warming–up" before engaging in any form of physical activity (especially exercises requiring only one or two short–duration, high–intensity power bursts) since the lactic acidosis would reduce the oxidative capacity of the working muscle during the first few bouts (119, 234). Second, in gated NMR experiments, where signal–to–noise and time resolution is enhanced by summing spectra acquired at identical time points during repeated bouts, there is an assumption that the metabolic events are identical from cycle to cycle. Although this appears to be a reasonable assumption for submaximal workloads (Figure 8 and Figure 15), it does not appear to hold for supramaximal workloads (Figure 14 and Figure 15). It would seem prudent not to include data from at least the first cycle in gated NMR experiments.

Viability of in vivo fiber typing by ^{31}P–NMRS

Can phosphocreatine transient analysis estimate skeletal muscle fiber distributions? From a global functional standpoint, yes, but not at the cellular level as has been proposed by others. Since recovery PCr time constants can be used to assess relative oxidative capacity of skeletal muscle (234), the results of and Figure 23 would suggest applying the unbiased NNLS method to PCA–corrected ^{31}P–NMR data can potentially resolve at least two fiber type populations. A major result of this study, however, is that we could not unambiguously identify the distribution of distinct fiber populations based solely upon a single global NMR derived parameter since essentially equivalent results are obtained from PCr transients from two diverse, hypothetical, fiber type distributions (Figure 26). This is at odds with the prevailing tendency in the *in vivo* ^{31}P–NMRS muscle energetics literature to correlate various NMR parameters with

histochemical fiber types usually based upon ATPase staining methods which give bi– or tri–partitite distributions (217, 308, 304, 236). Although these correlations are useful first approximations, they tend to grossly oversimplify the diverse metabolic profiles of mixed skeletal muscle tissue and thereby perpetuate the idea that only two or three discrete fiber type populations exist (e.g. Type I vrs. II or Type I vrs. IIA vrs. IIB). This is in spite of the fact that over the past three decades, invasive biopsy techniques of human and animal muscle have repeatedly provided profuse evidence that fiber–type distributions represent a continuum of energy–supply and energy–demand properties (e.g. ATPase activity, oxidative capacity, glycogen depletion, capillary density, etc.) rather than discrete stereotypes (83, 85, 187, 272, 284, 109, 261, 267). For example, Pette concluded that fiber typing based upon ATPase activity (i.e. Type I vrs. IIA vrs. IIB) and oxidative capacity (e.g. based upon succinate dehydrogenase activity) are not necessarily correlated since he observed considerable overlap of SDH activity between I, IIA, and IIB fibers–and inter–fiber variability (241). Additionally, Guth has shown a collection of putatively homogeneous fibers can exhibit different ATPase staining intensities (i.e. an intra–fiber variability) since the stain does not distinguish between myofibrillar ATPase, the SR Ca–ATPase, or the mitochondrial ATPase (113, 114). Furthermore, since these diverse fibers are arranged in a random spatial distribution within healthy muscle (152, 160, 284), the biopsy literature suggests completely non–invasive attempts to identify Type I and II fiber populations (an energy demand classification scheme) based solely upon an energy supply classification scheme (e.g. PCr recovery tau, Pi peak splitting) are inherently imprecise and can be misleading. This is further seriously complicated during *in vivo* experiments by variable inter–subject motor unit recruitment strategies (25, 26, 71, 37) and the inability to precisely define the muscle volume interrogated by the NMR transceiver coil (154, 155, 226).

On the other hand, comprehensive whole–muscle fiber type classification based upon invasive biopsies would require reporting several dozen metabolic, cellular, and functional parameters (e.g. protein isozymes profiles, mitochondrial content, enzymatic activities, time–to–fatigue, time–to–peak–tension, etc.) from several different geographic locations within the muscle. Since this would require numerous tissue samples and hence subject discomfort, it would be valuable to develop a taxonomy exploiting the non–invasive nature of ^{31}P–NMRS while attempting to acknowledge the continuum nature of fiber properties.

Although current technological limitations precludes ^{31}P–NMRS from resolving individual fiber type properties (107), a suggested first step would be to describe the global functional characteristics of a given volume of muscle by both an energy–supply parameter and an energy–demand parameter in response to a standardized workload. As discussed in this dissertation, the inherent high signal–to–noise of the PCr resonance coupled with the unbiased determination of time constants by the NNLS algorithm, make analyzing PCr recovery transients a suitable method for assessing global relative oxidative capacity as the energy–supply parameter. ATP cost of contraction determined by the time–zero derivative of [PCr] at the onset of stimulation (104) or by the slope of [PCr] versus time during ischemic stimulation (25, 26) could serve as the energy–demand parameter. (In order to minimize the confounding effects of inter–subject differential motor unit recruitment and fatigue responses on ATP cost, it is necessary to use brief bouts of suprathreshold motor unit stimulation by either direct nerve contact in animal studies or via percutaneous electrodes in human studies.). After measuring these two non–invasive parameters in different animal models over a wide cross–section of subjects using standardized workloads, the goal would be to plot individual relative oxidative capacity versus ATP cost and look for clustering. If data point clusters did emerge, this would provide a basis for a completely non–

invasive, NMR–centric method of "fiber typing" which is relieved of the constraints imposed by confining global NMR parameters to specific enzymatic profiles obtained by biopsy. It is certainly acknowledged this proposed method does not actually "fiber type" in the cellular sense and would require agreement as to what constitutes a "standard workload". Its advantage, however, is it attempts to correlate two key functional parameters during *in vivo* whole–muscle exercise. This could provide a framework for systematically quantifying the effects of various athletic training regimens or neuromuscular pathologies. It should also be of use to investigators who wish to link the whole–body VO_2 slow–component (seen at workloads above the plasma lactic acid threshold) and fiber type distribution in exercises that activate a large fraction of the total muscle mass (246).

In summary, although previous ^{31}P–NMRS studies by others have shown the multicomponent nature of the PCr recovery time course after stimulation is most easily explained by fiber type heterogeneity, we have not found it possible to unambiguously identify distinct fiber type population distributions based exclusively on global NMR–dervived time constants since bimodal and Gaussian distributions give similar results. This certainly does not preclude the use of NMR to quantify more global parameters of muscle function.

CHAPTER 5
SUMMARY AND RECOMMENDATIONS

Summary

Previous comparative and human cross–sectional studies have suggested a link between PCr kinetics and skeletal muscle oxidative capacity over limited ranges of mitochondrial content. Data from the first investigation in this dissertation (Chapter 3) confirms that the PCr recovery rate constant is directly proportional to oxidative capacity over a 6–fold range of mitochondrial content in mammalian muscle. The practical application of this result is that relative skeletal muscle oxidative capacity can be assessed, non–invasely, by analysis of PCr recovery transients obtained via ^{31}P–NMRS. This data also suggests that submaximal workloads (i.e. workloads that can be maintained within the oxidative capacity of the muscle fibers without fatigue or acidosis) should be used since intracellular acidosis depresses the PCr recovery rate constant thereby confounding its correlation to relative oxidative capacity. Lastly, these results are consistent with the linear control model of oxidative phosphorylation by the cytoplasmic free energy of ATP hydrolysis.

Given the outcome of the first investigation, an attempt was made (Chapter 4) to unambiguously identify the distribution of distinct fiber populations by decomposing the global NMR–derived PCr recovery time constant into its constituent components. High signal–to–noise ^{31}P–NMRS data was obtained by spectral processing with the Principal Component Analysis algorithm and then summing across repeated stimulation–recovery cycles. The PCr recovery time constant from the high signal–to–noise dataset was decomposed using the Non–negative Least Squares (NNLS) algorithm, which eliminates investigator bias by not specifying the number of components *a priori*. This extensive data processing resolved at least two components for both submaximal or supramaximal

stimulation rates. Furthermore, it was argued that the presence of multiple components is best explained by fiber type heterogeneity rather than a proton–induced mass–action shift in the creatine kinase equilibrium reaction, as is commonly reported. Unfortunately, a modelling analysis comparing a discrete bimodal fiber type distribution versus a quasi–Gaussian fiber type distribution showed that similar results are obtained by the NNLS algorithm. This indicates that unambiguous fiber type determination at the cellular level is not currently possible with even high signal–to–noise ^{31}P–NMRS data. This conclusion runs contrary to the tendency in the *in vivo* NMR literature which suggests that various steady state and transient parameters can distinguish Type I verus Type II skeletal muscle fibers.

Recommendations for future studies

"As the island of knowledge expands, so does the shore of the unknown."
Anonymous

Perhaps the most intriguing discovery in this dissertation was identification of a very short PCr recovery time constant (approximately two seconds) using the NNLS algorithm (Table 8). Such rapid recovery components have not been reported in the mammalian muscle literature. A logical, but to date empirically unsupported, origin of this very fast component would be continued glycolytic flux into the early stages of recovery. If tenable, then resolving this rapid component is of interest to bioenergeticists on two counts. First, it contradicts the prevailing dogma which stipulates that significant glycolytic flux occurs only during stimulation and then abruptly ceases when stimulation stops. Second, the increase in intracellular protons from lactic acidosis in early recovery would necessarily change the cytosolic redox potential and possibly the redox potential in the mitochondrial matrix. This in turn could influence the mitochondrial ATP synthesis rate which is dependent upon the difference between the mitochondrial redox

potential and the cytosolic ΔG_{ATP}. Since the spectral time resolution used in this study was insufficient for us to conclude that the pH change during early recovery was due to continued glycolytic flux, it is incumbent to increase the time resolution to approximately one second/spectrum without sacrificing signal–to–noise by using gated ^{31}P–NMR experiments. If better time resolution suggests that the pH changes during early recovery are consistent with continued glycolytic flux, then corroboration from analyzing intracellular lactate kinetics would be required. This could be accomplished with ^{13}C–NMRS measurements of ^{13}C–labeled glucose–6–phosphate.

Another interesting finding in this dissertation was the identification of an increasing trend in end–stimulaiton pH as a function of cycle number after supramaximal workloads (Figure 15). It was postulated that increased blood flow during the later cycles was responsible for the attenuation of end–stimulation pH. This attenuation could be experimentally manipulated through the use of locally injected nitric oxide agonists or antagonists, which would vasodilate or vasoconstrict the vascular smooth muscle, respectively. If this pharmacological treatment alters the pattern of end–stimulation pH as a function of cycle number, this would support the hypothesis that blood flow (hence convective O_2 delivery) plays an important role in determining the skeletal muscle's redox state and dependence on anaerobic metabolism. Also, using the repeated stimulation–recovery protocol described in Chapter 4, the effects of aerobic training, which would presumably increase O_2 extraction capacity by increasing mitochondrial content, could be investigated. Aerobic training would be expected to attenuate the drop in end–stimulaiton pH during the first three cycles of supramaximal stimulation.

It would also be of interest to rigorously define the three–dimensional B_1 field pattern from the saddle–shaped surface coil used in Chapter 4. This would require using antenna theory along with computer numerical methods due to the complex

geometry of the transceiver coil. Once defined, the B_1 field pattern would be used in a computer simulation to interrogate a hypothetical, heterogenous muscle. The purpose would be to catalog the effects of different spatial distributions of fiber types on the transient and steady–state behavior of the global, NMR–derived, PCr time constant.

APPENDICES

Appendix A

Figure 27: ^{31}P–NMR Probe Photographs

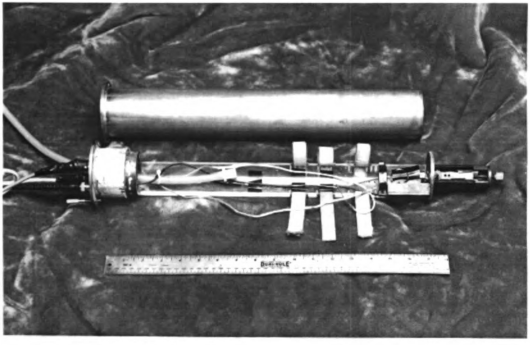

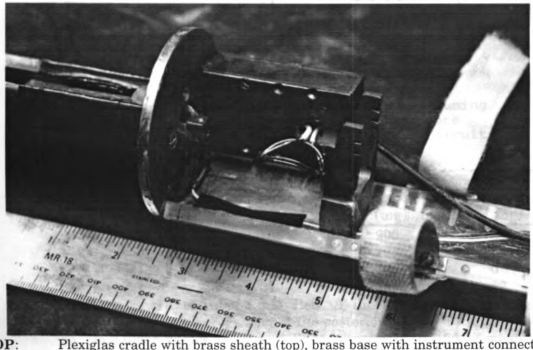

TOP: Plexiglas cradle with brass sheath (top), brass base with instrument connectors (left) and brass adjustable force transducer mount (right).

BOTTOM: Close up of box with LC–tank circuit with saddle shaped transceiver coil, adjustable force transducer mount and rigid brass posts to secure femur head.

Appendix B

Figure 28 & Table 9: *Leg cross-section*

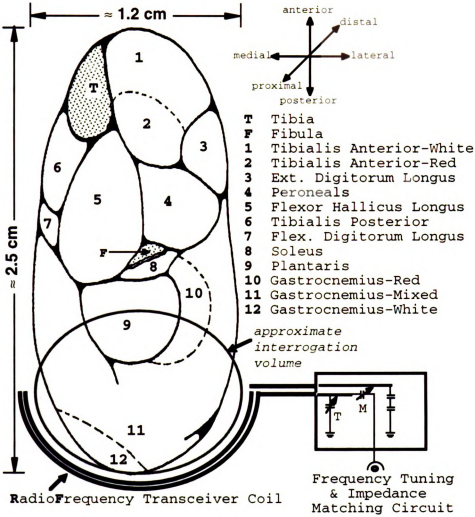

Posterior Leg Muscle	Fiber mass (mg)	FOG %	FOG mass (mg)	FG %	FG mass (mg)	SO %	SO mass (mg)
Plantaris	368	50	155	41	206	9	25
Gastroc–Red	135	62	76	8	12	30	47
Gastroc–White	116	16	10	84	106	0	0
Gastroc–Mixed	1764	28	310	65	1372	7	82

Above table is an excerpt of Table 2 from Ref. (8) illustrating the inter–muscle and intra–muscle fiber type heterogeneity of the posterior rat leg. Total mass of rat leg ≈ 5500mg. Only mean values are shown. SEM is typically 10–15% of mean (N=6).

Appendix C

Figure 29: Temperature Homeostasis

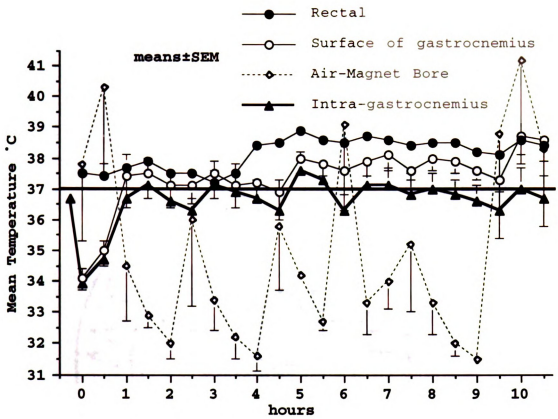

In this supplemental experiment, four rats of similar body mass to the main experiments (300–400g) underwent the identical surgical protocol as previously described in Chapter 4–Methods except that the bipolar electrode was not placed across the nerve. Since the nerve was not directly stimulated, force was not recorded. ^{31}P–NMR spectroscopy was continuously acquired (TR = 1.00 second, NS = 16) but not saved. In addition to the usual rectal temperature probe (YSI model 402A), a "banjo" temperature probe (YSI model 408) was secured underneath the skin directly on the epimysium of the gastrocnemius belly and a fine–tip temperature probe (YSI model 520) was bored ≈3–5mm into the gastrocnemius belly. Also, the ambient magnet bore air temperature was measured on the medial side of the hindlimb with a YSI probe model 405. The temperature controller used feedback from the rectal probe. Each probe underwent a separate 5–point calibration (31.0°, 34.5°, 35.5°, 37.0°, 40.0°) against an NIST certified partial immersion thermometer (OMEGA model ASTM–1C –20°– +150°C). in a temperature regulated water bath. Probe temperature (±0.1°C) was digitally recorded every 30 minutes for 10 hours. (Cole–Palmer temperature recorder model 8402—10). Note, for reference purposes, the duration of a single stimulation—recovery cycle is 11.4, 21.3, and 32.0 minutes for 0.75Hz, 2.0Hz and 5.0Hz respectively.

Appendix D

Figure 30: N versus Cycle Number

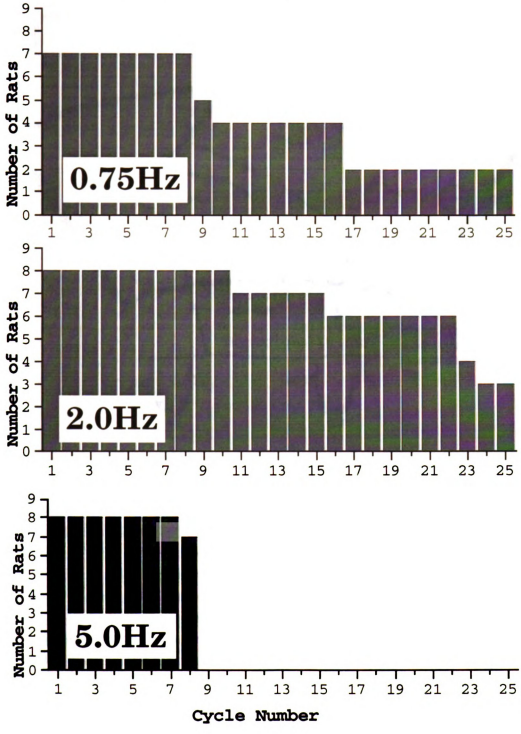

Appendix E

Figure 31: Methimazole Inhibition

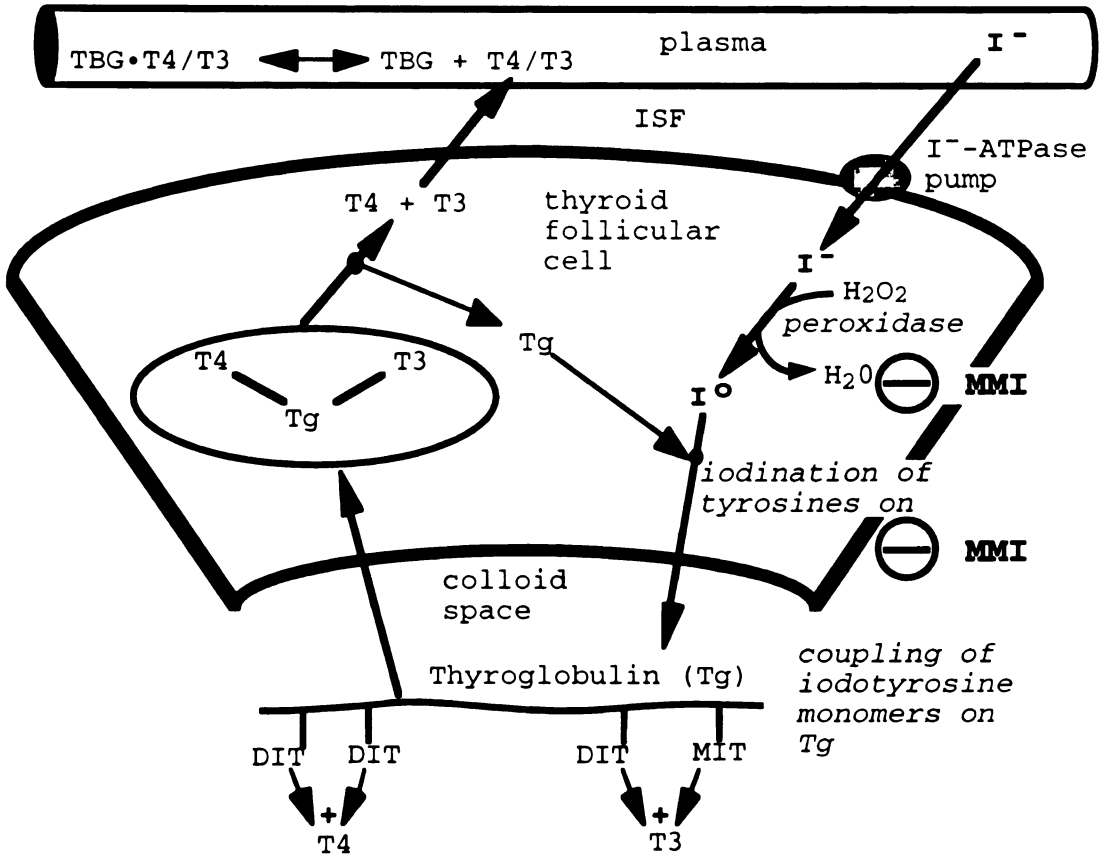

Dietary iodide is actively taken up by the thyroid follicular cell from the plasma via an ATPase pump and oxidized into iodine by the peroxidase enzyme found in the cytosol. One or two iodine atoms are then incorporated into tyrosine amino acids on the thyroglobulin molecule forming monoiodotyrosine or diiodotyrosine, respectively. Both the oxidation step and iodine incorporation step are blocked by methimazole. In the normally functioning thyroid follicular cell, iodine is added to the phenolic group of tyrosine molecules bound to thyroglobulin (Tg) forming monoiodotyrosine (MIT) or diiodotyrosine (DIT) monomers. The coupling of MITs and DITs forms thyroid hormone (MIT+DIT=T_3, triiodotyrosine; DIT+DIT=T_4, tetraiodotyrosine) and takes place within the colloid space on the thyroglobulin molecule. The thyroid cells export mostly T_4 and a little T_3 both of which bind to Thyroid Binding Globulin (TBG) in the plasma. T_4 is converted into the more biologically active form of T_3 by deiodinases located within the interstitial fluid of muscle and most other tissues.

Appendix F

Figure 32: Intensity-Duration Protocol

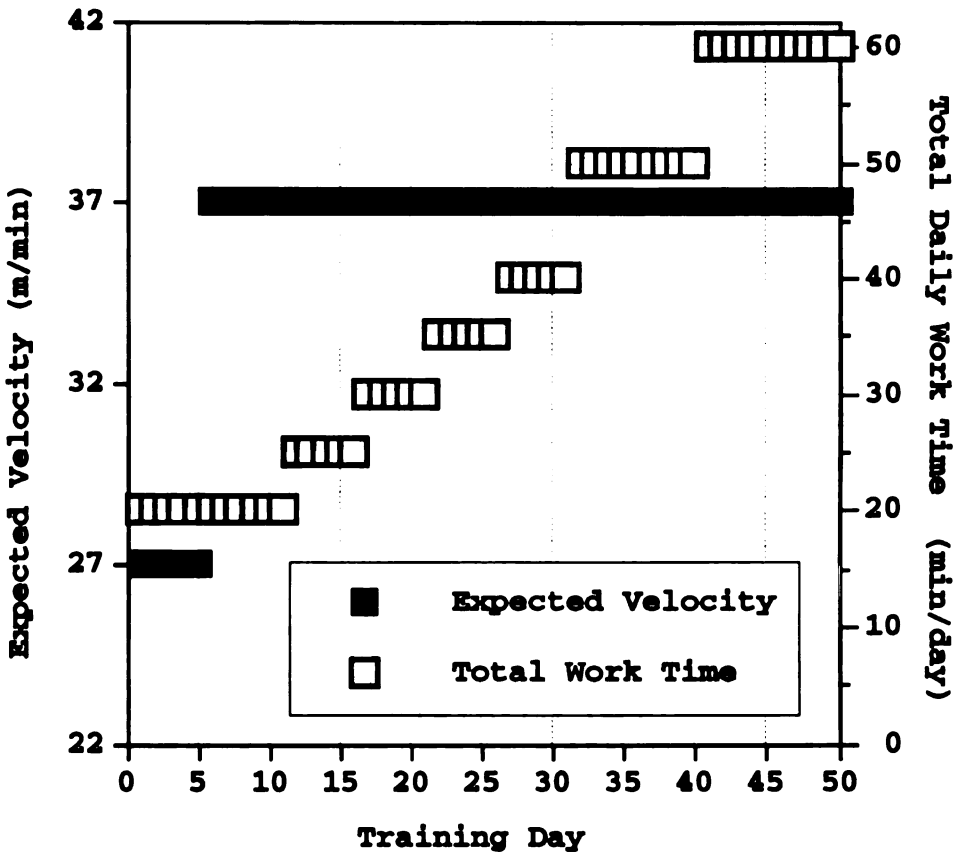

The above is a graphical representation of the controlled running wheel intensity–duration parameters used over the 10–week interval training period. These parameters nearly doubled the mitochondrial content in the superficial white gastrocnemius of the rat based upon citrate synthase activity. Modified from Hickson et al. (127). Rats running at 37m/min roughly corresponds to an intensity of 85-90% $VO2_{max}$ (270).

Appendix G

Figure 33: Training Compliance

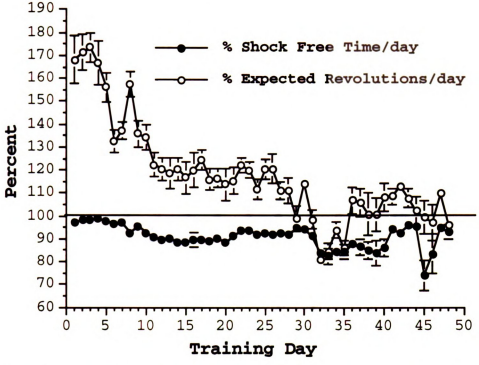

All values are mean±SEM (N=12). Graph indicates, as a group, the rats met or greatly exceeded the expected number of wheel revolutions per day for virtually the entire 10 week protocol. The training intensity and/or duration was progressively increased throughout the 10 week regimen as shown in Appendix F. The apparatus also recorded the amount of time per animal a mild constant current (≈ 0.5mAmp) was applied to the aluminum rungs of the running wheel to motivate the rat to run. This allowed calculation of % shock free time per day. The dip in compliance seen between days 30–36 correlates with the larger jump in training duration seen in Appendix F. Rats were not trained within 24 hours of start of their NMR experiment.

Appendix H

Figure 34: Methimazole Effects

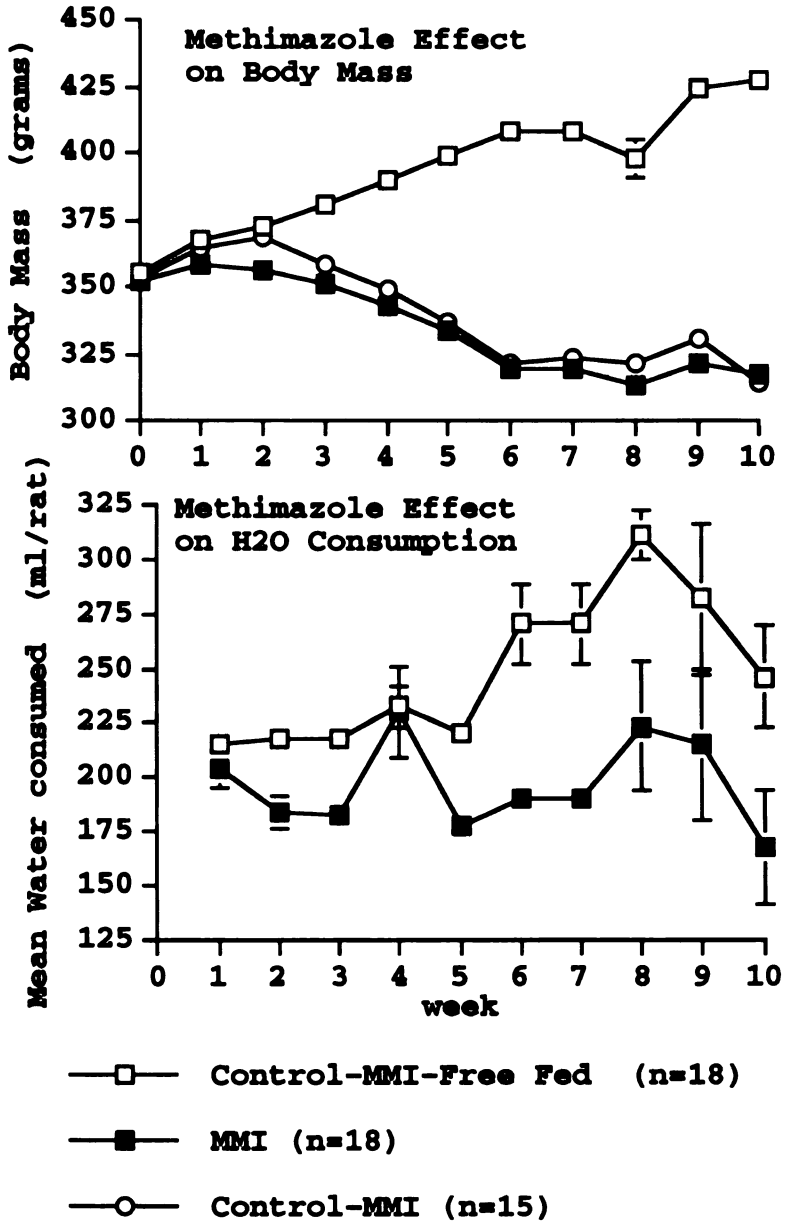

Points are means±SEM: **TOP GRAPH**, All rats from each group where weighed every Monday and Thursday within six hours of the start of their nocturnal cycle. The weekly body mass for one rat was taken as the average of the two values recorded and was averaged with others in the group. Rats in the Control–MMI group were limited to 35 g/day/cage of Purina Rat Chow to mirror the decline in body mass of the MMI rats. **BOTTOM GRAPH**, Total weekly water consumption for each cage was measured on Thursdays based upon the difference method using a graduated cylinder. This number was divided by the number of rats per cage and averaged with others. Square symbols in bottom graph represent all rats from both Control groups (n=33).

List of References

LIST OF REFERENCES

1. **Achten, E., M. VanCauteren, R. Willem, R. Luypaert, W. J. Malaisse, G. VanBosch, G. Delanghe, K. DeMeirleir, and M. Osteaux**. 31P–NMR spectroscopy and the metabolic properties of different muscle fibers. *Journal of Applied Physiology* 68(2): 644–649, 1990.

2. **Ackerman, J. J. H.** Surface (local) coils as NMR receivers. *Concepts in Magnetic Resonance* 2: 33–42, 1990.

3. **Ackerman, J. J. H., P. J. Bore, D. G. Gadian, T. H. Grove, and G. K. Radda**. N.m.r. studies of metabolism in perfused organs. *Phil. Transactions of the Royal Society of London B* 289: 425–436, 1980.

4. **Adams, G. R., J. M. Foley, and R. A. Meyer**. Muscle buffer capacity estimated from pH changes during rest–to–work transitions. *Journal of Applied Physiology* 69(3): 968–972, 1990.

5. **Andrew, E. R.**, Introduction to nuclear magnetic resonance. In: *NMR in Physiology and Biomedicine*, edited by R. J. Gillies, Orlando, 1994, pp. 1–23.

6. **Argov, Z., N. DeStefano, and D. L. Arnold**. ADP recovery after a brief ischemic exercise in normal and diseased human muscle–a 31P MRS study. *NMR in Biomedicine* 9(4): 165–172, 1996.

7. **Argov, Z., J. Maris, L. Damico, M. Koruda, Z. Roth, J. S. Leigh, and B. Chance**. Continuous, graded steady–state muscle work in rats studied by *in vivo* 31P–NMR. *Journal of Applied Physiology* 63(4): 1428–1433, 1987.

8. **Armstrong, R. B., and R. O. Phelps**. Muscle fiber type composition of the rat hindlimb. *American Journal of Anatomy* 171: 259–272, 1984.

9. **Arnold, D. L., P. M. Matthews, and G. K. Radda**. Metabolic recovery after exercise and the assessment of mitochondrial function *in vivo* in human skeletal muscle by means of 31P NMR. *Magnetic Resonance in Medicine* 1: 307–315, 1984.

10. **Baldwin, K. M., G. H. Klinkerfuss, R. L. Terjung, P. A. Mole, and J. O. Holloszy**. Respiratory capacity of white, red, and intermediate muscle: adaptive response to exercise. *American Journal of Physiology* 222(2): 373–378, 1972.

11. **Baldwin, K. M., and C. M. Tipton**. Work and metabolic patterns of fast and slow twitch skeletal muscle contracting *in situ*. *European Journal of Physiology* 334: 345–356, 1972.

12. **Baldwin, K. M., W. W. Winder, R. L. Terjung, and J. O. Holloszy**. Glycolytic enzymes in different types of skeletal muscle: adaptation to exercise. *American Journal of Physiology* 225(4): 962–966, 1973.

13. **Bar, A., J.-A. Simoneau, and D. Pette**. Altered expression of myosin light-chain isoforms in chronically stimulated fast-twitch muscle of the rat. *European Journal of Biochemistry* 178(3): 591–594, 1989.

14. **Barker, R. D. J., T. G. Cartledge, F. Dewhurst, and R. O. Jenkins**, *Principles of Cell Energetics.* edited by G. D. Weston, Biotechnology by Open Learning, Butterworth-Heinemann, Oxford, 1992.

15. **Barnard, R. J., V. R. Edgerton, T. Furukawa, and J. B. Peter**. Histochemical, biochemical, and contractile properties of red, white, and intermediate fibers. *American Journal of Physiology* 220(2): 410–414, 1971.

16. **Barnard, R. J., V. R. Edgerton, and J. B. Peter**. Effect of exercise on skeletal muscle II. Contractile properties. *Journal of Applied Physiology* 28(6): 767–770, 1970.

17. **Barnard, R. J., V. R. Edgerton, and J. B. Peter**. Effect of exercise on skeletal muscle I. Biochemical and histochemical properties. *Journal of Applied Physiology* 28(6): 762–766, 1970.

18. **Barstow, T. J., A. M. Jones, P. H. Nguyen, and R. Casaburi**. Influence of muscle fiber type and pedal frequency on oxygen uptake kinetics of heavy exercise. *Journal of Applied Physiology* 81(4): 1642–1650, 1996.

19. **Bassett, D. R., and E. T. Howley**. Maximal oxygen uptake: "classical" versus "contemporary" viewpoints. *Medicine & Science in Sports & Exercise* 29(5): 591–603, 1997.

20. **Beard, H. H.**, *Creatine and Creatinine Metabolism.* Chemical Publishing Co., Brooklyn, 1943.

21. **Bendahan, D., S. Confort-Gouny, G. Kozak-Reiss, and P. J. Cozzone**. Heterogeneity of metabolic response to muscular exercise in humans: New criteria of invariance defined by *in vivo* phosphorus-31 NMR spectroscopy. *FEBS Letters* 272(1–2): 155–158, 1990.

22. **Bergmeyer, H. U.**, Ed., Metabolites 2: Tri- and Dicarboxylic Acids, Purines, Pyrimidines and Derivatives, Coenzymes, Inorganics, In: *Methods of Enzymatic Analysis*, Vol. VII, VCH, Weinheim, 1985.

23. **Binzoni, T., and P. Cerretelli**. Bioenergetic approach to transfer function of human skeletal muscle. *Journal of Applied Physiology* 77(4): 1784–1789, 1994.

24. **Binzoni, T., G. Ferretti, K. Schenker, and P. Ceretelli**. Phosphocreatine hydrolysis by 31P-NMR at the onset of constant-load exercise in humans. *Journal of Applied Physiology* 73(4): 1644–1649, 1992.

25. **Blei, M. L., K. E. Conley, and M. J. Kushmerick**. Separate measures of ATP utilization and recovery in human skeletal muscle. *Journal of Physiology* 465: 203–222, 1993.

26. **Blei, M. L., K. E. Conley, I. R. Odderson, P. C. Esselman, and M. J. Kushmerick**. Individual variation in contractile cost and recovery in a human skeletal muscle. *Proceedings of the National Academy of Science USA* 90(August): 7396–7400, 1993.

27. **Bloch, F.** Nuclear induction. *Physical Review* 70(7, 8): 460–474, 1946.

28. **Bodner, G. M.** Metabolism Part II: The Tricarboxylic Acid (TCA), Citric Acid, or Krebs Cycle. *Journal of Chemical Education* 63(8): 673–677, 1986.

29. **Boicelli, C. A., A. M. Baldassarri, C. Borsetto, and F. Conconi**. An approach to noninvasive fiber type determination by NMR. *International Journal of Sports Medicine* 10: 53–54, 1989.

30. **Booth, F. W., and D. B. Thomason**. Molecular and cellular adaptations of muscle in response to exercise: Perspectives of various models. *Physiological Reviews* 71(2): 541–585, 1991.

31. **Bracewell, R. N.**, *The Fourier Transform and Its Application.* 2nd, Revised Ed., edited by S. W. Director, Circuits and Systems, McGraw–Hill, New York, 1986.

32. **Brooke, M. H., and K. K. Kaiser**. Muscle fiber types: How many and what kind? *Archives of Neurology* 23(October): 369–379, 1970.

33. **Brown, T., and R. Stoyanova**. NMR spectral quantitation by principal–component analysis. II Determination of frequency and phase shifts. *Journal of Magnetic Resonance Series B* 112: 32–43, 1996.

34. **Buchner, E.** Alkoholische gahrung ohne hefezellen. *Berlin d. Deutsch Chem. Gesellsch* 30: 117–124, 1897.

35. **Buller, A. J., J. C. Eccles, and R. M. Eccles**. Interactions between motoneurones and muscles in respect of the characteristic speeds of their responses. *Journal of Physiology* 150: 417–439, 1960.

36. **Burke, R. E.** Motor unit types of cat triceps surae muscle. *Journal of Physiology* 193: 141–160, 1967.

37. **Burke, R. E.**, Motor units: anatomy, physiology, and functional organization. In: *Handbook of Physiology, Section 1, The Nervous System*, edited by V. B. Brooks, Bethesda, American Physiological Society, 1981, Vol. 2 (part 1), pp. 345–422.

38. **Burke, R. E., D. N. Levine, F. E. Zajac, P. Tsairis, and W. K. Engel.** Mammalian motor units: Physiological–histochemical correlation in three types in cat gastrocnemius. *Science* 174(November 12): 709–712, 1971.

39. **Burt, C. T., T. Glonek, and M. Barany**. Analysis of phosphate metabolites, the intracellular pH, and the state of adenosine triphosphate in intact muscle by phosphorous nuclear magnetic resonance. *Journal of Biological Chemistry* 251(9): 2584–2591, 1976.

40. **Cain, D. F., and R. E. Davies**. Breakdown of adenosine triphosphate during a single contraction of working muscle. *Biochemical and Biophysical Research Communications* 8(5): 361–366, 1962.

41. **Caiozzo, V. J., and F. Haddad**. Thyroid hormone: Modulation of muscle, structure, function, and adaptive responses to mechanical loading. *Exercise Science and Sports Review* 24: 321–361, 1996.

42. **Canfield, P., and G. Marechal**. Equilibrium of nucleotides in frog sartorius muscle during an isometric tetanus at 20°C. *Journal of Physiology (London)* 232: 453–466, 1973.

43. **Carlson, F. D., D. Hardy, and D. R. Wilkie**. The relation between heat produced and phosphorylcreatine split during isometric contraction of frog's muscle. *Journal of Physiology* 189: 209–235, 1967.

44. **Carlson, F. D., D. J. Hardy, and D. R. Wilkie**. Total energy production and phosphocreatine hydrolysis in the isotonic twitch. *Journal of General Physiology* 46: 851–882, 1963.

45. **Carlson, F. D., and A. Siger**. The mechanochemistry of muscular contraction I. The isometric twitch. *Journal of General Physiology* 44: 33–60, 1960.

46. **Challiss, R. A. J., M. J. Blackledge, and G. R. Radda**. Spatial heterogeneity of metabolism in skeletal muscle *in vivo* studies by 31P–NMR spectroscopy. *American Journal of Physiology (Cell Physiology)* 254(23): C417–C422, 1988.

47. **Chanaud, C. M., C. A. Pratt, and G. E. Loeb**. Functionally complex muscles of the cat hindlimb: V. The roles of histochemical fiber–type regionalization and mechanical heterogeneity in differential muscle activation. *Experimental Brain Research* 85: 300–313, 1991.

48. **Chance, B., S. Eleff, J. S. Leigh, D. Sokolow, and A. Sapega**. Mitochondrial regulation of phosphocreatine/inorganic phospate ratios in exercising human muscle: A gated 31P NMR study. *Proceedings of the National Academy of Science USA* 78(11): 6714–6718, 1981.

49. **Chance, B., J. S. Leigh, B. J. Clark, J. Maris, J. Kemt, S. Nioka, and D. Smith**. Control of oxidative metabolism and oxygen delivery in human skeletal muscle: A steady–state analysis of the work/energy cost transfer function. *Proceedings of the National Academy of Sciences USA* 82: 8384–8388, 1985.

50. **Chance, B., J. S. Leigh, J. Kent, and K. McCully**. Metabolic control principles and 31P–NMR. *Federation Proceedings* 45: 2915–2920, 1986.

51. **Chance, B., J. S. Leigh, J. Kent, K. McCully, S. Nioka, B. J. Clark, J. M. Maris, and T. Graham**. Multiple controls of oxidative metabolism in living tissues as studied by phosphorous magnetic resonance. *Proceedings of the National Academy of Science USA* 83: 9458–9462, 1986.

52. **Chance, B., and G. R. Williams**. Respiratory enzymes in oxidative phosphorylation. *Journal of Biological Chemistry* 217: 395–451, 1955.

53. **Chance, B., and G. R. Williams**. The respiratory chain and oxidative phosphorylation. *Advances in Enzymology* 17: 65–134, 1956.

54. **Chasiotis, D., K. Sahlin, and E. Hultman**. Regulation of glycogenolysis in human muscle at rest and during exercise. *Journal of Applied Physiology (Respiratory, Environmental, Exercise Physiology)* 53(3): 708–715, 1982.

55. **Close, R. I.** Dynamic properties of mammalian skeletal muscle. *Physiological Reviews* 52(1): 129–197, 1972.

56. **Coggan, A. R., R. J. Spina, and D. S. King**. Histochemical and enzymatic comparison of the gastrocnemius muscle of young and elderly men and women. *Journal of Gerontology: Biological Sciences* 47(3): B71–B76, 1992.

57. **Connett, R. J.** Glycolytic regulation during an aerobic rest–to–work transition in dog gracilis muscle. *Journal of Applied Physiology* 63(6): 2366–2374, 1987.

58. **Connett, R. J., and K. Sahlin**, Control of glycolysis and glycogen metabolism. In: *Handbook of Physiology Section 12: Exercise: Regulation and Integration of Multiple Systems*, edited by L. B. Rowell, and J. T. Shepherd, New York, Oxford University Press, 1996, pp. 870–911.

59. **Cooley, J. W., and J. W. Tukey**. An algorithm for the machine calculation of complex Fourier series. *Mathematics of Computation* 19(April): 297–301, 1965.

60. **Cooper, D. S., D. Kieffer, V. Saxe, H. Mover, F. Maloof, and E. C. Ridgway**. Methimazole pharmacology in the rat: studies using a newly developed radioimmunoassay for methimazole. *Endocrinology* 114(3): 786–793, 1984.

61. **Crow, M. T., and M. J. Kushmerick**. Chemical energetics of slow– and fast–twitch muscles of the mouse. *Journal of General Physiology* 79: 147–166, 1982.

62. **Curtin, N. A., M. J. Kushmerick, R. W. Wiseman, and R. C. Woledge**. Recovery after contraction of white muscle fibres from the dogfish Scyliorhinus canicula. *Journal of Experimental Biology* 200: 1061–1071, 1997.

63. **Curtin, N. A., and R. C. Woledge**. Energy changes and muscular contraction. *Physiological Reviews* 58(3): 690–761, 1978.

64. **Dainty, M., A. Kleinzeller, A. S. C. Lawrence, M. Miall, J. Needham, D. M. Needham, and S.–C. Shen**. Studies on the anomalous viscosity and flow–birefringence of protein solutions. *Journal of General Physiology* 27: 355–399, 1944.

65. **Davies, K. J. A., L. Packer, and G. A. Brooks**. Biochemical adaptation of mitochondria, muscle, and whole–animal respiration to endurance training. *Archives of Biochemistry and Biophysics* 209(2): 539+554, 1981.

66. **Dawson, M. J., D. G. Gadian, and D. R. Wilkie**. Contraction and recovery of living muscles studied by 31P nuclear magnetic resonance. *Journal of Physiology* 267: 703–735, 1977.

67. **Dawson, M. J., D. G. Gadian, and D. R. Wilkie**. Muscle fatigue investigated by phosphorus nuclear magnetic resonance. *Nature* 274(August 31): 861–866, 1978.

68. **Dawson, M. J., D. G. Gadian, and D. R. Wilkie**. Studies of the biochemistry of contracting and relaxing muscle by the use of 31P n.m.r. in conjunction with other techniques. *Philosophical Transactions of the Royal Society of London B* 289: 445–455, 1980.

69. **Defuria, R. R., and M. J. Kushmerick**. ATP utilization associated with recovery metabolism in anaerobic frog muscle. *American Journal of Physiology (Cell Physiology)* 232(1): C30–C36, 1977.

70. **DeRuiter, C. J., A. deHaan, and A. J. Sargeant**. Repeated force production and metabolites in two medial gastrocnemius muscle compartments of the rat. *Journal of Applied Physiology* 79(6): 1855–1861, 1995.

71. **DeRuiter, C. J., P. E. M. H. Habets, A. DeHaan, and A. J. Sargeant**. In vivo IIX and IIB fiber recruitment in gastrocnemius muscle of the rat is compartment related. *Journal of Applied Physiology* 81(2): 933–942, 1996.

72. **Diehl, P., E. Fluck, H. Gunther, R. Kosfeld, and J. Seelig**, Eds., In: *In–Vivo Magnetic Resonance Spectroscopy III: In–Vivo MR Spectroscopy–Potential and Limitations*, Vol. 28, Springer–Verlag, Berlin, 1992.

73. **DiPrampero, P. E., and R. Margaria**. Relationship between O2 consumption, high energy phosphates and the kinetics of the O2 debt in exercise. *European Journal of Physiology* 304: 11–19, 1968.

74. **DiPrampero, P. E., and R. Margaria**. Mechanical efficiency of phosphagen (ATP + CP) splitting and its speed of resynthesis. *European Journal of Physiology* 308: 197–202, 1969.

75. **Druyan, R., B. DeBernard, and M. Rabinowitz**. Turnover of cytochromes labeled with γ–aminolevulinic acid–^{3}H in rat liver. *Journal of Biological Chemistry* 244(21): 5874–5878, 1969.

76. **Dubowitz, V., and A. B. Everson-Pearse**. A comparative histochemical study of oxidative enzyme and phosphorylase activity in skeletal muscle. *Histochemie* 2: 105–117, 1960.

77. **Dudley, G. A., W. M. Abraham, and R. L. Terjung**. Influence of exercise intensity and duration on biochemical adaptations in skeletal muscle. *Journal of Applied Physiology (Respiratory, Environmental, Exercise Physiology)* 53(4): 844–850, 1982.

78. **Dudley, G. A., P. C. Tullson, and R. L. Terjung**. Influence of mitochondrial content on the sensitivity of respiratory control. *Journal of Biological Chemistry* 262(19): 9109–9114, 1987.

79. **Ebashi, S.** Calcium binding activity of vesiculare relaxing factor. *The Journal of Biochemistry* 50(3): 236–244, 1961.

80. **Edgerton, V. R.**, Ph.D. Thesis, *Histochemical changes in rat skeletal muscle after exercise.*, Michigan State University, 1968.

81. **Edgerton, V. R.** Mammalian muscle fiber types and their adaptability. *American Zoologist* 18: 113–125, 1978.

82. **Edgerton, V. R., L. Gerchman, and R. Carrow**. Histochemical changes in rat skeletal muscle after exercise. *Experimental Neurology* 24: 110–123, 1969.

83. **Edgerton, V. R., J. L. Smith, and D. R. Simpson**. Muscle fibre type populations of human leg muscles. *Histochemical Journal* 7(3): 259–266, 1975.

84. **Edwards, R. H. T., R. C. Harris, E. Hultman, and L.-O. Nordesjo**. Phosphagen utilization and resynthesis in successive isometric contractions, sustained to fatigue, of the quadriceps muscle in man. *Journal of Physiology (London)* 224(1): 40P–41P, 1972.

85. **Elder, G. C. B., K. Bradbury, and R. Roberts**. Variability of fiber type distributions within human muscles. *Journal of Applied Physiology (Respiratory, Environmental, Exercise Physiology)* 53(6): 1473–1480, 1982.

86. **Embden, G., and E. Grafe**. Uber den einflub der muskelarbeit auf die phosphorsaureausscheidung. *Zeitschrift f Physiological Chemistry* 113: 108–137, 1921.

87. **Engelhardt, W. A., and M. N. Ljubimowa**. Myosine and adenosinetriphosphatase. *Nature* 144: 668–669, 1939.

88. **Engelman, T. W.** On the nature of muscular contraction. *Proceedings of the Royal Society of London Serial B* 411: 411–435, 1895.

89. **English, A. E., M. L. G. Joy, and R. M. Henkelman**. Pulsed NMR relaxometry of striated muscle fibers. *Magnetic Resonance in Medicine* 21: 264–281, 1991.

90. **English, A. W., S. L. Wolf, and R. L. Segal**. Compartmentalization of muscle and their motor nuclei: The partitioning hypothesis. *Physical Therapy* 73: 857–867, 1993.

91. **Ennor, A. H., and J. F. Morrison**. Biochemistry of the phosphagens and related guanidines. *Physiological Reviews* 38(October): 631–674, 1958.

92. **Farrar, T. C., and E. D. Becker**, *Pulse and Fourier Transform NMR: Introduction to Theory and Methods.* Academic Press, New York, 1971.

93. **Fenn, W. O.** The relation between the work performed and the energy liberated in muscular contraction. *Journal of Physiology* 58: 373–395, 1923.

94. **Fiske, C. H., and Y. Subbarow**. The nature of the inorganic phosphate in voluntary muscle. *Science* 65(1686): 401–403, 1927.

95. **Fiske, C. H., and Y. Subbarow**. The isolation and function of phosphocreatine. *Science* 67(Feb. 10): 169–170, 1928.

96. **Fiske, C. J., and Y. Subbarow**. Phosphocreatine. *Journal of Biological Chemistry* 81: 629–679, 1929.

97. **Fitts, R. H., F. W. Booth, W. W. Winder, and J. O. Holloszy**. Skeletal muscle respiratory capacity, endurance, and glycogen utilization. *American Journal of Physiology* 228(4): 1029–1033, 1975.

98. **Fitts, R. H., and J. J. Widrick**. Muscle mechanics: Adaptations with exercise–training. *Medicine and Science in Sports and Exercise* 24: 427–473, 1996.

99. **Fletcher, W. M., and F. G. Hopkins**. Lactic acid in amphibian muscle. *Journal of Physiology* 35: 247–309, 1907.

100. **Fletcher, W. M., and F. G. Hopkins**. The respiratory process in muscle and the nature of muscular motion. *Proceedings of the Royal Society of London Serial B* 89: 444–467, 1917.

101. **Flinn, R. A., and P. K. Trojan**, *Engineering Materials and Their Applications.* 3rd Ed., Houghton Mifflin Co., Boston, 1986.

102. **Foley, J. M., G. R. Adams, and R. A. Meyer**. Different effects of gradual vs. acute adenine nucleotide depletion on ATP cost of muscle contraction. *American Journal of Physiology (Cell Physiology)* 267(36): C1177–C1184, 1994.

103. **Foley, J. M., S. J. Harkema, and R. A. Meyer**. Decreased ATP cost of isometric contractions in ATP–depleted rat fast–twitch muscle. *American Journal of Physiology (Cell Physiology)* 261(30): C872–C881, 1991.

104. **Foley, J. M., and R. A. Meyer**. Energy cost of twitch and tetanic contractions of rat muscle estimated in situ by gated 31P–NMR. *NMR in Biomedicine* 6: 32–38, 1993.

105. **Fruton, J. S.**, *Molecules and Life: Historical Essays on the Interplay of Chemistry and Biology.* Wiley–Interscience, New York, 1972.

106. **Funk, C. I., A. J. Clark, and R. J. Connett**. A simple model of aerobic metabolism: applications to work transitions in muscle. *American Journal of Physiology (Cell Physiology)* 258(27): C995–C1005, 1990.

107. **Gadian, D. G.**, *NMR and its application to living systems.* 2nd Ed., Oxford University Press, Oxford, 1995.

108. **Gillies, R. J., K. Ugurbil, J. A. Den_Hollander, and R. B. Shulman**. 31P NMR studies of intracellular pH and phosphate metabolism during cell division cycle of *Saccharomyces cerevisiae. Proceedings of the National Academy of Sciences USA* 78(4): 2125–2129, 1981.

109. **Gollnick, P. D., R. B. Armstrong, C. W. Saubert, K. Piehl, and B. Saltin**. Enzyme activity and fiber composition in skeletal muscle of untrained and trained men. *Journal of Applied Physiology* 33(3): 312–319, 1972.

110. **Gordon, T., and M. C. Pattullo**. Plasticity of muscle fiber and motor units types. *Exercise Science and Sports Review* 21: 331–362, 1993.

111. **Gower, D., and K. M. Kretzschmar**. Heat production and chemical change during isometric contraction of rat soleus muscle. *Journal of Physiology* 258: 659–671, 1976.

112. **Graham, S. J., P. L. Stanchev, and M. J. Bronskill**. Criteria for analysis of multicomponent tissue T2 relaxation data. *Magnetic Resonance in Medicine* 35: 370–378, 1996.

113. **Guth, L.** Fact and artifact in the histochemical procedure for myofibrillar ATPase. *Experimental Neurology* 41: 440–450, 1973.

114. **Guth, L., and H. Yellin**. The dynamic nature of the so–called "fiber types" of mammalian skeletal muscle. *Experimental Neurology* 31: 277–300, 1971.

115. **Gyulai, L., Z. Roth, J. S. Leigh, and B. Chance**. Bioenergetic studies of mitochondrial oxidative phosphorylation using 31phosphorus NMR. *Journal of Biological Chemistry* 260: 3947–3953, 1985.

116. **Hames, B. D.**, *Gel Electrophoresis of Proteins.* 2nd Ed., edited by D. Rickwood, and B. D. Hames, The Practical Approach Series, IRL Press, Oxford, 1990.

117. **Harden, A., and W. J. Young**. The alcoholic ferment of yeast–juice. *Proceedings of the Royal Society of London Serial B* 77: 405–420, 1906.

118. **Harkema, S. J., G. R. Adams, and R. A. Meyer**. Acidosis has no effect on the ATP cost of contractions in cat fast– and slow–twitch skeletal muscles. *American Journal of Physiology (Cell Physiology)* 272(41): C485–C490, 1997.

119. **Harkema, S. J., and R. A. Meyer**. Effects of acidosis on control of respiration in skeletal muscle. *American Journal of Physiology (Cell Physiology)* 272(41): C491–C500, 1997.

120. **Harris, R. C., R. H. T. Edwards, E. Hultman, L.–O. Nordesjo, B. Nylind, and K. Sahlin**. The time course of phosphorylcreatine resynthesis during recovery of the quadriceps muscle in man. *European Journal of Physiology* 367: 137–142, 1976.

121. **Hartner, K.–T., and D. Pette**. Fast and slow isoforms of troponin I and troponin C: Distribution in normal rabbit muscles and effects of chronic stimulation. *European Journal of Biochemistry* 188: 261–267, 1990.

122. **Haynes, R. C.**, Thyroid and antithyroid drugs. In: *Goodman and Gilman's The Pharmacological Basis of Therapeutics*, (8th Ed.), edited by A. Goodman–Gilman, T. W. Rall, A. S. Nies, and P. Taylor, New York, Pergamon Press, 1990, pp. 1373–1376.

123. **Heckman, C. J., and T. G. Sandercock**. From motor unit to whole muscle properties during locomotor movements. *Exercise Science and Sports Review* 24: 109–133, 1996.

124. **Heineman, F. W., J. Eng, B. A. Berkowitz, and R. S. Balaban**. NMR Spectral analysis of kinetic data using natural lineshapes. *Magnetic Resonance in Medicine* 13: 490–497, 1990.

125. **Henneman, E., and C. B. Olson**. Relations between structure and function in the design of skeletal muscles. *Journal of Neurophysiology* 28: 581–598, 1965.

126. **Hermann, L.** Beitrage zur physiologie und physik des nerven. *European Journal of Physiology* 109: 95–144, 1905.

127. **Hickson, R.** Skeletal muscle cytochrome c and myoglobin, endurance, and frequency of training. *Journal of Applied Physiology (Respiratory, Environmental, Exercise Physiology)* 51(3): 746–749, 1981.

128. **Hill, A. V.** The energy degraded in the recovery processes of stimulated muscles. *Journal of Physiology* 46: 28–80, 1913.

129. **Hill, A. V.** Thermodynamics in physiology. *Nature* 113(2850): 859–862, 1924.

130. **Hill, A. V.** The recovery heat–production in oxygen after a series of muscle twitches. *Proceedings of the Royal Society of London Serial B* 103: 183–191, 1928.

131. **Hill, A. V.** The revolution in muscle physiology. *Physiological Reviews* 12: 56–67, 1932.

132. **Hill, A. V.** The mechanical efficiency of frog's muscle. *Proceedings of the Royal Society of London Serial B* 127: 434–451, 1939.

133. **Hill, A. V.** A discussion on muscular contraction and relaxation: their physical and chemical basis. *Proceedings of the Royal Society of London Serial B* 137: 40–87, 1950.

134. **Hill, A. V.** A challenge to biochemists. *Biochimica et Biophysica Acta* 4: 4–11, 1950.

135. **Hill, A. V.**, *Trails and Trials in Physiology*. Williams & Wilkins Co., Baltimore, 1965.

136. **Hill, D. K.** The time course of the oxygen consumption of stimulated frog's muscle. *Journal of Physiology* 98: 207–227, 1940.

137. **Hohorst, J. J., M. Reim, and H. Bartels**. Studies on the creatine kinase equilibrium in muscle and the significance of ATP and ADP levels. *Biochemical and Biophysical Research Communications* 7(2): 142–146, 1962.

138. **Holloszy, J. O.** Biochemical adaptations in muscle: Effects of exercise on mitochondrial oxygen uptake and respiratory enzyme activity in skeletal muscle. *Journal of Biological Chemistry* 242(9): 2278–2282, 1967.

139. **Holloszy, J. O., and L. B. Oscai**. Effect of exercise on α–glycerophosphate dehydrogenase activity in skeletal muscle. *Archives of Biochemistry and Biophysics* 130: 653–656, 1969.

140. **Holloszy, J. O., L. B. Oscai, I. J. Don, and P. A. Mole**. Mitochondrial citric acid cycle and related enzymes: Adaptive response to exercise. *Biochemical and Biophysical Research Communications* 40(6): 1368–1373, 1970.

141. **Homsher, E., and C. J. Kean**. Skeletal muscle energetics and metabolism. *Annual Review of Physiology* 40: 93–131, 1978.

142. **Hood, D. A., J. Gorski, and R. L. Terjung**. Oxygen cost of twitch and tetanic isometric contractions of rat skeletal muscle. *American Journal of Physiology (Endocrinol. Metab.)* 250(13): E449–E456, 1986.

143. **Hoult, D. I.** The magnetic resonance myth of radio waves. *Concepts in Magnetic Resonance* 1: 1–5, 1989.

144. **Hoult, D. I., S. J. W. Busby, D. G. Gadian, G. K. Radda, R. E. Richards, and P. J. Seeley**. Observation of tissue metabolites using 31P nuclear magnetic resonance. *Nature* 252(November 22): 285–287, 1974.

145. **Houmard, J. A., R. Smith, and G. L. Jendrasiak**. Relationship between MRI relaxation time and muscle fiber composition. *Journal of Applied Physiology* 78(3): 807–809, 1995.

146. **Hultman, E., J. Bergstrom, and N. M. Anderson**. Breakdown and resynthesis of phosphorylcreatine and adenosine triphosphate in connection with muscular work in man. *Scandinavian Journal of Clinical Laboratory Investigations* 19: 56–66, 1967.

147. **Hunter, A.**, *Creatine and Creatinine.* Longmans, Green and Co. LTD, London, 1928.

148. **Huxley, H., and J. Hanson**. Structural changes in muscle during contraction: Changes in the cross–striations of muscle during contraction and stretch and their structural interpretation. *Nature* 173(4412): 973–976, 1954.

149. **Iotti, S., R. Lodi, C. Frassineti, P. Zaniol, and B. Barbiroli**. In vivo assessment of mitochondrial functionality in human gastrocnemius muscle by 31P MRS. *NMR in Biomedicine* 6(4): 248–253, 1993.

150. **Izumo, S., B. Nadal-Ginard, and V. Mahdavi**. All members of the MHC multigene family respond to thyroid hormone in a highly tissue–specific manner. *Science* 231: 597–600, 1986.

151. **Jackman, M. R., and W. T. Willis**. Characteristics of mitochondria isolated from type I and type IIb skeletal muscle. *American Journal of Physiology (Cell Physiology)* 270(39): C673–C678, 1996.

152. **James, N. T.** The distribution of type I and type II fibres in muscles. *Journal of Anatomy* 108: 612–613, 1971.

153. **Jansson, E., G. A. Dudley, B. Norman, and P. A. Tesch**. Relationship of recovery from intense exercise to the oxidative potential of skeletal muscle. *Acta Physiologica Scandinavica* 139(1): 147–152, 1990.

154. **Jeneson, J. A. L., S. J. Nelson, D. B. Vigneron, J. S. Taylor, J. Murphy-Boesch, and T. R. Brown**. Two–dimensional 31P–chemical shift imaging of intramuscular heterogeneity in exercising human forearm muscle. *American Journal of Physiology (Cell Physiology)* 263(32): C357–C364, 1992.

155. **Jeneson, J. A. L., J. O. vanDobbenburgh, C. J. A. vanEchteld, C. Lekkerkerk, W. J. M. Janssen, L. Dorland, R. Berger, and T. R. Brown**. Experimental design of 31P MRS assessment of human forearm muscle function: Restrictions imposed by functional anatomy. *Magnetic Resonance in Medicine* 30: 634–640, 1993.

156. **Ji, L. L., F. W. Stratman, and H. A. Lardy**. Chronic exercise training alters kinetic properties of rat skeletal muscle and myocardial lactate dehydrogenase. *FEBS Letters* 208(2): 297–300, 1986.

157. **Jobsis, F. F.** Energy utilization and oxidative recovery metabolism in skeletal muscle. *Current Topics in Bioenergetics* 3: 279–349, 1969.

158. **Jobsis, F. F., and J. C. Duffield**. Oxidative and glycolytic recovery metabolism in muscle. *Journal of General Physiology* 50: 1009–1047, 1967.

159. **Jobsis, F. F., and J. C. Duffield**. Force, shortening, and work in muscular contraction: Relative contributions to overall energy utilization. *Science* 156(June 9): 1388–1392, 1967.

160. **Johnson, M. A., J. Polgar, D. Weightman, and D. Appleton**. Data on the distribution of fibre types in thirty–six human muscles: An autopsy study. *Journal of the Neurological Sciences* 18: 111–129, 1973.

161. **Jones, J. H., and S. L. Lindstedt**. Limits to maximal performance. *Annual Review of Physiology* 55: 547–569, 1993.

162. **Kalckar, H. M.**, *Biological Phosphorylations: Development of Concepts.* Prentice–Hall, Englewood Cliffs, 1969.

163. **Karlsson, J., B. Sjodin, A. Thorstensson, B. Hulten, and K. Frith**. LDH isozymes in skeletal muscles of endurance and strength trained athletes. *Acta Physiologica Scandinavica* 93: 150–156, 1975.

164. **Kelso, T. B., D. R. Hodgson, A. R. Visscher, and P. D. Gollnick**. Some properties of different skeletal muscle fiber types: comparison of reference bases. *Journal of Applied Physiology* 62(4): 1436–1441, 1987.

165. **Kemp, G. J.** Interactions of mitochondrial ATP synthesis and the creatine kinase equilibrium in skeletal muscle. *Journal of Theoretical Biology* 170: 239–246, 1994.

166. **Kemp, G. J., D. J. Taylor, and G. K. Radda**. Control of phosphocreatine resynthesis during recovery from exercise in human skeletal muscle. *NMR in Biomedicine* 6: 66–72, 1993.

167. **Kemp, G. J., D. J. Taylor, and G. K. Radda**. The production, buffering, and efflux of protons in human skeletal muscle during exercise and recovery. *NMR in Biomedicine* 6: 73–83, 1993.

168. **Kemp, G. J., C. H. Thompson, A. L. Sanderson, and G. K. Radda**. pH control in rat skeletal muscle during exercise, recovery from exercise, and acute respiratory acidosis. *Magnetic Resonance in Medicine* 31: 103–109, 1994.

169. **Krebs, H. A., and R. L. Veech**. Equilibrium relations between pyridine nucleotides and adenine nucleotides and their roles in the regulation of metabolic processes. *Advances in Enzyme Regulation* 7: 397–413, 1969.

170. **Kretzschmar, K. M., and D. R. Wilkie**. A new approach to freezing tissues rapidly. *Journal of Physiology (London)* 202: 66P–67P, 1969.

171. **Kuby, S. A., L. Noda, and H. A. Lardy**. Adenosinetriphosphate–creatine transphosphorylase III: Kinetic Studies. *Journal of Biological Chemistry* 210: 65–83, 1954.

172. **Kushmerick, M. J.**, Energetics of muscle contraction. In: *Handbook of Physiology, Section 10, Skeletal Muscle*, edited by L. H. Peachey, R. H. Adrian, and S. R. Gieger, Bethesda, American Physiological Society, 1983, pp. 189–236.

173. **Kushmerick, M. J., and R. E. Davies**. The chemical energetics of muscle contraction: II. The chemistry, efficiency and power of maximally working sartorius muscles. *Proceedings of the Royal Society of London Serial B* 174: 315–353, 1969.

174. **Kushmerick, M. J., R. E. Larson, and R. E. Davies**. The chemical energetics of muscle contraction: I. Activation heat, heat of shortening and ATP utilization for activation–relaxation processes. *Proceedings of the Royal Society of London Serial B* 174: 293–314, 1969.

175. **Kushmerick, M. J., and R. A. Meyer**. Chemical changes in rat leg muscle by phosphorus nuclear magnetic resonance. *American Journal of Physiology (Cell Physiology)* 248: C542–C549, 1985.

176. **Kushmerick, M. J., R. A. Meyer, and T. R. Brown**. Regulation of oxygen consumption in fast– and slow–twitch muscle. *American Journal of Physiology (Cell Physiology)* 263(32): C598–C606, 1992.

177. **Kushmerick, M. J., and R. J. Paul**. Relationship between initial chemical reactions and oxidative recovery metabolism for single isometric contractions of frog sartorius at 0°C. *Journal of Physiology* 254: 711–727, 1976.

178. **Kushmerick, M. J., and R. J. Paul**. Aerobic recovery metabolism following a single isometric tetanus in frog sartorius muscle at 0°C. *Journal of Physiology* 254: 693–709, 1976.

179. **Langone, J.**, *Superconductivity*. Contemporary Books, Chicago, 1989.

180. **Lapaglia, S. R.**, Molecular spectra and molecular symmetry–Introduction to magnetic resonance spectroscopy. In: *Introduction to Quantum Chemistry*, 1971, pp. 238–255.

181. **Larsson, L., X. Li, A. Teresi, and G. Salviati**. Effects of thyroid hormone on fast– and slow–twitch skeletal muscles in young and old rats. *Journal of Physiology* 481(1): 149–161, 1994.

182. **Laughlin, M. H., and R. B. Armstrong**. Muscular blood flow distribution patterns as a function of running speed in rats. *American Journal of Physiology (Heart and Circulatory Physiology)* 243(12): H296–H306, 1982.

183. **Laughlin, M. H., R. J. Korthuis, D. J. Duncker, and R. J. Bache**, Control of blood flow to cardiac and skeletal muscle during exercise (Chapter 16). In: *Handbook of Physiology Section 12: Exercise: Regulation and Integration of Multiple Systems*, edited by L. B. Rowell, and J. T. Shepard, New York, Oxford University Press, 1996, pp. 705–769.

184. **Lawson, C. L., and R. J. Hanson**, *Solving least squares problems*. Prentice–Hall, Inc., Englewood Cliffs, 1974.

185. **Lawson, J. W. R., and R. L. Veech**. Effects of pH and free Mg2+ on the Keq of the creatine kinase reaction and other phosphate hydrolyses and phosphate transfer reactions. *Journal of Biological Chemistry* 254(July 25): 6528–6537, 1979.

186. **Leberer, E., and D. Pette**. Immunochemical quantification of sarcoplasmic reticulum Ca–ATPase, of calsequestrin and of parvalbumin in rabbit skeletal muscles of defined fiber composition. *European Journal of Biochemistry* 156: 489–496, 1986.

187. **Lexell, J., D. Downham, and M. Sjostrom**. Distribution of different fibre types in human skeletal muscles: Fiber type arrangement in m. vastus lateralis from three groups of healthy men between 15 and 83 years. *Journal of the Neurological Sciences* 72: 211–222, 1986.

188. **Lipmann, F.** Metabolic generation and utilization of phosphate bond energy. *Advances in Enzymology and Related Areas of Molecular Biology* 1: 99–162, 1941.

189. **Lohmann, K.** The chemistry of muscle contraction (translated from German). *Naturwiss* 22: 409–414, 1934.

190. **Lundsgaard, E.** The significance of the phenomenon "alactacid muscle contractions" for an interpretation of the chemistry of muscle contraction (translated from German). *Danske Hospitalstidende* 75: 84–95, 1932.

191. **Mackie, B. G., and R. L. Terjung**. Blood flow to different skeletal muscle fiber types during contraction. *American Journal of Physiology (Heart Circ. Physiology)* 245(14): H265–275, 1983.

192. **Malher, M.** First–order kinetics of muscle oxygen consumption, and an equivalent proportionality between QO2 and phosphorylcreatine level: implications for the control of respiration. *Journal of General Physiology* 86: 135–165, 1985.

193. **Margaria, R., H. T. Edwards, and D. B. Dill**. The possible mechanisms of contracting and paying the oxygen debt and the role of lactic acid in muscular contraction. *American Journal of Physiology* 106(3): 680–715, 1933.

194. **Marquardt, D. W.** An algorithm for least squares estimation of parameters. *Journal of the Society of Industrial and Applied Mathematics* 11: 431–441, 1963.

195. **Marsh, G. D., D. H. Paterson, J. J. Potwarka, and R. T. Thompson**. Transient changes in muscle high–energy phosphates during moderate exercise. *Journal of Applied Physiology* 75(2): 648–656, 1993.

196. **Martinas, K., L. Ropolyi, and P. Szegedi**, Thermodynamics: History and Philosophy, Conference: *History of Thermodynamics–Facts, Trends, Debates*, World Scientific Publishing Co., Veszprem, Hungary, 1990, p. 527.

197. **McAllister, R. M., R. W. Ogilvie, and R. L. Terjung**. Functional and metabolic consequences of skeletal muscle remodeling in hypothyroidism. *American Journal of Physiology (Endocrinology Metabolism)* 260(23): E272–E279, 1991.

198. **McAllister, R. M., and R. L. Terjung**. Acute inhibition of respiratory capacity of muscle reduces peak oxygen consumption. *American Journal of Physiology (Cell Physiology)* 259(28): C889–C896, 1990.

199. **McAllister, R. M., and R. L. Terjung**. Training–induced muscle adaptations: increased performance and oxygen consumption. *Journal of Applied Physiology* 70(4): 1569–1574, 1991.

200. **McCully, K. K., M. A. Forciea, L. M. Hack, E. Donlon, R. W. Wheatley, C. A. Oatis, T. Goldberg, and B. Chance**. Muscle metabolism in older subjects using 31P magnetic resonance spectroscopy. *Canadian Journal of Physiology and Pharmacology* 69: 576–580, 1991.

201. **McFarland, E. W., M. J. Kushmerick, and T. S. Moerland**. Activity of creatine kinase in a contracting mammalian muscle of uniform fiber type. *Biophysical Journal* 67(5): 1912–1924, 1994.

202. **Mendel, L. B., and W. C. Rose**. Experimental studies on creatine and creatinine. *Journal of Biological Chemistry* 10: 213–264, 1911.

203. **Meyer, R. A.** A linear model of muscle respiration explains monoexponential phosphocreatine changes. *American Journal of Physiology (Cell Physiology)* 254(23): C548–C553, 1988.

204. **Meyer, R. A.** Linear dependence of muscle phosphocreatine kinetics on total creatine content. *American Journal of Physiology (Cell Physiology)* 257(26): C1149–C1157, 1989.

205. **Meyer, R. A., and G. R. Adams**. Stoichiometry of phosphocreatine and inorganic phosphate changes in rat skeletal muscle. *NMR in Biomedicine* 3(5): 206–210, 1990.

206. **Meyer, R. A., G. R. Adams, M. J. Fisher, P. F. Dillon, J. M. Krisanda, T. R. Brown, and M. J. Kushmerick**. Effects of decreased pH on force and phosphocreatine in mammalian skeletal muscle. *Canadian Journal of Physiology and Pharmacology* 69: 305–310, 1991.

207. **Meyer, R. A., T. R. Brown, B. L. Krilowicz, and M. J. Kushmerick**. Phosphagen and intracellular pH changes during contraction of creatine–depleted rat muscle. *American Journal of Physiology (Cell Physiology)* 250(19): C264–C274, 1986.

208. **Meyer, R. A., T. R. Brown, and M. J. Kushmerick**. Phosphorus nuclear magnetic resonance of fast– and slow–twitch muscle. *American Journal of Physiology (Cell Physiology)* 248(17): C279–C287, 1985.

209. **Meyer, R. A., M. J. Fisher, S. J. Nelson, and T. R. Brown**. Evaluation of manual methods for integration of *in vivo* phosphorus NMR spectra. *NMR in Biomedicine* 1(3): 131–135, 1988.

210. **Meyer, R. A., and J. M. Foley**. Testing models of respiratory control in skeletal muscle. *Medicine and Science in Sports and Exercise* 26(1): 52–57, 1994.

211. **Meyer, R. A., and J. M. Foley**, Cellular processes integrating the metabolic response to exercise (Chapter 18). In: *Handbook of Physiology Section 12: Exercise: Regulation and Integration of Multiple Systems*, edited by L. B. Rowell, and J. T. Shepard, New York, Oxford University Press, 1996, pp. 841–869.

212. **Meyer, R. A., M. J. Kushmerick, and T. R. Brown**. Application of 31P–NMR spectroscopy to the study of striated muscle metabolism. *American Journal of Physiology (Cell Physiology)* 242(11): C1–C11, 1982.

213. **Meyer, R. A., H. L. Sweeney, and M. J. Kushmerick**. A simple analysis of the "phosphocreatine shuttle". *American Journal of Physiology (Cell Physiology)* 246(15): C365–C377, 1984.

214. **Meyer, R. A., and R. L. Terjung**. Differences in ammonia and adenylate metabolism in contracting fast and slow muscle. *American Journal of Physiology (Cell Physiology)* 237(6): C111–C118, 1979.

215. **Meyerhoff, O.**, *The transformation of energy in muscle.* Chemical Dynamics of Life Phenomena, Lippincott Comp., Philadelphia, 1925.

216. **Mitchell, P.** Coupling of phosphorylation to electron and hydrogen transfer by a chemio–osmotic type of mechanism. *Nature* 191(4784): 144–148, 1961.

217. **Mizuno, M., N. H. Secher, and B. Quistorff**. 31P–NMR spectroscopy, rsEMG, and histochemical fiber types of human wrist flexor muscles. *Journal of Applied Physiology* 76(2): 531–538, 1994.

218. **Mole, P. A., K. M. Baldwin, R. L. Terjung, and J. O. Holloszy**. Enzymatic pathways of pyruvate metabolism in skeletal muscle: adaptations to exercise. *American Journal of Physiology* 224(1): 50–54, 1973.

219. **Mommaerts, W. F. H. M.** Energetics of muscular contraction. *Physiological Reviews* 49(3): 427–508, 1969.

220. **Mommaerts, W. F. H. M., and J. C. Rupp**. Dephosphorylation of adenosine triphosphate in muscular contraction. *Nature* 168(4283): 957, 1951.

221. **Monsieurs, K., L. Heytens, C. Kloeck, J.–J. Martin, F. Wuyts, and L. Bossaert**. Slower recovery of muscle phosphocreatine in malignant hyperthermia–susceptible individuals assessed by 31P–MR spectroscopy. *Journal of Neurology* 255(10): 651–656, 1997.

222. **Moon, R. B., and J. H. Richards**. Determination of intracellular pH by 31P magnetic resonance. *Journal of Biological Chemistry* 248(20): 7276–7278, 1973.

223. **Naqui, A., and B. Chance**. Steady–state kinetic approaches to complex biological systems. *Cell Biophysics* 11(December): 159–176, 1987.

224. **Nash, S. G.**, *A history of scientific computing.* ACM Press History Series, Addison–Wesley Publishing Co., New York, 1990.

225. **Needham, D. M.**, *Machina Carnis: The biochemistry of muscular contraction in its historical development.* Cambridge University Press, Cambridge, 1971.

226. **Nelson, S., J. S. Taylor, D. B. Vigneron, J. Murphy-Boesh, and T. R. Brown**. Metabolite images of the human arm: Changes in spatial and temporal distribution of high energy phosphates during exercise. *NMR in Biomedicine* 4: 268–273, 1991.

227. **Newton, K., W. Steeds, and T. K. Garrett**, *The Motor Vehicle.* 12th Ed., Butterworth–Heinemann, Oxford, 1996.

228. **Noakes, T. D.** Challenging beliefs: ex Africa semper aliquid novi. *Medicine & Science in Sports & Exercise* 29(5): 571–590, 1997.

229. **Noakes, T. D.** Maximal oxygen uptake: "classical" versus "contemporary" viewpoints: a rebuttal. *Medicine & Science in Sports & Exercise* 30(9): 1381–1398, 1998.

230. **Noda, L., S. A. Kuby, and H. A. Lardy**. Adenosinetriphosphate–creatine transphosphorylase IV: Equilibrium studies. *Journal of Biological Chemistry* 210: 83–95, 1954.

231. **Odeblad, E., and G. Lindstrom**. Some preliminary observations on the proton magnetic resonance in biologic samples. *Acta Radiologica* 43: 469–475, 1955.

232. **Odum, H. T., R. J. Beyers, and N. E. Armstrong**. Consequences of small storage capacity in nanoplankton pertinent to measurement of primary production in tropical waters. *Journal of Marine Research* 21(3): 191–198, 1963.

233. **Padykula, H. A., and G. F. Gauthier**. Cytochemical studies of adenosine triphosphatases in skeletal muscle fibers. *The Journal of Cell Biology* 18: 87–107, 1963.

234. **Paganini, A. T., J. M. Foley, and R. A. Meyer**. Linear dependence of muscle phosphocreatine kinetics on oxidative capacity. *American Journal of Physiology (Cell Physiology)* 272(41): C501–C510, 1997.

235. **Painter, P. L.** Exercise in end–stage renal disease. *Exercise Science and Sports Review* 16: 305–339, 1988.

236. **Park, J. H., R. L. Brown, C. R. Park, K. McCully, M. Cohn, J. Haselgrove, and B. Chance**. Functional pools of oxidative and glycolytic fibers in human muscle observed by 31P magnetic resonance spectroscopy during exercise. *Proceedings of the National Academy of Science USA* 84: 8976–8980, 1987.

237. **Paton, D. N.** Creatin[e] excretion in the bird and its significance. *Journal of Physiology* 39: 495–504, 1910.

238. **Pekelharing, C. A., and C. J. C. VanHoogenhuyze**. Die bildung des kreatins im muskel beim tonus und bei der starre. *Zeitschrift f Physiological Chemistry* 64: 262–293, 1910.

239. **Peter, J. B., R. J. Barnard, V. R. Edgerton, C. A. Gillespie, and K. E. Stemple**. Metabolic profiles of three fiber types of skeletal muscle in guinea pigs and rabbits. *Biochemistry* 11(14): 2627–2633, 1972.

240. **Pette, D.** Activity–induced fast to slow transitions in mammalian muscle. *Medicine and Science in Sports and Exercise* 16(6): 517–528, 1984.

241. **Pette, D.** Metabolic heterogeneity of muscle fibers. *Journal of Experimental Biology* 115: 179–189, 1985.

242. **Pette, D., and R. S. Staron**. Cellular and molecular diversities of mammalian skeletal muscle fibers. *Review of Physiology, Biochemistry and Pharmacology* 116: 1–76, 1990.

243. **Phillips, S. K., M. Takei, and K. Yamada**. The time course of phosphate metabolites and intracellular pH using 31P NMR compared to recovery heat in rat soleus muscle. *Journal of Physiology* 460(January): 693–704, 1993.

244. **Piiper, J., P. E. DiPrampero, and C. P.** Oxygen debt and high–energy phosphates in gastrocnemius muscle of the dog. *American Journal of Physiology* 215(3): 523–531, 1968.

245. **Piiper, J., and P. Spiller**. Repayment of O2 debt and resynthesis of high–energy phosphates in gastrocnemius muscle of the dog. *Journal of Applied Physiology* 28(5): 657–662, 1970.

246. **Poole, D. C., T. J. Barstow, G. A. Gaesser, W. T. Willis, and B. J. Whipp**. VO2 slow component: physiological and functional significance. *Medicine & Science in Sports & Exercise* 26: 1354–1358, 1994.

247. **Purcell, E. M., H. C. Torrey, and R. V. Pound**. Resonance absorption by nuclear magnetic moments in a solid. *Physical Review* 69: 37–38, 1946.

248. **Radda, G. K., and P. J. Seeley**. Recent studies on cellular metabolism by nuclear magnetic resonance. *Annual Review of Physiology* 41: 749–69, 1979.

249. **Radmer, R. J., and B. Kok**, Light conversion efficiency in photosynthesis. In: *Encyclopedia of Plant Physiology*, edited by A. Pirson, and M. H. Zimmermann, Berlin, Springer–Verlag, 1977, Vol. 5, pp. 125–135.

250. **Rall, J. A.** Energetics of skeletal muscle contraction: Implications of fiber types. *Exercise Sports Science Review* 13: 33–74, 1985.

251. **Ranvier, M. L.** Proprietes et structures differentes des muscles rouges et des muscles blancs, chez les lapins (French: Difference in the properties and structure of the red and white muscle of rabbits). *Comptes Rendus Academie des Sciences* 77: 1030–1034, 1873.

252. **Rassier, D. E., L. A. Tubman, and B. R. MacIntosh**. Length–dependent potentiation and myosin light chain phosphorylation in rat gastrocnemius muscle. *American Journal of Physiology (Cell Physiology)* 273(42): C198–C204, 1997.

253. **Reiser, P. J., and B. T. Stokes**. Development of contractile properties in avian embryonic skeletal muscle. *American Journal of Physiology (Cell Physiology)* 242(11): C52–C58, 1982.

254. **Robinson, D. M., R. W. Ogilvie, P. C. Tullson, and R. L. Terjung**. Increased peak oxygen consumption of trained muscle requires increased electron flux capacity. *Journal of Applied Physiology* 77(4): 1941–1952, 1994.

255. **Rome, L. C., R. P. Funke, R. McNeill-Alexander, G. Lutz, H. Aldridge, F. Scott, and M. Freadman**. Why animals have different muscle fibre types. *Nature* 335(October 27): 824–827, 1988.

256. **Roy, R. R., K. M. Baldwin, and V. R. Edgerton**. The plasticity of skeletal muscle: Effects of neuromuscular activity. *Exercise Science and Sports Review* 19: 269–312, 1991.

257. **Sahlin, K.** Intracellular pH and energy metabolism in skeletal muscle of man. *Acta Physiologica Scandinavica Suppl.* 455: 1–56, 1978.

258. **Sahlin, K., R. C. Harris, and E. Hultman**. Creatine kinase equilibrium and lactate content compared with muscle pH in tissue samples obtained after isometric exercise. *Biochemical Journal* 152: 173–180, 1975.

259. **Sahlin, K., R. C. Harris, and E. Hultman**. Resynthesis of creatine phosphate in human muscle after exercise in relation to intramuscular pH and availability of oxygen. *Scandinavian Journal of Clinical Laboratory Investigations* 39: 551–558, 1979.

260. **Sahlin, K., R. C. Harris, B. Nylind, and E. Hultman**. Lactate content and pH in muscle samples obtained after dynamic exercise. *European Journal of Physiology* 367: 143–149, 1976.

261. **Saltin, B., and P. D. Gollnick**, Skeletal muscle adaptability: significance for metabolism and performance. In: *Handbook of Physiology, Section 10, Skeletal Muscle*, edited by L. D. Peachey, R. H. Adrian, and S. R. Gieger, Bethesda, American Physiological Society, 1983, pp. 555–631.

262. **Saltin, B., and S. Strange**. Maximal oxygen uptake: "old" and "new" arguments for a cardiovascular limitation. *Medicine & Science in Sports & Exercise* 24(1): 30–37, 1992.

263. **Samuels, H. H., B. M. Forman, Z. D. Horowitz, and Z. S. Ye**. Regulation of gene expression by thyroid hormone. *Annual Review of Physiology* 51: 623–639, 1989.

264. **Sandberg, J. A., and F. D. Carlson**. The length dependence of phosphorylcreatine hydrolysis during and isometric tetanus. *Biochemische Zeitschrift* 345: 212–231, 1966.

265. **Sandow, A.** Excitation–contraction coupling in muscular response. *Yale Journal of Biology and Medicine* 25: 176–201, 1952.

266. **Sapega, A. A., D. P. Sokolow, T. J. Graham, and B. Chance**. Phosphorus nuclear magnetic resonance: a non–invasive technique for study of muscle bioenergetics during exercise. *Medicine and Science in Sports and Exercise* 19(4): 410–420, 1987.

267. **Schiaffino, S., V. Hanzlikova, and S. Pierobon**. Relations between structure and function in rat skeletal muscle fibers. *The Journal of Cell Biology* 47: 107–119, 1970.

268. **Schiaffino, S., and C. Reggiani**. Myosin isoforms in mammalian skeletal muscle. *Journal of Applied Physiology* 77(2): 493–501, 1994.

269. **Shaw, T. M., and R. H. Elsken**. Nuclear magnetic resonance absorption in hygroscopic materials. *Journal of Chemical Physics* 18: 1113–1114, 1950.

270. **Shepherd, R. E., and P. D. Gollnick**. Oxygen uptake of rats at different work intensities. *European Journal of Physiology* (362): 219–222, 1976.

271. **Simon, R., and A. Smith**, *Superconductors.* Plenum Press, New York, 1988.

272. **Simoneau, J.–A., and C. Bouchard**. Human variation in skeletal muscle fiber–type proportion and enzyme activities. *American Journal of Physiology (Endocrinology and Metabolism)* 257(20): E567–E572, 1989.

273. **Singer, J. R.** Blood flow rates by nuclear magnetic resonance measurements. *Science* 130: 1652–1653, 1959.

274. **Soderlund, K., and E. Hultman**. ATP and phosphocreatine changes in single human muscle fibers after intense electrical stimulation. *American Journal of Physiology (Endocrinology and Metabolism)* 261(24): E737–741, 1991.

275. **Sommerville, J., and U. Sheer**, *Electron Microscopy in Molecular Biology: A Practical Approach.* IRL Press, Oxford, 1987.

276. **Spriet, L. L., K. Soderlund, J. A. Thomson, and E. Hultman**. pH measurement in human skeletal muscle samples: effect of phosphagen hydrolysis. *Journal of Applied Physiology* 61(5): 1949–1954, 1986.

277. **Srere, P. A.**, Citrate synthase. In: *Methods in Enzymology*, 1969, Vol. 13, pp. 3–11.

278. **Stainsby, W. N.** Oxygen uptake for isotonic and isometric twitch contractions of dog skeletal muscle in situ. *American Journal of Physiology* 219(2): 435–439, 1970.

279. **Stainsby, W. N., and J. T. Fales**. Oxygen consumption for isometric tetanic contractions of dog skeletal muscle in situ. *American Journal of Physiology* 224(3): 687–691, 1973.

280. **Stein, J. M., and H. A. Padykula**. Histochemical classification of individual skeletal muscle fibers of the rat. *American Journal of Anatomy* 110: 103–115, 1962.

281. **Stoyanova, R., A. C. Kuesel, and T. R. Brown**. Application of principal–component analysis for NMR spectral quantitation. *Journal of Magnetic Resonance, Series A* 115: 265–269, 1995.

282. **Sugden, P. H., and E. A. Newsholme**. The effects of ammonium, inorganic phosphate and potassium ions on the activity of phosphofructokinases from muscle and nervous tissues of vertebrates and invertebrates. *Biochemical Journal* 150: 113–122, 1975.

283. **Sullivan, T. E., and R. B. Armstrong**. Rat locomotory muscle fiber activity during trotting and galloping. *Journal of Applied Physiology (Respiratory, Evironmental, Exercise Physiology)* 44(3): 358–363, 1978.

284. **Susheela, A. K., and J. N. Walton**. Note on the distribution of histochemical fibre types in some normal human muscles: A study on autopsy material. *Journal of the Neurological Sciences* 8: 201–207, 1969.

285. **Sweeney, H. L., M. J. Kushmerick, K. Mabuchi, F. A. Sreter, and J. Gergely**. Myosin alkali light chain and heavy chain variations correlate with altered shortening velocity of isolated skeletal muscle fibers. *Journal of Biological Chemistry* 263(18): 9034–9039, 1988.

286. **SzentGyorgi, A.** Studies on muscle. *Acta Physiologica Scandinavica* 8(Suppl. 25): 3–115, 1945.

287. **Takahashi, H., M. Inaki, K. Fujimoto, S. Katsauta, I. Anno, M. Niitsu, and Y. Itai**. Control of the rate of phosphocreatine resynthesis after exercise in trained and untrained human quadriceps muscles. *European Journal of Applied Physiology* 71(5): 396–401, 1995.

288. **Takahashi, H., S. Kuno, S. Katsuta, H. Shimojo, K. Masuda, H. Yoshioka, I. Anno, and Y. Itai**. Relationships between fiber composition and NMR measurements in human skeletal muscle. *NMR in Biomedicine* 9: 8–12, 1996.

289. **Talmadge, R. J., and R. R. Roy**. Electrophoretic separation of rat skeletal muscle myosin heavy–chain isoforms. *Journal of Applied Physiology* 75(5): 2337–2340, 1993.

290. **Taylor, D. J., P. J. Bore, P. Styles, D. G. Gadian, and G. Radda, K.** Bioenergetics of intact human muscle a 31P nuclear magnetic resonance study. *Molecular Biology in Medicine* 1: 77–94, 1983.

291. **Taylor, D. J., P. Styles, P. M. Matthews, D. A. Arnold, D. G. Gadian, P. Bore, and G. K. Radda**. Energetics of human muscle: exercise–induced ATP depletion. *Magnetic Resonance in Medicine* 3: 44–54, 1986.

292. **Taylor, H. L., E. Buskirk, and A. Henschel**. Maximal oxygen intake as an objective measure of cardio–respiratory performance. *Journal of Applied Physiology* 8: 73–80, 1955.

293. **Terjung, R. L.** Cytochrome C turnover in skeletal muscle. *Biochemical and Biophysical Research Communications* 66(1): 173–178, 1975.

294. **Terjung, R. L.** Muscle fiber involvement during training of different intensities and durations. *American Journal of Physiology* 230(4): 946–950, 1976.

295. **Terjung, R. L., and B. Mackie–Engbretson**. Blood flow to different rat skeletal muscle fiber type sections during isometric contraction in situ. *Medicine and Science in Sports and Exercise* 20(5): S124–S130, 1988.

296. **Thompson, C. H., G. J. Kemp, A. L. Sanderson, and G. K. Radda**. Skeletal muscle mitochondrial function studied by kinetic analysis of postexercise phosphocreatine resynthesis. *Journal of Applied Physiology* 78(6): 2131–2139, 1995.

297. **Thompson, W. H.** The metabolism of voluntary muscle. I: The effect of prolonged excitation of motor nerves on the creatine content of limb muscles. *Quarterly Journal of Experimental Physiology* 11(3): 223–230, 1917.

298. **Thunberg, T.** Zur kenntis des kreatins (To the knowledge the creatine). *Zentralblatt fur Physiologie* 20: 915–916, 1911.

299. **Traficante, D. D.** Impedance: what it is and why it must be matched. *Concepts in Magnetic Resonance* 1: 73–92, 1989.

300. **Traficante, D. D.** Introduction to transmission lines. *Concepts in Magnetic Resonance* 5: 57–86, 1993.

301. **Uyeno, K., and T. Mitsuda**. Creatine formation during tonic muscle contractions. *Journal of Physiology (London)* 57: 313–317, 1923.

302. **Vandenborne, K., K. McCully, H. Kakihira, M. Prammer, L. Bolinger, J. A. Detre, K. DeMeirleir, G. Walter, B. Chance, and J. S. Leigh**. Metabolic heterogeneity in human calf muscle during maximal exercise. *Proceedings of the National Academy of Science USA* 88(July): 5714–5718, 1991.

303. **Vandenborne, K., G. Walter, J. S. Leigh, and G. Goelman**. pH heterogeneity during exercise in localized spectra from single human muscles. *American Journal of Physiology (Cell Physiology)* 265(65): C1332–C1339, 1993.

304. **Vandenborne, K., G. Walter, L. Ploutz-Synder, R. Staron, A. Fry, K. DeMeirleir, G. A. Dudley, and J. S. Leigh**. Energy rich phosphates in slow and fast human skeletal muscle. *American Journal of Physiology (Cell Physiology)* 268(37): C869–C876, 1995.

305. **Veech, R. L., J. W. R. Lawson, N. W. Cornell, and H. A. Krebs**. Cytosolic phosphorylation potential. *Journal of Biological Chemistry* 254(14): 6538–6547, 1979.

306. **Vincent, A., and J. McD.Blair**. The coupling of the adenylate kinase and creatine kinase equilibrium. Calculation of substrate and feedback signal levels in muscle. *FEBS Letters* 7(3): 239–244, 1970.

307. **Wagner, P. D.** Determinants of maximal oxygen transport and utilization. *Annual Review of Physiology* 58: 21–50, 1996.

308. **Walter, G., K. Vandenborne, K. K. McCully, and J. S. Leigh**. Noninvasive measurement of phosphocreatine recovery kinetics in single human muscle. *American Journal of Physiology (Cell Physiology)* 272(41): C525–C534, 1997.

309. **Wasserman, K.** Coupling of external to cellular respiration during exercise: the wisdom of the body revisited. *American Journal of Physiology (Endocrinology and Metabolism)* 266(29): E519–E539, 1994.

310. **Weber, A., and H. H. Weber**. Zur thermodynamik der kontraktion des fasermodells. *Biochimica et Biophysica Acta* 7: 339–348, 1951.

311. **Wells, R. L., and W. W. Heusner**. A controlled running wheel for small animals. *Laboratory Animal Science* 21(6): 904–910, 1971.

312. **Wheeler, T. J., and J. M. Lowenstein**. Adenylate deaminase from rat muscle. *The Journal of Biological Chemistry* 254(18): 8994–8999, 1979.

313. **Whittall, K. P., and A. L. Mackay**. Quantitative interpretation of NMR relaxation data. *Journal of Magnetic Resonance* 84: 134–152, 1989.

314. **Wilkie, D. R.** Thermodynamics and the interpretation of biological heat measurements. *Progress in Biophysics and Biophysical Chemistry* 10: 259–298, 1960.

315. **Wilkie, D. R.** Heat, work, and phosphorylcreatine break–down in muscle. *Journal of Physiology* 195(1): 157–183, 1968.

316. **Wilkie, D. R.**, Muscle as a thermodynamic machine. In: *Ciba Foundation Symposium*, Amsterdam, Elsevier, 1975, Vol. 31, pp. 327–339.

317. **Winegrad, S.** Intracellular calcium movements of frog skeletal muscle during recovery from tetanus. *Journal of General Physiology* 51: 65–83, 1968.

318. **Wiseman, R. W., and M. J. Kushmerick**. Creatine kinase equilibration follows solution thermodynamics in skeletal muscle. *Journal of Biological Chemistry* 270(21): 12428–12438, 1995.

319. **Woittiez, R. D., G. C. Baan, P. A. Huijing, and R. H. Rozendal**. Functional characteristics of the calf muscles of the rat. *Journal of Morphology* 184: 375–387, 1985.

320. **Woledge, R. C.** Heat production and chemical change in muscle. *Progress in Biophysics and Molecular Biology* 22: 37–74, 1971.

321. **Woledge, R. C., N. A. Curtin, and E. Homsher**, *Energetic Aspects of Muscle Contraction.* edited by P. F. Baker, Monographs of the Physiological Society, Vol. 41, Academic Press, San Diego, 1985.

322. **Wu, K.-D., and J. Lytton**. Molecular cloning and quantification of sarcoplasmic reticulum Ca2+–ATPase isoforms in rat muscles. *American Journal of Physiology (Cell Physiology)* 264(33): C333–C341, 1993.

323. **Yoshida, T., and H. Watari**. 31P–nuclear magnetic resonance spectroscopy study of the time course of energy metabolism during exercise and recovery. *European Journal of Applied Physiology* 66: 494–499, 1993.

324. **Yoshida, T., H. Watari, and K. Tagawa**. Effects of active and passive recoveries on splitting of the inorganic phosphate peak determined by 31P–nuclear magnetic resonance spectroscopy. *NMR in Biomedicine* 9: 13–19, 1996.

INDEX

—A—

A.V. Hill, 11, 13, 15, 21, 24
acetylcholine, 125
Achilles tendon, 48, 72
Achten, 42, 144
acidification, 3, 50, 55, 61, 88, 124
actin, 12, 17
adenine nucleotides, 22, 25, 121, 157
adenosine, 7, 12, 125, 147, 155, 161, 162
adenosine triphosphate, 12, 147, 155, 161
ADP, 7, 14, 15, 25, 38, 42, 121, 122, 144, 154
aerobic capacity, 1, 73
aerobic training, 2, 32, 40, 132
alactacid oxygen debt, 24
alkalinization, 55, 88
amino groups, 35
AMP, 10, 15, 25, 38
AMP deaminase, 38
amphibolic, 65
analog, 34, 40, 65
anaplerotic, 65
anastomoses, 125
apyrase A, 40
artifactual hydrolysis, 16
ATP, vii, 1, 2, 10, 12, 15, 21, 23, 29, 30, 35, 40, 45, 46, 49, 51, 54, 55, 57, 58, 61, 62, 63, 65, 69, 121, 122, 123, 125, 128, 130, 146, 149, 150, 152, 153, 154, 157, 165, 167
ATP consumption, 17
ATP demand, 1, 14, 23, 29, 40
ATP hydrolysis, 21, 38, 46, 130
ATP supply, 1, 14, 26, 44
ATP synthesis, 40, 123, 157
ATPase, 1, 12, 18, 22, 26, 28, 29, 31, 40, 66, 69, 127, 139, 153, 158, 169

—B—

B1, 50, 74, 132
Barnard, 27, 28, 145, 163
basal metabolic rate, 24
beer, 8
biexponential, 39, 115, 120, 124
bimodal, 3, 29, 116, 117, 118, 129, 131
biopsies, 1, 2, 70, 128
bisphosphoglycerate, 37
Blei, 42, 69, 146
blood flow, 16, 25, 33, 43, 123, 132, 158
Bo, 35, 50
Boltzmann, 35
Brooke, 26, 28, 146
Bruker, v, 50, 73
Buchner, 8, 146
buffer, 9, 17, 46, 144
Burke, 26, 28, 146, 147

—C—

Cain, 14, 15, 147
calcium, 18, 20, 29, 45, 96, 106, 169
Calcium Theory, 18
calf, 42, 168, 169
calsequestrin, 20, 158
capacitor, 11, 15, 41, 44
capillary, 4, 125, 127
capillary density, 4, 127
carbonyl, 35
cardiovascular, 1, 31, 67, 165
Carlson, 17, 30, 147, 165
Carnot, 5
cat, 6, 67, 120, 122, 123, 146, 147, 153
Challenge to Biochemists, 13
Chance, 13, 39, 144, 147, 148, 153, 159, 161, 162, 165, 168
charge, 11, 44
chemical energy balance method, vii, 30
chemical potential, 10, 12, 25
chemical shift, 37, 51, 76, 95, 156
chemiosmotic hypothesis, 25
chemomechanical, 15
Cholesky decomposition, 51
circuit model, 40, 65
citrate synthase, 2, 31, 49, 59, 60, 61, 64, 140
Clausius, 5
Clayeperon, 5
CO2, 7, 23

computational efficiency, 33
Connett, 38, 148, 152
continuum, 27, 127
Cooley, 33, 148
copper, 33
Cori, 8
creatine, 3, 6, 9, 12, 15, 25, 35, 39, 45, 46, 49, 55, 59, 65, 120, 121, 122, 131, 154, 157, 158, 160, 162, 164, 167, 168
creatine kinase, 9, 14, 15, 25, 38, 39, 46, 65, 121, 122, 131, 154, 157, 158, 160, 168
Curtin, 125, 149, 169
cytochrome C, 47, 49, 52, 65
cytochrome oxidase, 24

—D—

D.K. Hill, 24, 30
Dainty, 12, 149
Dalton, 5
Davies, 14, 22, 147, 149, 157
Dawson, 37, 149
developmental stage, 27
diaphragm, 18
diiodotyrosine, 139
DiPrampero, 39, 150, 163
dog, 30, 38, 148, 163, 166
dogfish, 122, 125, 149
Dubowitz, 26, 28, 150

—E—

Ebashi, 18, 150
Edgerton, 27, 145, 150, 163, 164
Edwards, 125, 150, 153, 159
efficiency, vii, 15, 20, 23, 33, 45, 150, 154, 157, 163
eigenvectors, 75
elastic component, 21, 106
elderly, 43, 148
electron microscopy, 18
electron pairs, 35
electron transport chain, 31
electron withdrawing groups, 35
Embden, 6, 151
endergonic, 10
endurance capacity, 31
endurance training, 31, 149
energy balance, vii, 19, 23, 30
energy cost, 15, 30, 44, 148
energy currency, 14
energy demand, 34, 45, 127
Engelmann, 5
engine, 5, 6, 20
enthalpy, 15, 20, 23
epoxy, 16
equilibrium, 15, 25, 38, 39, 65, 121, 122, 131, 154, 157, 164, 168
ethanol, 8
exercise biochemistry, 31
exergonic, 10
explained enthalpy, 19
external work, 9, 17, 21
extraction, 16, 132

—F—

FAD, 15
Fast Fourier Transform, 33
fast twitch muscle, 31
fatigue, 4, 9, 26, 28, 42, 50, 66, 128, 130, 149, 150
FDNB, 14, 16, 22
femur, 48, 72
Fenn, 17, 151
Fenn Effect, 17
fermentation, 8
FFT, 33
FG, 2, 32, 136
fiber recruitment, 1, 149
fiber type distributions, 3, viii, x, 2, 45, 69, 116, 117, 122, 126, 150
fiber type heterogeneity, 29, 121, 129, 131, 136
fiber typing, viii, 1, 2, 42, 126, 127
FID, 36
First Law of Thermodynamics, 19
fish, 26
Fisk, 9
Fletcher, 8, 151, 152
fluorodinitrobenzene, 14
FOG, 2, 32, 136
Foley, v, 44, 144, 152, 160, 162
follicular cells, 47
Fourier transform, 3, 33, 51, 74
free energy, 15, 21, 26, 38, 46, 130
Free Induction Decay, 36
frequency distribution, 29, 34
frequency domain, 36, 51

frog, 13, 16, 21, 30, 37, 38, 120, 147, 149, 154, 158, 169

—G—

G6P, 11
gastrocnemius, 2, ix, 3, 30, 49, 50, 52, 55, 61, 70, 96, 120, 124, 137, 140, 147, 148, 149, 155, 163, 164
gating, 39
Gauss, 33
Gaussian, 3, 27, 29, 76, 116, 117, 118, 129, 131
gel electrophoresis, 2, 29
Gibbs, 5
glycogen, 8, 24, 38, 124, 127, 148, 151
glycogen depletion, 127
glycogen phosphorylase, 38, 124
glycolysis, 9, 14, 16, 21, 26, 37, 42, 66, 123, 125, 148
glycolytic flux, 9, 44, 95, 123, 131
glycolytic pathway, 7
Gower, 20, 152
Guth, 127, 153

—H—

Hanson, 14, 155, 158
Harden, 8, 153
Harkema, 123, 152, 153
heart, 7, 40
heat, v, vii, 5, 6, 16, 21, 23, 125, 147, 154, 157, 163, 169
heat capacity, 16
heat engine, 5, 6, 21
Helmholtz, 5
Henneman, 32, 154
Hermann, 40, 154
hexokinase, 27
hexose, 8, 37
hexose monophosphates, 8
Hill, 6, 11, 13, 15, 21, 24, 30, 146, 154
hindlimb, 6, 72, 123, 137, 144, 147
Holloszy, 31, 144, 151, 154, 155, 161
homogeneity of variance, 77
Hopkins, 8, 151, 152
HRT, 106
Hultman, 24, 30, 148, 150, 153, 155, 164, 165, 166
human, 3, 4, 24, 33, 40, 64, 69, 120, 121, 122, 124, 125, 127, 130, 144, 145, 146, 147, 148, 150, 155, 156, 157, 158, 161, 162, 164, 165, 166, 167, 168
Huxley, 14, 155
hypercapnic acidosis, 122, 123
hypothyroidism, 2, 43, 47, 159

—I—

ICF, x, 36, 39, 61, 62, 63, 64, 67, 88, 89, 90, 91, 92, 93, 94, 95, 123
IIA, 26, 28, 127
IIB, 26, 28, 127, 149
IIC, 26, 28
immunocytochemistry, 29
inner mitochondrial membrane, 25, 47, 65
inorganic phosphate, 6, 10, 69, 76, 151, 160, 166, 169
intermediary metabolism, 10
interpulse interval, 50, 74
interval training, 47, 140
intracellular pH, 2, 37, 55, 66, 73, 147, 152, 160, 161, 163
iodoacetate, 9, 16
isoenzymes, 1, 29
isometric, 2, x, 17, 21, 30, 38, 40, 49, 50, 52, 54, 58, 61, 62, 64, 67, 71, 72, 74, 86, 97, 98, 99, 100, 101, 102, 103, 104, 105, 124, 147, 150, 152, 155, 158, 164, 165, 166, 167
isometric tension, 17, 30
isothermal, 19, 21
isotonic, 17, 21, 147, 166
isovolumetric, 19

—J—

Joule, 5

—K—

Kelvin, 5
Kemp, 41, 157, 167
Krebs cycle, 26, 31, 52, 65
Kuby, 38, 157, 162
Kushmerick, 22, 30, 38, 40, 146, 149, 157, 158, 160, 161, 166, 169

—L—

labile phosphate, 16

lactacid oxygen debt, 24
lactate, 8, 9, 19, 25, 42, 125, 132, 156, 164
lactate dehydrogenase, 27, 156
lactate hypothesis, 8, 9
lactic acid, 7, 10, 20, 24, 95, 122, 124, 126, 129, 131, 159
lactic acidosis, 9, 122, 124, 126, 131
light microscope, 18
light microscopy, 18
linear control model, 130
lineshape, 29, 75, 76, 110, 111
linewidth, 34, 42, 51, 110, 111
linewidth broadening, 37, 42, 51
Lipmann, 10, 12, 37, 158
Lohmann, 9, 37, 159
longitudinal relaxation, 70
Lorentzian, 34, 76
Lundsgaard, 9, 14, 159

—M—

magnet, 34, 43, 49, 50, 72, 73, 75, 110, 137
magnetic field, 34, 50, 74
magnetic moments, 33, 163
Mahler, 40
malate dehydrogenase, 27
malignant hyperthermia, 67, 161
Margaria, 24, 30, 150, 159
Marsh, 125, 159
material science, 33
maximal velocity, 21, 44
Mayer, 5
McCully, 43, 148, 159, 162, 168
mechanical efficiency, 21, 154
metabolic capacitor, 11, 41
metabolic networks, 11, 12, 25, 29, 34
methimazole, 2, 47, 52, 139
Method of Natural Lineshapes, 51, 76
Meyer, v, 38, 40, 144, 152, 153, 157, 160, 161, 162
Meyerhof, 8
microfilament, 96
Mitchell, 25, 161
mitochondrial matrix, 26, 31, 52, 68
MMI, 2, 47, 50, 52, 54, 55, 58, 61, 66, 142
model, 14, 22, 40, 46, 49, 59, 65, 72, 78, 116, 117, 130, 137, 152, 160
Modelling, 3, viii, 116
momentum, 123
Mommarets, 13
monoexponential, 3, 24, 30, 41, 46, 51, 58, 67, 114, 116, 118, 120, 124, 160
monoiodotyrosine, 139
motivation, 7, 15, 43
motor unit, 4, 26, 28, 32, 122, 127, 147, 152, 153
motorneuron, 27, 66
multicomponent, 121, 122, 129, 152
muscle biopsies, 2, 70
muscle fatigue, 4, 9, 50
myasthenia gravis, 7
myosin, 1, 12, 17, 21, 26, 28, 29, 31, 43, 49, 52, 66, 96, 121, 145, 164, 167
myosin ATPase, 1, 22, 26, 28, 31, 43, 66
myosin heavy chain, 29, 49, 52
myosin light chain, 29, 164
myosin regulatory light chain, 96
myothermal, 16, 23

—N—

NAD, 15, 25
Needham, 8, 149, 161
network, 18, 25
niobium, 33
nitrogen, 24, 35, 49
NMR, 1, 2, 3, vii, x, xi, 3, 32, 35, 43, 48, 53, 56, 64, 69, 71, 73, 75, 77, 79, 110, 112, 113, 122, 125, 126, 130, 132, 135, 137, 141, 144, 145, 146, 147, 148, 151, 152, 153, 155, 157, 160, 161, 162, 163, 166, 167
NNLS, 3, ix, x, 76, 77, 112, 114, 115, 116, 119, 124, 126, 131
Noda, 38, 157, 162
normality, 77
numerical methods, 33

—O—

O2, 7, 29, 30, 40, 65, 132, 150, 163
O2 consumption, 7, 30, 150
Odum, 40, 162
optimal length, 17
oxidative capacity, 2, vii, x, 2, 3, 23, 29, 31, 40, 45, 46, 51, 60, 61, 64, 69, 116, 117, 121, 123, 126, 130, 162

oxidative metabolism, 15, 23, 39, 50, 61, 66, 78, 123, 148
oxidative phosphorylation, 14, 16, 21, 59, 130, 148, 153
oxygen consumption, 1, 3, 24, 29, 30, 38, 40, 45, 48, 73, 86, 123, 154, 157, 159, 164

—P—

Padykula, 18, 162, 166
Parnas, 8
parvalbumin, 20, 158
Passive tension, 49, 72
PCA, 3, x, 3, 75, 110, 111, 112, 126
PCr, 2, vii, viii, ix, x, 2, 3, 5, 6, 9, 12, 15, 20, 23, 29, 30, 35, 38, 45, 46, 49, 50, 51, 54, 55, 57, 58, 60, 61, 62, 63, 64, 69, 75, 76, 78, 80, 81, 82, 83, 84, 85, 86, 87, 88, 95, 110, 111, 112, 114, 115, 116, 117, 118, 119, 120, 121, 122, 124, 126, 130, 131
PCr breakdown, 9, 20, 30
PCr hydrolysis, vii, 6, 9, 13, 17, 20, 23, 30, 38, 44, 51, 55, 58, 88
PCr recovery, 2, viii, x, 3, 39, 45, 46, 58, 60, 61, 64, 70, 112, 114, 115, 116, 117, 118, 119, 120, 121, 122, 127, 130, 131
PCr/Tc, 66
PCrss, 44, 86, 87
pentobarbital, 48, 71
PEP, 11
peripheral vascular disease, 43
Peter, 25, 145, 163
Pette, 127, 145, 153, 158, 163
pH, 2, ix, x, 2, 26, 28, 36, 39, 45, 50, 51, 54, 55, 58, 59, 61, 62, 63, 64, 66, 69, 73, 75, 76, 88, 89, 90, 91, 92, 93, 94, 95, 121, 122, 123, 124, 132, 144, 147, 152, 157, 158, 160, 161, 163, 164, 166, 168
pH heterogeneity, 69, 168
pH inhomogeneity, 42
pH optima, 123
phosphagen, 9, 15, 44, 46, 150, 166
phosphate acceptor, 14
phosphocreatine, 2, vii, viii, 4, 5, 15, 21, 44, 46, 51, 69, 126, 147, 151, 157, 160, 161, 162, 165, 166, 167, 168
phosphofructokinase, 27, 38, 124
phosphorus, 1, 35, 56, 69, 74, 79, 145, 149, 157, 160
phosphoryl, 11, 15, 37, 43
photorespiration, 40
photosynthesis, 40, 163
photosynthetic efficiency, 23
Pi, 2, 6, 9, 25, 36, 39, 45, 51, 54, 55, 67, 69, 76, 88, 95, 122, 125, 127
Pi peak splitting, 42, 69, 127
Pi/PCr, 39
Piiper, 24, 30, 163
plankton (232), 40
plant, 7, 33
plantaris, 96
plants, 23
Plexiglas, 135
poultry, 26
power, 2, 36, 40, 45, 50, 73, 75, 110, 126, 157
Principal Component Analysis, 3, viii, 3, 71, 75, 110, 111, 130
proton, 25, 33, 50, 55, 69, 73, 88, 121, 131, 162
psoas, 14
pyridine nucleotides, 13, 25, 157
pyruvate, 31, 161

—Q—

Q10, 20
QO2, 1, 30, 32, 65, 159
quadriceps, 125, 150, 153, 166
quantum, 32

—R—

rabbit, 14, 26, 153, 158
Radda, 41, 144, 147, 155, 157, 163, 167
radiofrequency, 50, 74
rat, 2, v, 3, 18, 37, 38, 46, 47, 48, 64, 69, 71, 72, 73, 75, 79, 86, 110, 111, 112, 113, 114, 115, 120, 122, 123, 124, 136, 140, 141, 142, 144, 145, 149, 150, 152, 155, 156, 157, 160, 163, 164, 165, 166, 167, 168, 169
rate constant, 2, x, 39, 45, 46, 51, 59, 60, 64, 130
recovery, 2, viii, x, 3, 6, 8, 17, 23, 30, 38, 45, 46, 51, 55, 58, 60, 61, 63, 64, 70, 73, 74, 75, 76, 77, 79, 80, 81, 82,

83, 84, 85, 86, 87, 88, 89, 90, 91, 92, 93, 94, 95, 106, 112, 113, 114, 115, 116, 117, 118, 119, 120, 121, 122, 124, 126, 130, 131, 137, 144, 146, 149, 153, 154, 156, 157, 158, 161, 163, 168, 169
recovery kinetics, 2, 39, 120, 121, 122, 168
recruitment, 1, 32, 43, 69, 127, 149
rectal thermistor, 49, 72
rectus abdominus, 14
Red, 26, 28, 136
red blood cells, 33
relaxation time, 28, 29, 54, 70, 106, 155
resonance stabilization, 11
resonant frequency, 34
respiratory chain, 13, 148
Rupp, 13, 161

—S—

saddle shaped transceiver coil, 135
Sahlin, 25, 120, 148, 153, 164
Sandberg, 17, 165
Sandow, 18, 165
sarcoplasmic reticulum, 18, 158, 169
sartorius, 14, 20, 147, 157, 158
sciatic nerve, 4, 48, 72
SDH, 26, 28, 127
second law of thermodynamics, 5
Shepherd, 48, 148, 165
shortening, 17, 20, 23, 156, 157, 166
SigmaPlot, 51
signal processing, 32
Size Principle of motor unit recruitment, 32
Sliding Filament Theory, 14, 17
slow twitch muscle, 31
SO, 2, 32, 136
sodium azide, 24
soleus, 20, 67, 96, 120, 123, 152, 163
spatial distribution, 37, 127, 133
spectroscopy, 2, vii, 1, 32, 46, 69, 137, 144, 145, 147, 158, 160, 161, 162, 169
SR, 18, 22, 29, 43, 127
stackplots, x, 56, 79
staining, 1, 26, 28, 127
Stainsby, 30, 166
staircase phenomenon, 96
steam engine, 5, 20
Subbarow, 6, 151
submaximal, 2, vii, x, 3, 45, 46, 50, 55, 56, 57, 58, 60, 61, 66, 78, 116, 118, 119, 120, 124, 130
submaximal stimulation, 2, vii, 3, 45, 55, 56, 57, 58, 60, 61, 66, 120
succinate dehydrogenase, 26, 127
superconducting, 33, 50, 74, 110
superconducts, 33
supramaximal, 3, x, 4, 49, 64, 66, 72, 106, 120, 124, 132
surface coil, 49, 72, 73, 132

—T—

T1, 70
T2, 70, 152
tau, 115, 116, 117, 119, 127
Teflon, 16
temperature, 5, 13, 16, 44, 49, 71, 72, 137
Terjung, 32, 144, 150, 155, 159, 161, 164, 167
tetanic, 18, 21, 44, 54, 152, 155, 166
tetanic force, 54
thermochemistry, 15
thermodynamic efficiency, 15, 21, 23
thermodynamics, 5, 169
thermopiles, 16
Thunberg, 7, 167
thyroglobulin, 139
Thyroid Binding Globulin, 139
thyroid hormone, 27, 47, 139, 155, 158, 165
time constant, viii, 3, 38, 39, 45, 46, 47, 58, 70, 76, 77, 112, 114, 116, 119, 120, 123, 126, 130, 131
time to peak tension, 28, 29
titanium, 33
tortoise, 13
TPT, 106
TR, 50, 55, 56, 74, 137
Trained, 47, 50, 52, 53, 54, 55, 58, 61, 65
training, 2, 27, 31, 40, 47, 129, 132, 140, 141, 149, 151, 154, 156, 167
transient analysis, viii, 39, 69, 126
transmission cable, 40
transverse relaxation, 70

troponin, 20, 29, 153
TTI, 30
Tukey, 33, 51, 77, 148
twitch, 2, x, 14, 20, 21, 31, 38, 44, 46, 49, 50, 52, 54, 58, 61, 62, 66, 70, 72, 74, 86, 96, 97, 98, 99, 100, 101, 102, 103, 104, 105, 106, 108, 122, 144, 145, 147, 149, 152, 153, 155, 158, 160, 166
twitch force, x, 49, 52, 54, 61, 62, 67, 72, 96, 97, 98, 99, 100, 101, 102, 103, 104, 105, 106, 108
Type I, 1, 2, 26, 28, 42, 52, 70, 120, 127, 131
Type II, 1, 2, 26, 28, 42, 52, 70, 131
Type IIa, 52
Type IIb, 52

—U—

unexplained enthalpy, 20

—V—

velocity, 13, 21, 44, 48, 121, 166
velocity of shortening, 21
VO2max, 2, 1, 2, 31, 48

—W—

Walter, 124, 168
Watt, 22
Weber, 13, 168
White, 26, 28, 136
Wilkie, 21, 147, 149, 157, 169
Williams, 13, 148, 154
Winegrad, 18, 169
Woledge, 20, 149, 169
work, 5, 7, 9, 13, 15, 21, 31, 38, 39, 67, 70, 144, 148, 151, 152, 155, 156, 165, 169
wrist flexor, 39, 161

—Y—

Young, 8, 153

MICHIGAN STATE UNIV. LIBRARIES
31293018017404